UNIVERSITY OF SOUTHAMPTON

EVOLUTION AND STRUCTURE OF A SHELF COCCOLITHOPHORE BLOOM IN THE WESTERN ENGLISH CHANNEL

A satellite, airborne and ship study

Ph.D. Thesis
August 1994
Carlos Garcia-Soto
Department of Oceanography

To my wife Miren,
with her any season is Spring.

UNIVERSITY OF SOUTHAMPTON

ABSTRACT

FACULTY OF SCIENCE
OCEANOGRAPHY

Doctor of Philosophy

EVOLUTION AND STRUCTURE OF A SHELF COCCOLITHOPHORE BLOOM IN THE WESTERN ENGLISH CHANNEL: A SATELLITE AIRBORNE AND SHIP STUDY

by Carlos Garcia-Soto *(Ldo. Grado SB)*

The physical factors associated with the development, advection and disappearance of a bloom of the coccolithophore *Emiliania huxleyi* were investigated with AVHRR satellite imagery (thermal and visible bands) in the Western English Channel in June 1992 from an early reflective stage to a mature and dissipative phase (3-4 weeks life time). The physical processes that appeared important in patch evolution and structure were, differential stratification in an area of weak tidal currents, initial zero wind conditions (allowing local bloom development), later strengthening NE winds (driving the bloom within a coastal warm surface current), entrainment of the bloom water into the anticyclonic tidal circulation around the Isles of Scilly and finally bloom dispersal by mixing and flow divergence.

Ship and airborne surveys simultaneous to the satellite images investigated the extent to which the bloom changed the local optical properties (red beam attenuation coefficient, PAR diffuse attenuation coefficient, *in situ* reflectance spectra (415-660nm) and Airborne Thematic Mapper reflectance), and examined the distribution of the different *E.huxleyi* standing stocks (detached coccoliths, empty coccospheres and living *E.huxleyi* cells). The bloom vertical structure was characterised by sections of temperature, chlorophyll *a*, inorganic nutrients, particulate organic and inorganic carbon, C/N atom-ratio and non-coccolithophore phytoplankton species. The results were analysed in relation to the life history strategy of *E.huxleyi*, the regional redistribution of phytoplankton and chemical constituents, the biological impact of the bloom irradiance field, the development of coccolithophore optical algorithms and the differences between oceanic and shelf coccolithophore blooms.

The satellite time series of the present work is so far the most comprehensive remote sensing report of a coccolithophore bloom. The simultaneous sea-truth measurements show for the first time a section of hydrographic, biological and optical properties of a bloom of *Emiliania huxleyi*.

CONTENTS

V. GENERAL DISCUSSION AND CONCLUSIONS

LIST OF FIGURES

CHAPTER I. INTRODUCTION

CHAPTER II. LITERATURE REVIEW

Figure 2.4 Satellite visible images (AVHRR) of the central area of the 1991 *E.huxleyi* bloom in the North Atlantic for **A)** June 15, **B)** June 17, **C)** June 19 and **D)** June 21. Advection towards the north east within the North Atlantic Drift is apparent south of 61°N, whereas north of this latitude the overall movement is towards the West; some individual eddies appear to remain almost stationary. (from Holligan *et al.*, 1993a)

Figure 2.5 Coccolith backscattering at **A)** 436nm *vs.* coccolith concentration. The equation represents a best-fit polynomial to the data. (85% of the residual variance about the mean is explained). **B)** As panel A but with 546nm light (89% of the residuals about the mean is explained). For the coccolith concentrations shown here, however, the polynomial fit is not significantly better than a linear fit. **C)** Results of the reflectance model for blue light (436nm). Different lines represent different ratios of coccoliths to cells: hatched line 20 coccoliths/cell; dashed line, 50 coccoliths/cell; dash-dot line, 100 coccoliths/cell; striped line, 200 coccoliths/cell; solid line, 400 coccoliths/cell; line for 1,000 coccoliths /cell. **D)** As panel C, but for green (546nm) light. (from Balch *et al.*, 1991)

Figure 2.6 Global climatology of classified coccolithophore blooms (measuring >4,800km^2) in Coastal Zone Colour Scanner imagery from November 1978 to June 1986. The maximum extent of the blooms detected during this period is displayed in white shades. (from Brown and Yoder, 1994a)

Figure 2.7 A) Overview of major oceanic and atmospheric processes associated with *Emiliania huxleyi*. **B)** Strategy for modelling *Emiliania huxleyi* in the GEM (Global Emiliania Modelling) and EHUX (Emiliania HUXleyi) research programmes. (from Westbroek *et al.*, 1993)

Figure 2.8 The life history of *E.huxleyi* as interpreted from observations of laboratory cultures. 1) Normal vegetative propagation. 2) Aberrant mode of vegetative propagation. 3) Loss of the ability to make calcified coccoliths, N-cells appear. 4) Flagellated cells appear in pure cultures of N-cells. 5) Flagellated cells appear in pure cultures of C-cells. 6) Coccolith-covered cells appear in pure cultures of S-cells. (from Klaveness, 1972)

Figure 2.9 Concentration of cells of *Emiliania huxleyi* and detached coccoliths during a bloom in a mesocosm enclosure experiment in Kossfjorden, April 30- May 20, 1992. Note the massive shedding of coccoliths at the end of the bloom. (from Westbroek *et al.*, 1993)

CHAPTER III. EXPERIMENTAL WORK AND METHODS

Figure 3.1 **A)** AVHRR visible satellite image of two coccolithophore blooms observed in the Western English Channel and off Brittany on 12th June 1992, **B)** corresponding AVHRR infra-red satellite image, **C)** scanning electron micrograph of the morphotype of *E.huxleyi* cell found in the Western English Channel bloom, and **D)** AVHRR visible satellite image of the Western English Channel bloom on 25th June 1992 with location of sampling stations and 100m water depth contour.

CHAPTER IV. OBSERVATIONS

Figure 4.1 Combined AVHRR satellite reflectance (white contours) and thermal (background) images on **A)** 4th and **B)** 12th June 1992. A minimum reflectance contour of 0.6% with increments of 0.6% has been plotted. Warm waters are shown as dark shades and cool waters as white shades. "Cl" denotes regions covered by clouds. **C)** Stratification parameter (S) contours (high definition plot of numerical model by Pingree and Griffiths (1978)) overlaying Figure 4.1B. The tidal mixing areas of the region ($S \leq 1$) are identified with initials: Start Point (SP), Lizard Head (LH), Isles of Scilly (IS) and Lands End (LE).

Figure 4.2 Combined AVHRR satellite reflectance (white contours) and thermal (background) images on **A)** 17th, **B)** 20th and **C)** 25th June 1992. A minimum reflectance contour of 0.6% with increments of 0.6% has been plotted. Warm waters are shown as dark shades and cool waters as white shades. "Cl" denotes regions covered by clouds.

Figure 4.3 **A)** Time series of 3-days averaged "AVHRR reflectance" speed or coccolithophore bloom speed (cm/s) calculated from satellite reflectance images during the period 4th June-24th June. The method has been tested between days 25th

and 26th June 25th against the 24h averaged velocity (shaded area) of two drifting buoys deployed in the core of the coccolithophore bloom. **B)** Time series of N component of wind speed (m/s) and **C)** E component of wind speed (m/s) covering the period 4th June-1st July 1992.

Figure 4.4 AVHRR satellite reflectance contours for the sampling days **A)** 25th and **B)** 26th June 1992 (minimum reflectance contour: 0.6%; reflectance increments 0.4%). Also shown the ship's track (dotted line), the location of the stations (black triangles), the tidally corrected positions (white triangles) and the 5 days tracks (25th-30th June) of two Argos buoys deployed in the core of the coccolith patch (broad line). Note that on the second sampling day (26th June) the ship's track cut features that were changed little from the day before: a wave-like structure on the southern edge of the bloom and a detached reflective area at approximately 49 º 47'N 5º 30'W.

Figure 4.5 Surface distribution of **A)** temperature (ºC), **B)** chlorophyll *a* (mg/m^3) and **C)** beam attenuation coefficient at 660nm (m^{-1}) along the cruise track (dotted line). AVHRR satellite reflectance contours on 25th June (from Figure 5a) are shown as background.

Figure 4.6 Empirical relationships between **A)** beam attenuation coefficient at 660nm (m^{-1}) and AVHRR reflectance (%) (AVHRR discrete reflectance increments of ~0.165 correspond to the sensor sensitivity using the onboard calibration values); **B)** AVHRR reflectance (%; 3x3 pixels averages) and concentration of coccoliths (coccoliths/ml) (numbers 1 to 6 indicates sampling stations); and **C)** beam attenuation coefficient at 660nm (m^{-1}) and concentration of coccoliths (coccoliths/ml).

Figure 4.7 Vertical distribution of **A)** temperature (ºC), **B)** chlorophyll *a* (mg/m^3), **C)** nitrate concentration (μM) and **D)** phosphate concentration (μM).

Figure 4.8 Vertical distribution of **A)** concentration of *E.huxleyi* cells (cells/ml), **B)** concentration of detached coccoliths (coccoliths/ml x 10^3) and **c)** concentration of empty coccospheres (coccospheres/ml).

Figure 4.9 Vertical distribution of non-coccolithophore photosynthetic phytoplankton (cell/ml): **A)** diatoms (shaded section: *Nitzschia delicatissima*), **B)** dinoflagellates (shaded section: *Gyrodinium aureolum*) and **C)** flagellates.

Figure 4.10 Vertical distribution of **A)** particulate inorganic carbon (PIC; mgC/m^3), **B)** particulate organic carbon (POC; mgC/m^3), **C)** C/N ratio (by atoms).

Figure 4.11 A) Vertical distribution of PAR diffuse attenuation coefficient (k(PAR); m^{-1}), **B)** empirical relationship between k(PAR) (m^{-1}) and surface concentration of coccoliths (coccoliths/ml $x10^3$), **C)** empirical relationship between k(PAR) (m^{-1}) and AVHRR satellite reflectance (%), **D)** empirical relationship between k(PAR) (m^{-1}) and beam attenuation coefficient (m^{-1}) in the coccolithophore bloom compared with the same relationship for the English Channel waters in winter (broken line; R.D.Pingree, unpublished data) and **E)** empirical relationship between the inverse of Secchi disk depth (m^{-1}) and beam attenuation coefficient (m^{-1}) compared with the same relationship described in the English Channel waters in winter (broken line; Pingree *et al.*, 1986).

Figure 4.12 Spectrum of *in situ* surface reflectance (%) in the range of wavelengths 415-660nm at the coccolith patch core (stations 3 and 4), coccolith patch edges (stations 2 and 5), tidally mixed region (station 1) and open shelf waters (station 6). Vertical lines indicate the range of averaged values (stations 3/4 and 2/5). Dotted line (from 632 to 660nm) indicates an indirect calculation (Kirk, 1981) of the reflectance at 660nm from the beam attenuation coefficient value at this wavelength (c660) and using as absorption c660 ~$0.4m^{-1}$ for clear waters. Thin horizontal lines from 580nm to 680nm shows AVHRR reflectance values. Also shown for reference the absorption spectrum (m^{-1}) of a similar coastal *E.huxleyi* bloom in the Gulf of Maine (Balch *et al.*, 1991) (broken line).

Figure 4.13 A) Empirical relationship between reflectance at 632nm and at 554nm and **B)** empirical relationship between *in situ* reflectance at 632nm and satellite AVHRR reflectance (630nm meanwavelength; broadband 580-680nm); **C)** vertical distribution of *in situ* reflectance at 554nm.

Figure 4.14.- A) Satellite AVHRR reflectance (%) image of the eastern region of the coccolithophore bloom on 23rd June (14:04 GMT). Airborne Thematic Mapper (ATM) reflectance on the same area and day (11:16-11.54 GMT) at **B)** 450-520nm (band 2), **C)** 520-600nm (band 3), **D)** 605-625nm (band 4) and **E)** 630-625nm (band 5). Flight lines 1 to 5 are shown as dotted lines.

CHAPTER V. DISCUSSION AND CONCLUSIONS

Figure 5.1 A) Simplified reflectance model, derived from Balch *et al.* (1991), relating surface reflectance at 546nm (R_{546}, %) and coccolith concentration (coccoliths/ml). The model was formulated for three bloom coccolith/cell ratio: 50 (young bloom, upper thin line), 150 (old bloom; lower thin line) and 100 (broad line). The numerical expression in the figure was derived from the intermediate 100 coccoliths/cell ratio. The marks in the figure shows the observed distribution of *in situ* surface reflectance against *in situ* coccolith concentration overlaid on the modelling distribution. Numbers 1 to 6 indicate the coccolithophore bloom stations. White triangles represents direct measurements; black triangles indicates a better aproximation of the later values to the modelling curve after subtracting a reflectance shift of ~1%. The tidally mixed station 1 is shown as a large star and highlights the limitation of the model in regions with high loads of sediments in suspension. **B)** Theoretical relationship (lines) between *E.huxleyi* cell concentration (NC; cells/ml) and a reflectance ratio $RATIO_{436\text{-}546}$ derived from the two single band reflectance models (436 and 550nm) by Balch *et al.* (1991). The model was formulated for two distinct values of 436nm reflectance (R_{436}): 5% (low R_{436}; thin line) and 20% (high R_{546}, broad line). The distribution of *in situ* data (cell concentration *vs.* $RATIO_{436\text{-}546}$) was overlaid on the modelling distribution and marked and annotated as in the previous figure. B denotes *in situ* data from Table 1 of Balch *et al.* (1991) corresponding to a coastal *E.huxleyi* bloom in the Gulf of Maine on June 1988.

Figure 5.2 CZCS composite image of a large coccolithophore bloom in the Bay of Biscay in May 1986. The image has been produced by assigning the atmospherically corrected reflectances for band 1 (blue), 2 (green) and 3 (yellow) to blue, green and red colours in the image, thereby giving a seminatural colour image. Clear high salinity waters appear blue as a result of the lower absorption of blue light by seawater. The combined effects of backscattering and absorption give rise to the intermediate colour patterns of the different phytoplankton populations. Coccolithophores appear as white reflectances due to backscattering in all three visible bands. The image clearly shows the spatial scale of the coccolithophore bloom and in the eddy-like finestructure reveals how the bloom edges are evolving.

LIST OF TABLES

CHAPTER II. LITERATURE REVIEW

CHAPTER III. EXPERIMENTAL WORK AND METHODS

ACKNOWLEDGEMENTS

Completing a PhD is a worthwhile but a long and sometimes painful process. I am very grateful to my supervisors Ian Robinson at Southampton University and Robin Pingree at Plymouth Marine Laboratory who not only taught good research making but always gave their unconditional and wholehearted support.

The value of this work has been greatly enhanced through being done with the help of good scientists and research institutions:

Steve Groom and Kevin Morris from the NERC Image Analysis Unit at the University of Plymouth provided valuable supervision for the processing of the satellite and airborne images and offered valuable comments on the chapter on methods. Bablu Sinha initiated the corrections of the airborne data (see preliminary results with ATM band 2 in Sinha and Pingree, 1993). Derek Harbour identified and counted the phytoplankton taxa. Emilio Fernández analysed the C/N and calcium content. I would also like to thank the captain and crew of the R/V Squilla and NERC Piper aircraft for assistance during the field and airborne study. The satellite data was provided and extracted in near real-time thanks to the facilities of NERC Satellite Station at Dundee University. Patrick Holligan and Emilio Fernández provided a final critical commentary of the work.

This research was supported by the Project Ocean-Shelf Boundary Processes (IRP-2) of the Plymouth Marine Laboratory (NERC). Completion of the doctorate was enabled by a Sectoral Grant (C+M) of the Commission of the European Union (Programme MAST II).

GLOSSARY OF SYMBOLS

a	absorption coefficient
b	scattering coefficient
b_b	backscattering coefficient
c	beam attenuation coefficient (c=a+b)
L	upwelling radiance
Ed, Eu	downwelling and upwelling irradiance
Q	angular distribution function (Q=Eu/L)
K	diffuse attenuation coefficient (K = d[LnEd]/dz)
R	irradiance reflectance or reflectance (R = Eu/Ed)
D	Secchi disk depth
PAR	Photosynthetic Active Radiation (400-700nm)
AVHRR	Advanced Very High Resolution Radiometer
CZCS	Coastal Zone Colour Scanner
ATM	Airborne Thematic Mapper
TM	Thematic Mapper
SeaWiFS	Sea-viewing Wide-Field-of-view Sensor
S	Stratification parameter (notation by Pingree and Griffiths, 1978)
PIC	Particulate Inorganic Carbon
POC	Particulate Organic Carbon
TPC	Total Particulate Carbon
DOC	Dissolved Organic Carbon
DOP	Dissolved Organic Phosphorus
C/N	Carbon Nitrogen atom ratio
N/P	Nitrogen Phosphorus atom ratio
DMS	Dimethylsulphide
DMSP	Dimethylsulphoniopropionate
α^B	photosynthetic efficiency
P_m^B	potential maximum photosynthetic growth or assimilation number
I_K	photoadaptative term ($I_K = P_m^B/\alpha^B$)
I_o	PAR sea surface irradiance
I_*	I_o/I_K (notation by Platt, 1986)
C	surface chlorophyll *a* concentration
Ck	average chlorophyll *a* concentration in the first optical depth ($z = 1/K_{PAR}$)
Cav	average chlorophyll *a* concentration in the euphotic zone ($z = 4.6/K_{PAR}$)
P_T	primary production integrated over the euphotic zone ($z = 4.6/K_{PAR}$)

CHAPTER I. INTRODUCTION

A. THESIS OVERVIEW

Objectives

In 1991, when the author's PhD programme commenced, SeaWiFS, the first satellite colour sensor since the Coastal Zone Colour Scanner (CZCS; 1978-1986), was planned to be launched within three years time (General Science Corporation, 1991). The PhD programme therefore set out to investigate the biological and optical structure of phytoplankton blooms as a preparation for satellite colour research during the SeaWiFS era. The objective turned out to be a major priority of subsequent recommendations of a NASA colour research commitee (Hooker *et al.*, 1992; Abbot *et al.*, 1994).

The PhD focused mainly on blooms of the coccolithophore *Emiliania huxleyi*, a species of significance to the global carbon and sulphur cycles (Holligan and Balch, 1991). Four main reasons orientated the main efforts towards the investigation of blooms of this species:

(i) their detectability with the visible band of the AVHRR sensor (Groom and Holligan, 1987), thus compensating for the absence of the CZCS colour scanner (1978-1986) at the time of the investigations;

(ii) previous satellite reports of coccolithophore bloom occurrences in the Western English Channel (Groom and Holligan, 1987; Grepma, 1988), where a rapid response exercise with ship and airplane could be carried out;

(iii) the lack of *in situ* studies of these type of blooms at both ocean (Holligan *et al.*, 1983; Holligan *et al.*, 1993a) and shelf (Balch *et al.*, 1991) regions; and

(iv) the increasing interest of the international research community in the ecology of *Emiliania huxleyi* (e.g. EHUX (Emiliania HUXleyi) Programme; MAST 1992-1994).

An important planning tool for the investigations was the use of near real-time remote sensing (Cornillon *et al.*, 1988; Groom and Cooper, 1989). This technique was thought to be relevant to provide the start time and location for the *in situ* survey, to track the evolution of transient blooms and to frame the field sampling within a broader oceanographic context. The particular study was carried out as a rapid response survey in the Western English Channel in June 1992 using combined satellite-airborne-and-ship sampling. The specific objectives were:

(i) to identify physical factors controlling bloom evolution and structure,

(ii) to track the life history strategy of *Emiliania huxleyi* from remote sensing and field observations,

(iii) to examine the optical changes induced by a bloom in the water column and the biological significance of such changes, and

(iv) to propose possible coccolithophore algorithms for the future SeaWiFS colour sensor.

Organisation

The first section of this Introduction presents the overall aim of the PhD and the specific objectives of the present Thesis; the second section summarises the PhD research work preliminary to the main coccolithophore experiment. Chapter Two reviews the contribution of colour remote sensing to phytoplankton studies emphasising primary production and coccolithophore optics. The significance of *Emiliania huxleyi* for the global distribution of phytoplankton and the biogeochemical cycles of carbon and sulphur is later described. The last sections of the chapter analyse recent laboratory observations concerning the life cycle of *E.huxleyi*, the process of bloom formation and the environmental factors determining bloom abundance and termination; this provides a basis for the later interpretation of the observed results.

Chapter Three describes the experimental work during the 1992 coccolithophore bloom study (sampling strategy, satellite remote sensing, airborne remote sensing and *in situ* methods). Chapter Four analyses the three major sections of observations:

(i) the temporal evolution of the bloom (development, advection, disapearance),

(ii) the bloom physical and biological structure (underway measurements, vertical hydrography, standing stocks of *E.huxleyi*, distribution of non-coccolithophore species, particulate organic and inorganic carbon) and,

(iii) the optical properties of the bloom (PAR diffuse attenuation coefficient, in situ reflectance and airborne ATM reflectance).

Chapter Five (Discussion and Conclusions) addresses the questions posed by the specific objectives of the work, suggests further remote sensing research on *E.huxleyi* blooms and presents finally the Summary of the Thesis.

B. PRELIMINARY RESEARCH WORK

Up to the detection with the AVHRR visible band of a coccolithophore bloom that could initiate the main experiment, the PhD programme focused on coupling between AVHRR-observed thermal structures and *in situ* distributions of phytoplankton. The studies were carried out in conjunction with various research projects that provided access to field data; the specific areas of research were selected among several possible collaborations in order to keep the whole PhD research strongly unified within a common research topic (phytoplankton blooms and hydrodynamics), a common observational methodology (combined satellite and ship sampling) and a common area of study (Bay of Biscay and adjacent seas; see Figure 1.1). The investigations targetted two regular features with strong surface thermal manifestation but yet unknown biological response:

(i) the winter Slope Current along the Iberian and Cantabrian shelf-break (Pingree and Le Cann, 1989; 1990) (see January and February in Figure 1.1) and

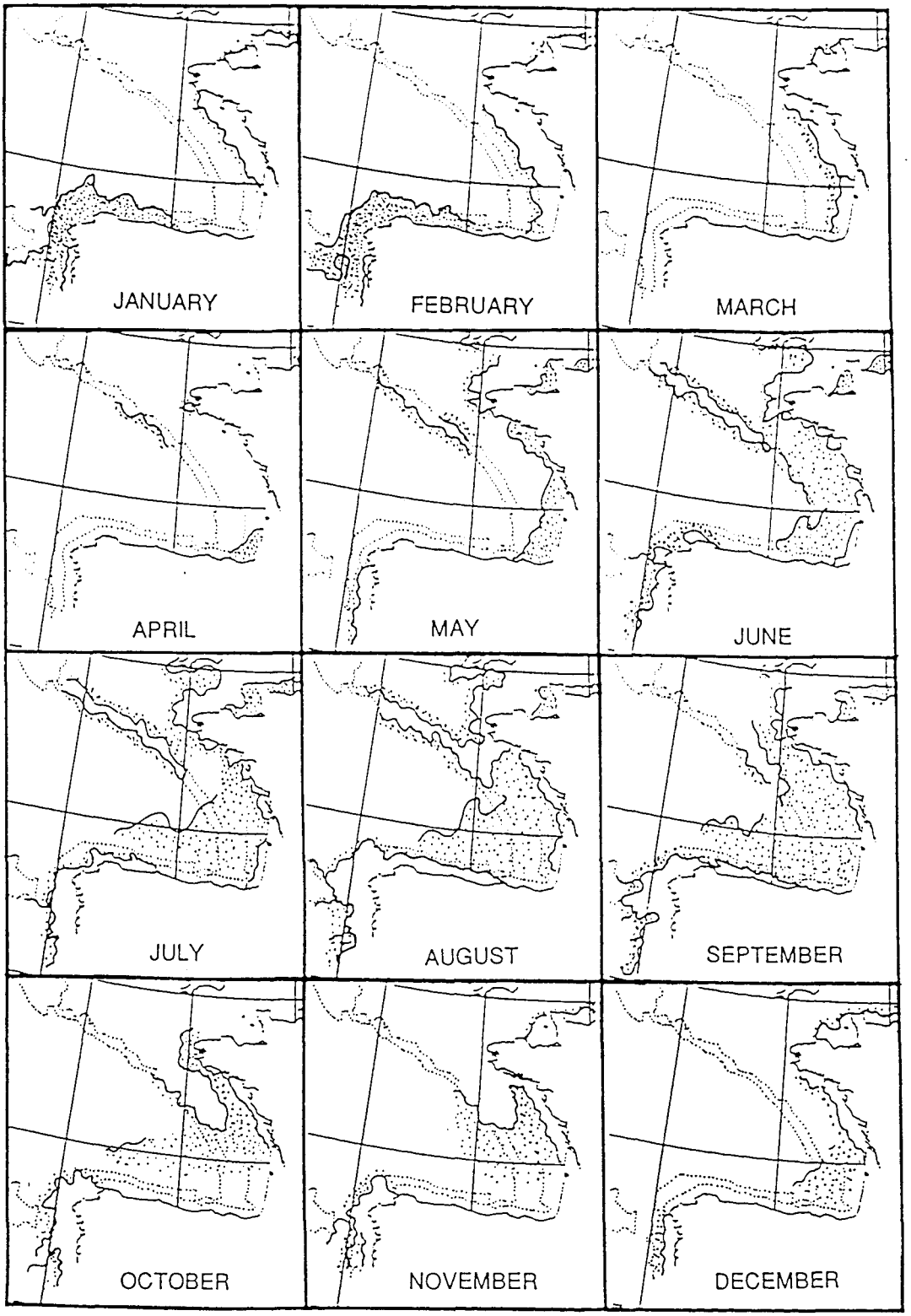

Figure 1.1 Satellite (AVHRR) monthly climatology (1981-1988) of regular thermal fronts (>0.5degC/5km and ≥50% occurrence) in the Bay of Biscay and adjacent seas. The warm side of the fronts is shown as a dotted area. (elaborated from SATMER (1983 to 1990) with permission of Centre de Meteorologie Spatiale du Lannion)

(ii) the local warm area of the SE Bay of Biscay in early spring (Hemery and Wald, 1986) (see April in Figure 1.1).

The results of these preliminary studies are summarised below and more detailed information can be found in original (Garcia-Soto *et al.*, 1991; Garcia-Soto and Madariaga, 1994) or joint (Fernández *et al.*, 1993b) publications.

Garcia-Soto *et al.* (1991)

Rationale and Objective

AVHRR images have recently revealed the existence of a thermohaline surface current 70-100km wide circulating poleward along the Iberian slopes and continuing with decreasing thickness along the Cantabrian slopes (Pingree and Le Cann, 1989, 1990). The IR satellite archive and long-term current meter measurements have described the seasonality of the flow lasting from October to April, when the summer upwelling winds advecting cool waters equatorward weaken or reverse (Pingree and Le Cann, 1989, 1992; Haynes and Barton, 1990). The current typically exhibits a surface temperature 0.5degC higher than the surrounding waters and extends from surface to 150-200m depth where it is mixed with the upper layer of the North Atlantic Central Water (NACW) (Frouin *et al.*, 1990; Haynes and Barton, 1990). Transects with the Undulating Oceanographic Recorder (UOR) across the N Iberian region in 1991 provided the opportunity to investigate the thermal fronts resulting at the boundaries of the Slope Current and the potential of these frontal regions to hold phytoplankton blooms.

Results and Conclusion

The comparison of thermal satellite images in April and May 1991 indicated that at the time of the investigations the strength of the winter warm flow was lessening and a situation of coastal upwelling was becoming established. UOR tows

(Figure 1.2) and stationary CTD profiles, close in time to the satellite observations, similarly identified the transitional stage across the shelf and slope regions. Cool (<12.3°C) and dense (>27.10kg/m^3) NACW waters, the source of the coastal upwelled waters of the area (Fraga, 1981), intercepted the warm (>12.6°C) waters of the winter slope flow at the mid-shelf stations. As initially hypothesised, a subsurface bloom of phytoplankton (up to 6mgChl*a*/m^3) was found at the strong density fronts arising due to the interaction of both water masses. The high vertical stability of these frontal regions made possible the occurrence of the bloom probably by decreasing the depth of the water column where the the plant cells were held, thereby allowing increased mean light levels. The wider significance of the results was that the anomalously warm Slope Current can sustain an important percentage of the regional biomass of primary producers some weeks before the initiation of the spring diatom bloom.

Garcia-Soto and Madariaga (1994)

Rationale and Objective

The Bay of Biscay is regularly characterised by the appearance of a local warm structure on its SE region appearing first in early spring and extending northward and westward during the following months (Hemery and Wald, 1986; see also Figure 1.1). The timing of the phenomenom reflects the local onset of the seasonal stratification and matches the initiation of other thermocline-dependent structures such as the Shelf-Break Cooling (Pingree and Mardell, 1981; Pingree, 1984) and the Ushant Front (Pingree and Griffiths, 1978; Pingree, 1980). During the first week of May 1991, the Undulating Oceanographic Recorder (UOR) was towed inside and progressively further from the warm feature along transects perpendicular to the Cantabrian coast (Figure 1.3). The transects allowed to investigate whether the timing of the spring phytoplankton bloom was coupled to the particular thermal distribution of the innermost Bay of Biscay.

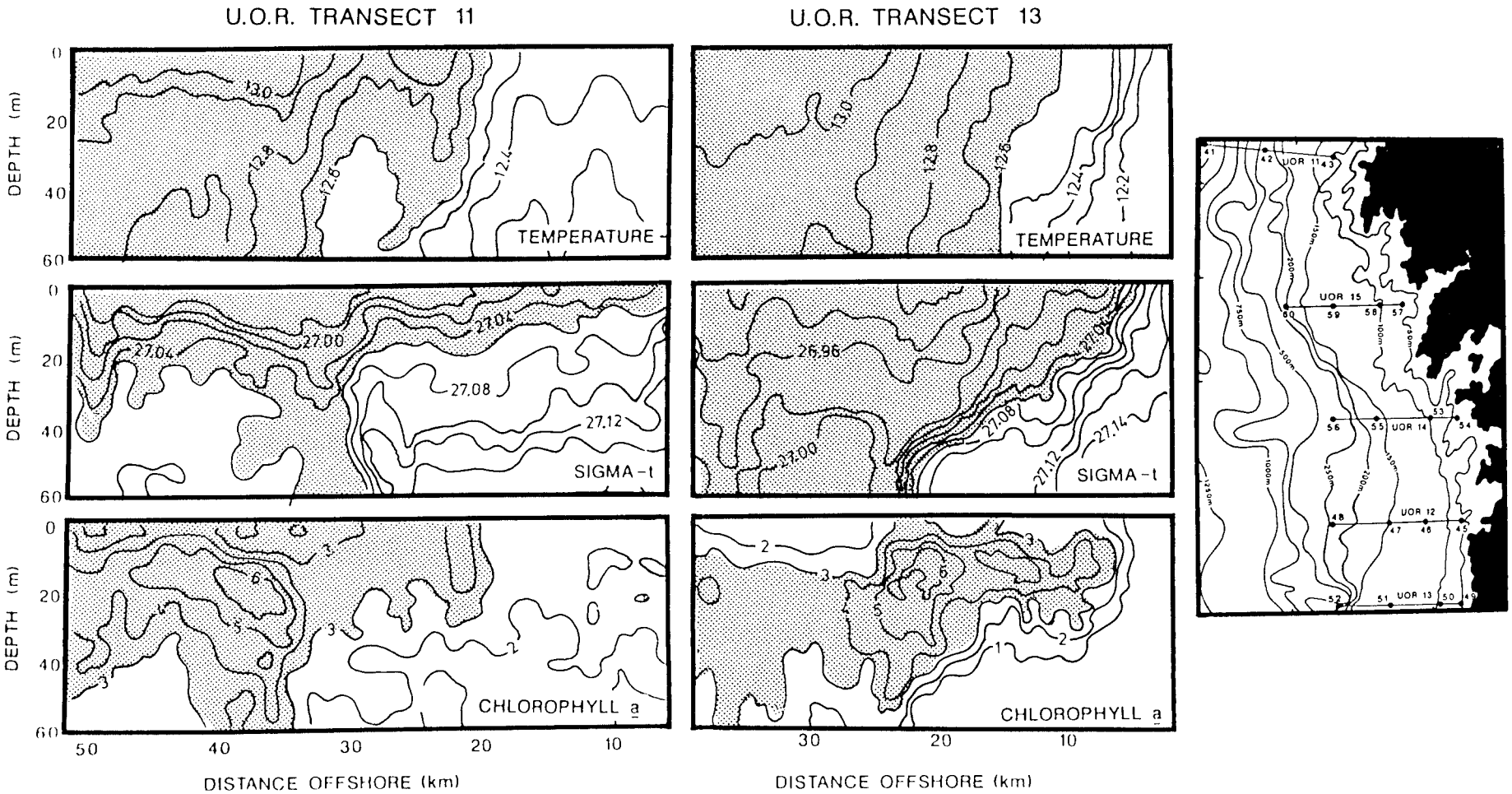

Figure 1.2 U.O.R. sections of temperature (°C), density (kg/m^3) and chlorophyll *a* concentration (mg/m^3) at the interface of slope water (shaded contours) and coastal upwelled water (clear contours) in the N Iberian region on 27th April (Transect 11) and 3rd May (Transect 13) 1991.

Results and Conclusion

The UOR sections of temperature in conjunction with AVHRR infra-red images identified the thermal transition from the warm and stratified structure of the inner corner of the Bay of Biscay (transect C) to a cooler (12.2°C) and vertically mixed outer water column (transect A). The three regional transects (A to C), despite being separated by only 30km, presented thermal profiles corresponding respectively to mid-April, beginning of May and mid-May according to the general hydrographic description of the area (Arias, 1980). The UOR distributions of chlorophyll *a* exhibited a similar spatial progression with values of phytoplankton biomass evolving from winter levels (1mgChl*a*/m^3) in the fully mixed transect A to bloom levels (up to 7mgChl*a*/m^3) in the stratified transect C. This local bloom (Transect C) originated not only from earlier stratification than in nearby regions (as hypothesised initially) but additionally from the presence of a large pool (diameter ~15km) of river-influenced waters (34.9-35.5psu) that strengthened the compartmentation of the water column. An important factor common to both physical processes (retainment of fluvial inputs and differential stratification), and ultimately related to the occurrence of the early spring bloom in the area, was the lower interchange of the local water masses with the Bay of Biscay oceanic waters.

These preliminary works overall demonstrated the great potential of infra-red remote sensing to develop novel hypotheses linking phytoplankton blooms to the physical environment but were limited by a sampling strategy planned for different objectives than those pursued by the author . The possibility of planning in full how and when to sample largely determined the greater success of the subsequent main coccolithophore experiment that is presented in this Thesis.

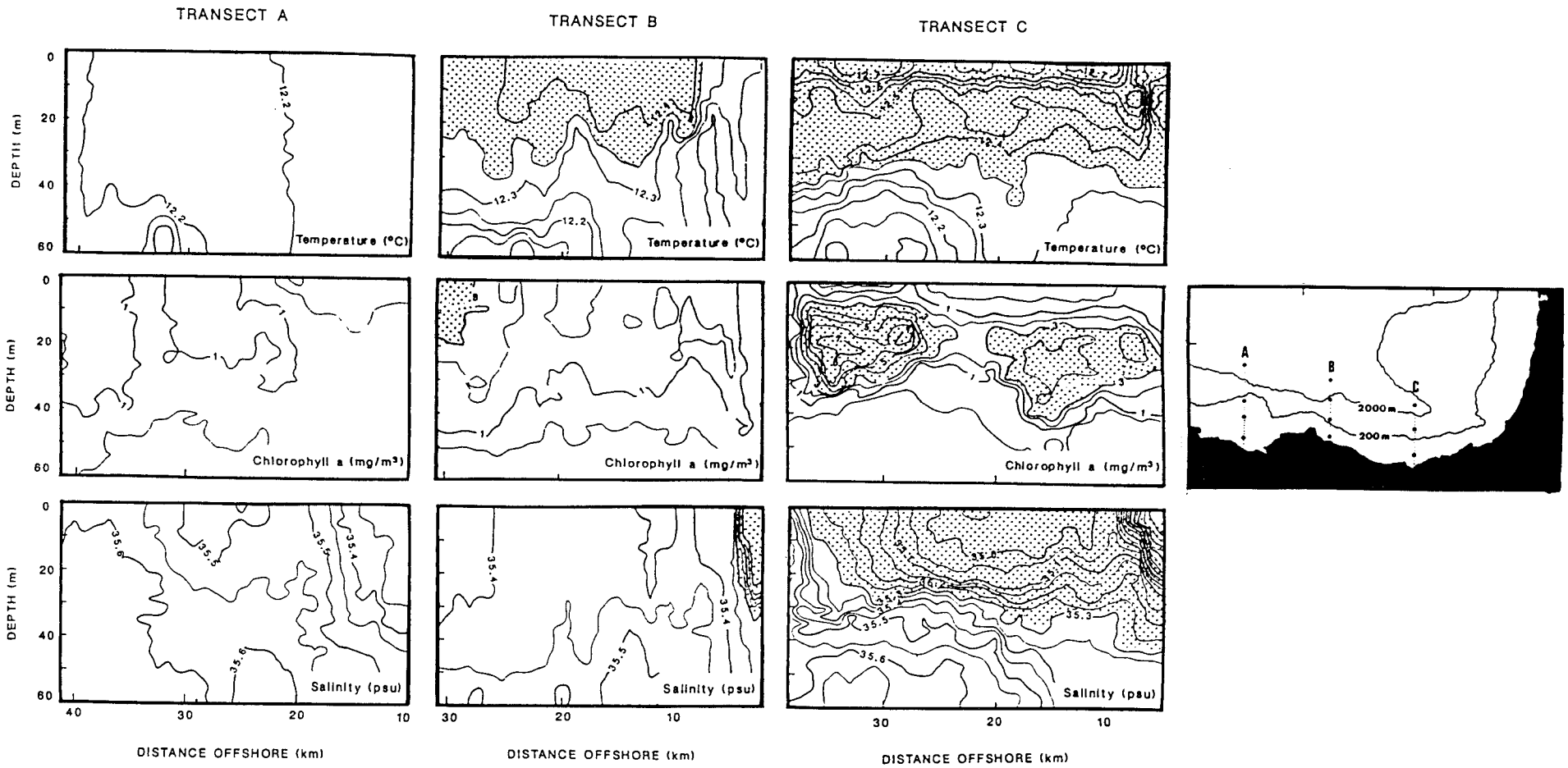

Figure 1.3 U.O.R sections of temperature (°C), chlorophyll *a* concentration (mg/m³) and salinity (psu) in the SE Bay of Biscay on 10th-12th May 1991.

CHAPTER II. LITERATURE REVIEW

The major contribution of remote sensing to biological oceanography lies in its ability to extend over time and space local measurements from *in situ* platforms such as ships and buoys. Both observing capabilities collect data which may be mutually exclusive but complementary, all of which are required to assess the problems of phytoplankton abundance and distribution. On their own, the satellite sensors are constrained to near surface observations, but they are the only method available today for investigating at a global scale key parameters such as phytoplankton biomass and primary production. The scope of this review is twofold, first to describe how ocean colour measurements are translated into phytoplankton concentration and, in combination with other satellite-derived parameters, into phytoplankton production; secondly, to analyse the main biological and optical findings relevant to interpret data of remote sensed blooms of the coccolithophore *Emiliania huxleyi*, the main topic of the Thesis.

A. COLOUR REMOTE SENSING AND PHYTOPLANKTON

Basic principles

Satellite colour sensors measure radiance at the top of the atmosphere that consists of a water-leaving signal and an atmospheric component which can be up to 95% of the total radiance detected. The removal of this atmospheric component is essential to estimate the water colour signal and this correction has attracted the attention of a considerable number of studies (*e.g.* Gordon, 1978, 1981; Sturm, 1981 for CZCS, and Tassan, 1987 for TM; see Robinson, 1985 for a wide review). The radiance due to the atmosphere consists of light scattered by molecular (Rayleigh) and aerosol (Mie) particles. Rayleigh scattering can be predicted and removed and present

methods of atmospheric correction (Gordon *et al.*, 1988a) incorporate multiple scattering. Calculation of the aerosol component presents a greater difficulty due to its variable temporal and spatial distribution. Measurements at red or infra-red wavelengths where the water leaving radiance is assumed to be zero allow relatively good corrections.

In discussing ocean colour, ocean waters are commonly divided into case 1 and case 2 waters (Morel and Prieur, 1977). Case 1 waters are those whose optical properties are largely determined by the presence of phytoplankton pigments and their derivative products; they represent normal oceanic conditions where particulate and dissolved substances are predominantly of biogenic origin. The absorption and backcattering by phytoplankton, containing chlorophyll *a*, makes the reflectance spectrum of pure sea water decrease at wavelengths below 540nm and increase at higher wavelengths (Figure 2.1A; Robinson, 1983). Increments in chlorophyll *a* concentration will strengthen this effect, causing the appearance of two distinct reflectance minima at 440nm and 660nm associated with the peaks of maximum chlorophyll *a* absorption. Modification of this "standard" reflectance spectrum can derive from the presence of pigment degradation products in aged phytoplankton populations and from accessory pigments of specific phytoplankton taxa (the red blooms of some dinoflagellates are an extreme example; *e.g.* Carder and Steward, (1985)). Dissolved organic compounds (DOC) from phytoplankton exudates and zooplankton excretion absorb additionally at blue wavelengths giving a reflectance difficult to separate from that of chlorophyll *a*.

Environments where the absorption and backscattering values are not linked solely to phytoplankton optics are classified as Case 2 waters (Morel and Prieur, 1977); the main subcategories include waters dominated by suspended inorganic sediments and those with a high content of dissolved organic matter from decayed

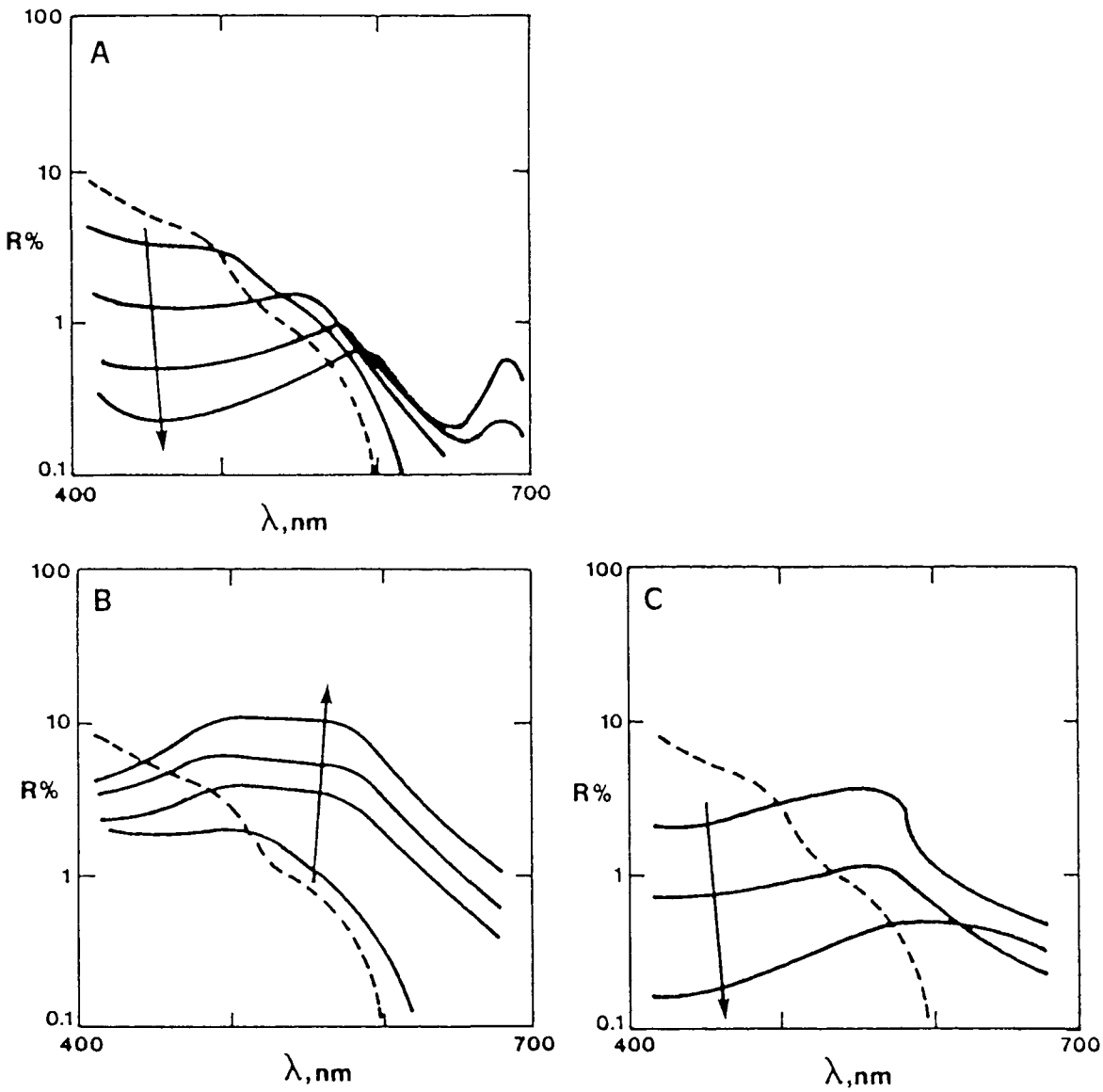

Figure 2.1 Typical reflectance spectra from A) case 1, phytoplankton dominated, water, B) case 2 water dominated by sediments in suspension and C) case 2 water dominated by yellow substance (gelbstoff). The arrows show respectively the effect of increasing concentration of chlorophyll, suspended sediments and gelbstoff. The dashed line is the clear-water reflectance spectrum. (from Robinson, 1983)

terrestrial vegetation (Gelbstoff or yellow substance). The backscattering by sediments in suspension is characterised by a weak spectral dependency and increases the reflectance of pure sea water at almost all wavelengths (see Figure 2.1B; Robinson, 1983). This standard spectral shape can however be modified by colour and size distribution of sediments from diverse origins (fluvial discharges, resuspension from the bottom, coastal erosion and waste dumping). Gelbstoff typically colours the water yellow or brown due to strong absorption at the blue wavelengths (Figure 2.1C, Robinson, 1983); in this case the similarities with the chlorophyll-dominated reflectance spectrum have wider implications for the calculation of satellite derived pigments.

Colour sensors

The earliest satellite information of water colour came from the sensors with high spatial resolution: Multi-Spectral Scanner (MSS), Thematic Mapper (TM) and High-Resolution Visible sensor (HRV) (Table 2.1; Robinson, 1989). TM is provided with a blue band (450-520nm) and an improved radiometric sensitivity that allows the retrieval of some quantitative information in coastal and estuarine regions (Tassan, 1987). Its characteristic broad bandwidth (optimised for studies of land resources) however, only permits detection of very strong coloured structures. A further problem results from a low repeat cycle (16-18 days in MSS and TM and 26 days in HRV) that limits tracking the short time evolution of any feature.

The Coastal Zone Colour Scanner (CZCS; Hovis *et al.*, 1980) (Table 2.1; Robinson, 1989) was the first sensor designed for phytoplankton studies. Although planned as a 1-year mission (1978-1979), CZCS operated until June 1986 producing over 15,000 scenes (Esaias *et al.*, 1986; Feldman *et al.*, 1989). Its radiometric

Sensor		MSS	TM	HRV	CZCS	AVHRR	ATM	FLI	SeaWiFS	MERIS
Waveband	1		450-520	500-590	433-453	580-680	420-450	up to	402-422	400-
	2		520-600	600-680	510-530	725-1100	450-520	64 bands	433-453	1050 in
	3		630-690	790-900	540-560	+	520-600	of 5 nm	490-510	at least
	4	500-600	760-900		660-680		605-625	width	555-575	15 bands
	5	600-700	+		700-800		630-690	in a	655-675	with
	6	700-800			+		695-750	sparse	745-785	1.25 nm
	7	800-1100					760-900	spatial	843-887	resolution
	8						910-1050	mode	+	
	9						1550-1750			
Scanline field of view		7.5°	7.5°		39°	55.4°	36°		58°	41°
Satellite/ vehicle		Landsat 1-4	Landsat 4,5	SPOT	Nimbus-7	TIROS /NOAA	Aircraft	Aircraft	Satellite ?	Columbus
Orbit period, min		103	99	101	105	102	variable		100	100
Height, km		908	705	822	950	815-860	according		700	824
Pixel size, m		76	30	20 (10*)	825	1100	to the		1130	260-520
Swath width, km		185	185	60	1640	2580	operation		2800	1500
Typical revisit, d		18	16	26	2	1	of the		1	2
Period of operation		1972-83	1982-	1986-	1978-86	1978-	aircraft		1992?	1997?

+ The thermal infra-red bands are not included. * Band 1 (panchromatic) only.
MSS: Multi-Spectral Scanner. TM: Thematic Mapper. HRV: High-Resolution Visible sensor. CZCS: Coastal Zone Color Scanner. AVHRR: Advanced Very High Resolution Radiometer. ATM: Airborne Thematic Mapper. FLI: Fluorescence Line Imager. SeaWiFS: Sea-viewing Wide Field-of-view Sensor. MERIS: Medium Resolution Imaging Spectrometer

Table 2.1 Specifications of some ocean colour sensors. (from Robinson, 1989). The present wavelength ranges of the bands 3, 4, 5 and 6 of SeaWiFS are respectively 480-500, 500-520, 545-565 and 660-680 (Hooker *et al.*, 1992).

sensitivity was optimised for oceanic areas, the visible detectors were built in narrow wavebands (20nm) to expose small changes of ocean colour and the 443nm band was specifically designed to measure the absorption maximum by chlorophyll *a*. Other CZCS improvements included the possibility of tilting (±20°) the angle of view of the sensor to avoid sunglint, a high repeat cycle (2 days at the Equator and 1 day at temperate latitudes) and a broad swath coverage (1,638km wide) with a good spatial resolution (0.825km x 0.825km at nadir). After the end of the CZCS mission the visible band of the meteorological sensor Advanced Very High Resolution Radiometer (AVHRR) (Table 2.1; Robinson, 1989) has allowed continuation of some phytoplankton studies (*e.g.* coccolithophore blooms; Groom and Holligan, 1987) at a very similar temporal and spatial scale.

Airborne sensors (see ATM and FLI in Table 2.1; Robinson, 1989) flying at lower altitudes and on flexible surveys can achieve a much higher spatial resolution (down to 1m) and sampling frequency than satellites. Though the spatial extent of the observed area is limited by their narrow swath width, this can be overcome by composing a set of flight runs. The early sensor Airborne Thematic Mapper (ATM; Daedalus) has relatively wide bands and, similarly to the equivalent satellite sensor (Landsat Thematic Mapper), only detects marine structures with very strong colour signatures (*e.g.* Garcia and Robinson, 1991). Subsequent imagers such as FLI (Fluorescence Line Imager; Gower and Borstad, 1981; Gower *et al.*, 1987)) and CASI (Compact Airborne Spectral Imager; Borstad *et al.*, 1989) provides greater spectral resolution (few nanometres), spectral flexibility (the bands can be configured) and improved sensitivity (signal to noise ratios of up to 200 to 1). These instruments were specifically built to image the absorption and the sun-stimulated fluorescence of chlorophyll *a*.

Two new colour sensors are planned to be launched by NASA and ESA within the next five years: the Sea-viewing Wide Field of view Sensor (SeaWiFS, 1995) and the Medium Resolution Imaging Spectrometer (MERIS, 1998) (Table 2.1; Robinson, 1989). SeaWiFS (General Science Corporation, 1991) is effectively a development of the CZCS with two improved aspects: two additional bands in the mid blue (510nm) and far blue (412nm) should permit the separation of the signals due to chlorophyll *a* and dissolved organic carbon (DOC) and two additional near infra-red bands (765nm and 865nm) should improve the atmospheric correction in coastal regions. The much finer spectral resolution makes MERIS a completely different type of sensor comparable to the airborne FLI and CASI sensors

Phytoplankton biomass and attenuation coefficient

Phytoplankton biomass in Case 1 waters is generally estimated from CZCS information using the standard NASA algorithms (Gordon *et al.*, 1983; Gordon and Morel, 1983). These expressions are based on statistical log-transformed regressions between chlorophyll concentration and a ratio of blue (443nm) to green (550nm) upwelling radiances (Lu^{λ}) with the form:

$$Ck = A(Lu443/Lu550)^{B}$$

The constants A and B are determined empirically from *in situ* measurements of surface chlorophyll and upwelling radiance; the blue and green wavelengths are chosen respectively at the spectral regions of maximum and minimum chlorophyll *a* absorption. With high chlorophyll *a* concentrations (>1.5 mg/m^3), and therefore high absorption values, Lu443 in CZCS band 1 approximates zero and is replaced in the algorithm by Lu520 in the green CZCS band 2 (520nm). The following 3-band algorithm has been recently proposed to avoid problems derived from switching the 2-band algorithms:

$$Ck = 5.56 * [Lu443 + Lu520/Lu550]^{-2.252}$$ (Müller-Karger *et al.*, 1990).

These satellite-derived values represent the concentration of chlorophyll *a* plus phaeophytin *a* (one of its degradation products) since both pigments have a similar blue absorption spectrum. The estimates have an acuracy of ±30% (Gordon *et al.*, 1985) and, being derived from water-leaving radiances, are an optically weighted concentration of pigments over the depth from which the light is reflected (Gordon and Clark, 1980). It has been calculated (Gordon and McCluney, 1985) that 90% of the detected signal originates in the first optical depth, defined as the depth at which natural sunlight has decayed to 1/e of its surface values. The chlorophyll content of Case 2 waters cannot be in general estimated from CZCS information (Viollier and Sturm, 1984; Bricaud and Morel, 1987); a notable exception are large areas of sediment-dominated Case 2 waters where chlorophyll and sediments covary (Mitchelson, 1984; Mitchelson *et al.*, 1986).

The diffuse attenuation coefficient (K) is an additional property that can be inferred from satellite ocean colour. It is significant to phytoplankton studies as it measures the penetration of the natural light in the water column. Austin and Petzold (1981) (Figure 2.2) related K to the ratio of CZCS water leaving radiances (Lu^{λ}) for two wavelengths using an algorithm similar to that for the chlorophyll with the form:

$$K^{\lambda}\text{-}Kw^{\lambda} = A^{\lambda}(Lu443/Lu550)^{B\lambda}$$

K^{λ} represents the total vertical extinction coefficient, Kw^{λ}, is the K value for pure sea water and A^{λ} and B^{λ} are parameters derived empirically from spectral data over a wide range of ocean locations. Two K algorithms (K490 and K520) have been formed using the ratio of the CZCS radiances at 443nm and 550nm. The technique is not however restricted to the specific wavelengths utilised by the remote sensor.

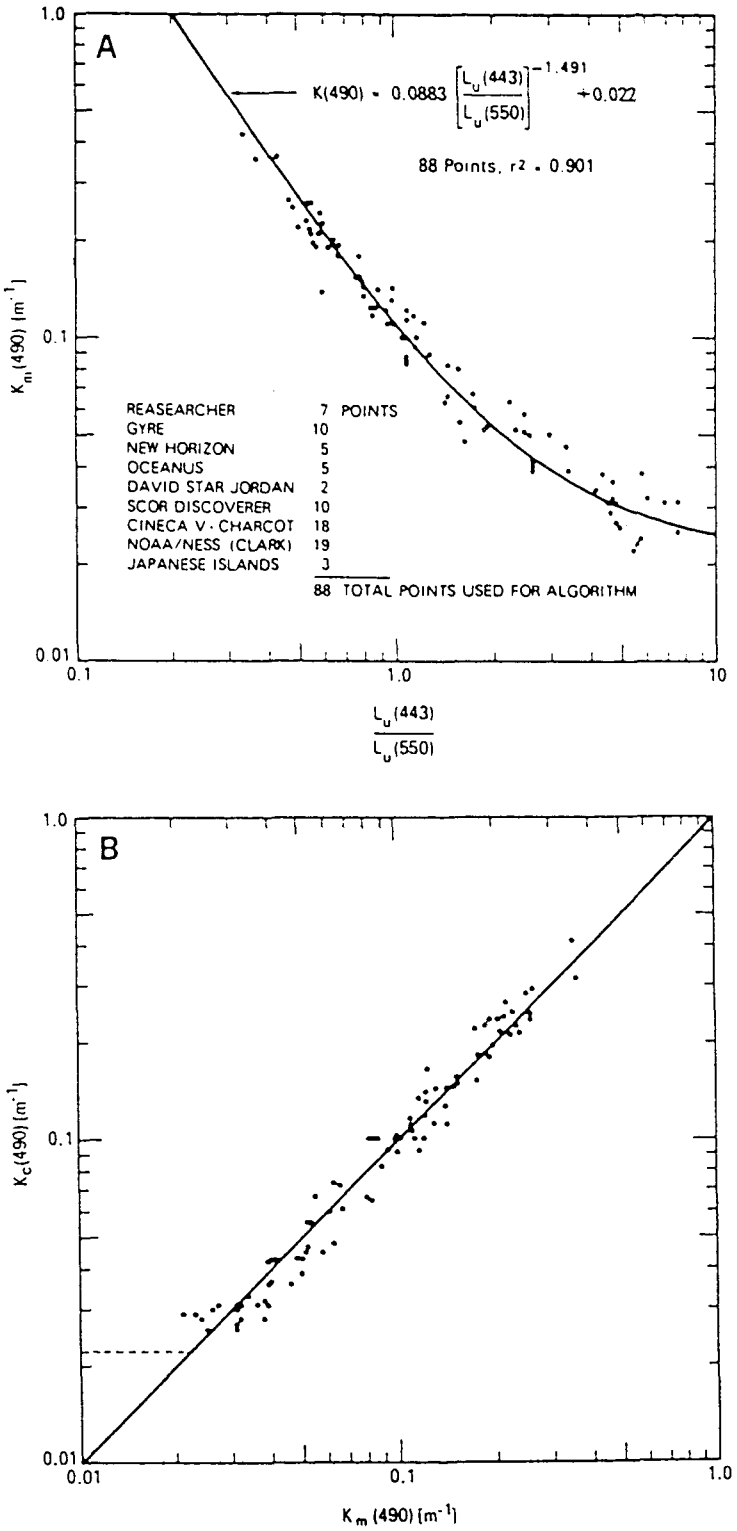

Figure 2.2 A) Relationship between vertical extinction coefficient at 490nm (K(490)) and the ratio of CZCS upwelling radiances at 443nm (band 1) and 550nm (band 3). B) Regression of calculated values of K(490) against the measured values. (from Austin and Petzold, 1981)

Primary production (empirical algorithms)

Water column primary production (P_T) was first estimated from satellite pigment concentration (Ck) using empirical correlations between field chlorophyll and primary production data from the Southern Californian Bight (Smith *et al.*, 1982; Brown *et al.*, 1985). These early expressions explained typically 30-35% of the variance in integral primary production when tested against a large set of *in situ* data of the region (Balch *et al.*, 1989). The regional algorithm with the best performance (40%; Balch *et al.*, 1989) had the form:

$$\ln P_T = 3.06 + 0.5 \ln Ck - 0.24 PTA + 0.25 DL$$ (Eppley *et al.*, 1985),

and included in addition to chlorophyll concentration (Ck), day-length in hours (DL) (an approximation to seasonal changes in irradiance and temperature) and Scripp's Pier temperature anomaly (PTA) (reflecting variation of availability of nutrients).

Over a large oceanic extent (from the Peruvian upwelling to the Arctic region) a reasonable relationship was found (Eppley *et al.*, 1985) between primary production (P_T) and a wide range of surface chlorophyll concentrations (Ck) (0.05-100mg Chl*a*/m^3):

$$P_T = 1{,}000\ Ck^{0.5}.$$

The algorithm relationship exhibited however strong regional differences and when applied later to smaller ranges of chlorophyll (Campbell and O'Reilly, 1988) was lost among the scatter of the data. Very similar expressions to that described by Eppley *et al.* (1985) had been observed between surface chlorophyll concentration (C) and the average chlorophyll concentration in the euphotic zone (Cav) (above 1% light level):

$$Cav = 0.95\ C^{0.788}$$ (Smith and Baker, 1978)

$$Cav = 1.10\ C^{0.890}$$ (Brown *et al.*, 1985)

which suggested that part of the variability of the algorithm given by Eppley *et al.*

(1985) was reflecting the large regional variability in the ratio of near-surface biomass to depth averaged biomass. Oligotrophic waters present in general a characteristic subsurface chlorophyll maximum that makes Cav exceed Ck, the reversed situation ocurs in eutrophic waters where the maximum chlorophyll concentrations are normally found near the surface.

Primary production (P-I algorithms)

The empirical algorithms relied on a constant relationship between production and chlorophyll. Several authors (*e.g.* Harrison and Platt, 1986; Garcia-Soto *et al.*, 1990) have however shown that diverse factors such as light or nutrients can change this relation. Among the alternative algorithms the most generally applied are the P-I algorithms. These expressions specify primary production as a function of the chlorophyll biomass, the light field and two of the three photosynthetic parameters of the Photosynthesis-Irradiance (P-I) curve: the initial slope or photosynthetic efficiency (α^B; mgC/mgChl*a*.E.h), the potential maximum photosynthetic growth or assimilation number (P_m^B; mgC/mgChl*a*.m^2) and the irradiance at which photosynthesis saturates or photoadaptative term ($I_K = P_m^B/\alpha^B$; E/m^2.h) (see Jassby and Platt (1976) for a review of the different mathematical functions of the P-I curve). The following equation from Talling (1957) is normally stated in calculations of integrated primary production from remote sensing data:

$$P_T/C=[Ln(2*I_*)]*(P_m^B/K)$$

$$I_* = I_o/I_K \text{ (notation by Platt, 1986)}$$

C (mgChl*a* /m^3) represents a chlorophyll concentration distributed homogeneously in the photic zone and is approximated by the CZCS estimate in the top optical depth (Ck). I_o is the surface irradiance (W/m^2), which can be calculated from remote sensing of cloud cover (Bishop and Marra, 1984; Bishop and Rossow, 1991). K (m^{-1})

is the PAR vertical extinction coefficient, potentially derived from satellite information as K490 or K520 in CZCS (Austin and Petzold, 1981). I_o and K define together the underwater light field for phytoplankton growth. The variations in nutrient concentration and temperature are assumed to be included as variations of P_m^B or I_K.

A major set of P-I algorithms is based on the empirical observation that I_* tends to have a constant value of ~5 and proposes the following simplified equation:

$$P_T/Ck = 2.3P_m^B/K \text{ (Eppley } et\ al.\text{, 1987)}$$

Identical expressions can be found in Bannister (1974), Smith and Baker (1978) and Harris *et al.* (1980). Banse and Yong (1990) have recently included a small variation by changing P_m^B to the biomass normalised photosynthetic rate between the 20% and the 50% light levels.

The alternative set of algorithms redefines the $Ln(2*I_*)$ term of Talling (1957) first to a linear function of I_* (Platt, 1986; Lewis *et al.*, 1986) and later to a more accurate polynomial function of I_* (Platt *et al.*, 1990); the expressions normally substitute I_K for the equivalent term P_m^B/α^B. Consecutive developments of the Platt (1986) algorithm have incorporated models for the non-uniform vertical distribution of chlorophyll in the entire photic zone (expressed in terms of the satellite chlorophyll concentration (Ck) and three additional parameters; Platt *et al.*, 1988) and for the spectral absorption characteristics of pigments and water (Platt and Sathyendranath, 1988; Sathyendranath *et al.*, 1989). The algorithm by Platt and Sathyendranath (1988) has already been applied to estimate the monthly water-column primary production of the North Atlantic divided into 11 hydrographic provinces according to latitude and depth (Figure 2.3; Platt *et al.*, 1991).

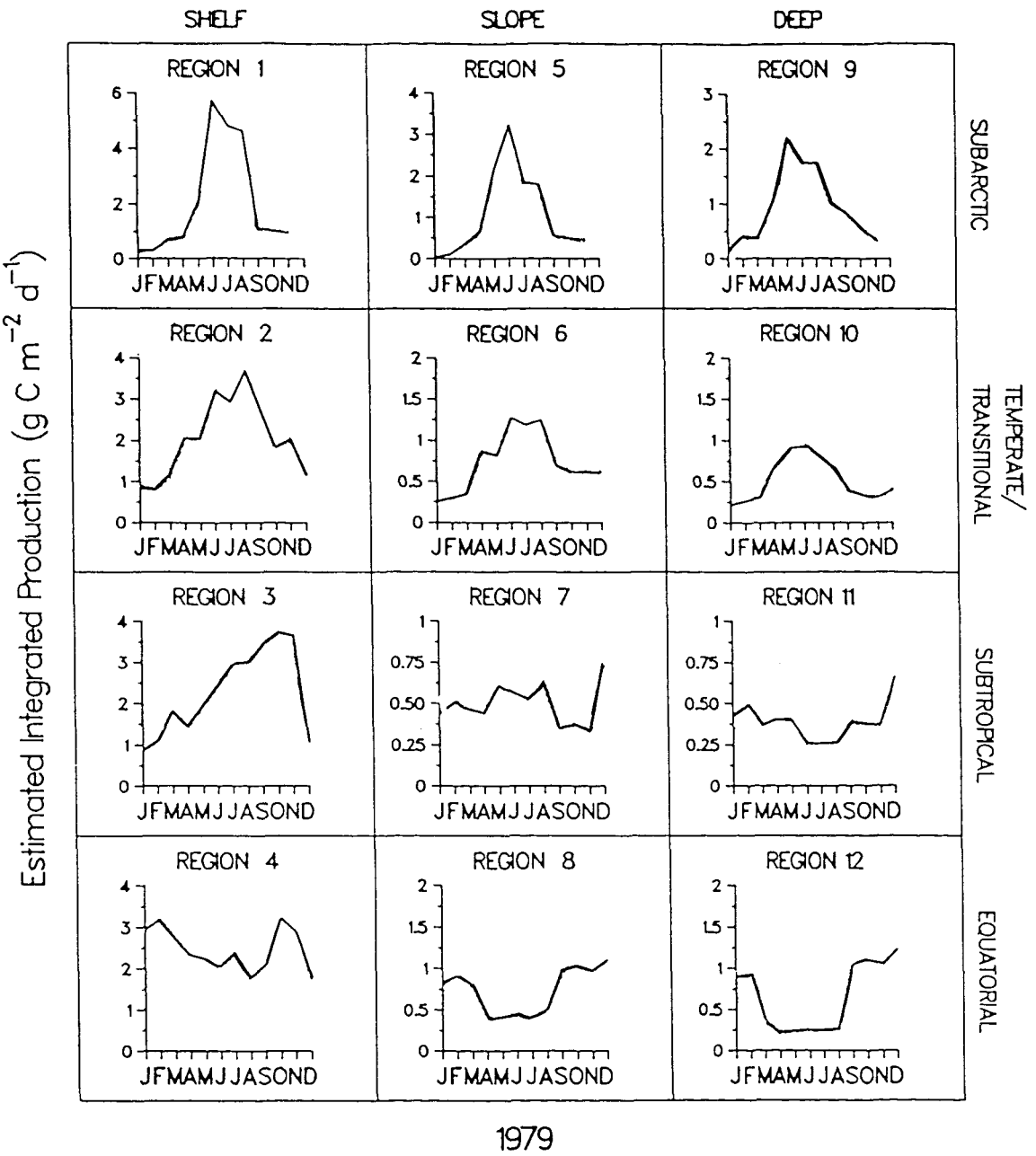

Figure 2.3 Satellite estimates of monthly primary production in the North Atlantic basin subdivided in 12 provinces according to latitude and depth. The method of Platt and Sathyendranath (1988) has been applied. (from Platt *et al.*, 1991)

When tested against a large data set of *in situ* data (Balch *et al.*, 1992a; Platt and Sathyendranath, 1993; Balch, 1993) the algorithms based on the simple $2.3P_m{}^BB/K$ expression (Smith and Baker, 1978; Eppley *et al.*, 1987; Banse and Yong, 1990) account for 60-65% of the variance of the integrated primary production. The explained variance is by contrast reduced to 30-35% (Balch *et al.*, 1992a; Platt and Sathyendranath, 1993; Balch, 1993) in the simple (Lewis *et al.*, 1986) or the complex (Platt and Sathyendranath, 1988) algorithms derived from Platt (1986) that incorporate absolute irradiance (I_o) and the photoadaptative term (I_K). These results have raised some criticism about the incorrect pooling of data when comparing models (Platt and Sathyendranath, 1993; Sathyendranath and Platt 1993) or by contrast lead to the conclusion that model complexity has not kept pace with model performance (Balch, 1993). Both models have also been considered complementary (Parslow and Harris, 1990) to the extent that their difference in realisation could reflect regional differences in the amount of phytoplankton adaptation to short term light variability. The first type of algorithms ($2.3P_m{}^BB/K$) assumes that physiological or community adaptation leads to an I_* value of about 5. This unchanged I_o/I_K ratio could be expected if such adaptation occurs in a shorter time than the day-to-day light fluctuations. By contrast, if the adaptation takes place over a longer time scale the $2.3P_m{}^BB/K$ model could fail to explain important variations of P_T that could be otherwise predicted by the algorithms derived from Platt (1986).

Coccolithophores

Light backscattering by *Emiliania huxleyi* represents a special case of biological effects on remote sensing, with satellite (CZCS) reflectance values exceeding 30% in blooms of this species compared to 3-5% during its absence. Investigation of these reflectance signals was initiated by the need to correct errors in the CZCS estimation of near-surface chlorophyll (Holligan *et al.*, 1983; Viollier and Sturm, 1984); it was

estimated from a theoretical radiance model (Gordon *et al.*, 1988b), that an increment of backscatter independent of chlorophyll of $0.0125m^{-1}$ would overestimate chlorophyll concentrations smaller than $0.3mg/m^3$ and underestimate larger concentrations. The special optics of the coccolithophores have originated two new research lines: the potential use of the reflective coccoliths as passive tracers of water movement (Holligan, 1987) and the quantification of surface coccolith concentrations from ship-underway and spacecraft optical data (Holligan and Balch, 1991; Holligan *et al.*, 1993a).

The low sinking rate of the detached coccoliths (~0.1m/day; Honjo, 1976) and the entrainment of high densities of these particles on eddies and plumes (Holligan, 1987) has long been recognised as the base of a possible method for tracking sea surface velocity using remote sensed coccolithophore blooms. This technique would have the advantage of using a very conservative motion tracer, thus improving the current methods based on CZCS data (Garcia and Robinson, 1989, limited by active phytoplankton growth) and on infra-red AVHRR data (Emery *et al.*, 1986; limited by temperature degradation) (see Wahl and Simpson (1990) for a detailed review). Retrieving sea surface velocity from a sequence of images of oceanic eddy-like blooms requires today the use of complex and time consuming image processing techniques allowing for rotation and deformation (*e.g.* Jain, 1989). The advection of blooms in these regions has consequently been interpreted loosely and within a previously known broad circulation pattern (Figure 2.4; Holligan *et al.*, 1993a). At the shelf regions by contrast, the coccolithophore blooms are not normally entrained on eddy fields and offer the best possibility of retrieving sea surface velocity (translational velocity in this case). The only limitation to be overcome for that future study is the distinction between real circulation and development of new blooms using a satellite time series at sufficiently short time intervals (Holligan *et al.*, 1989).

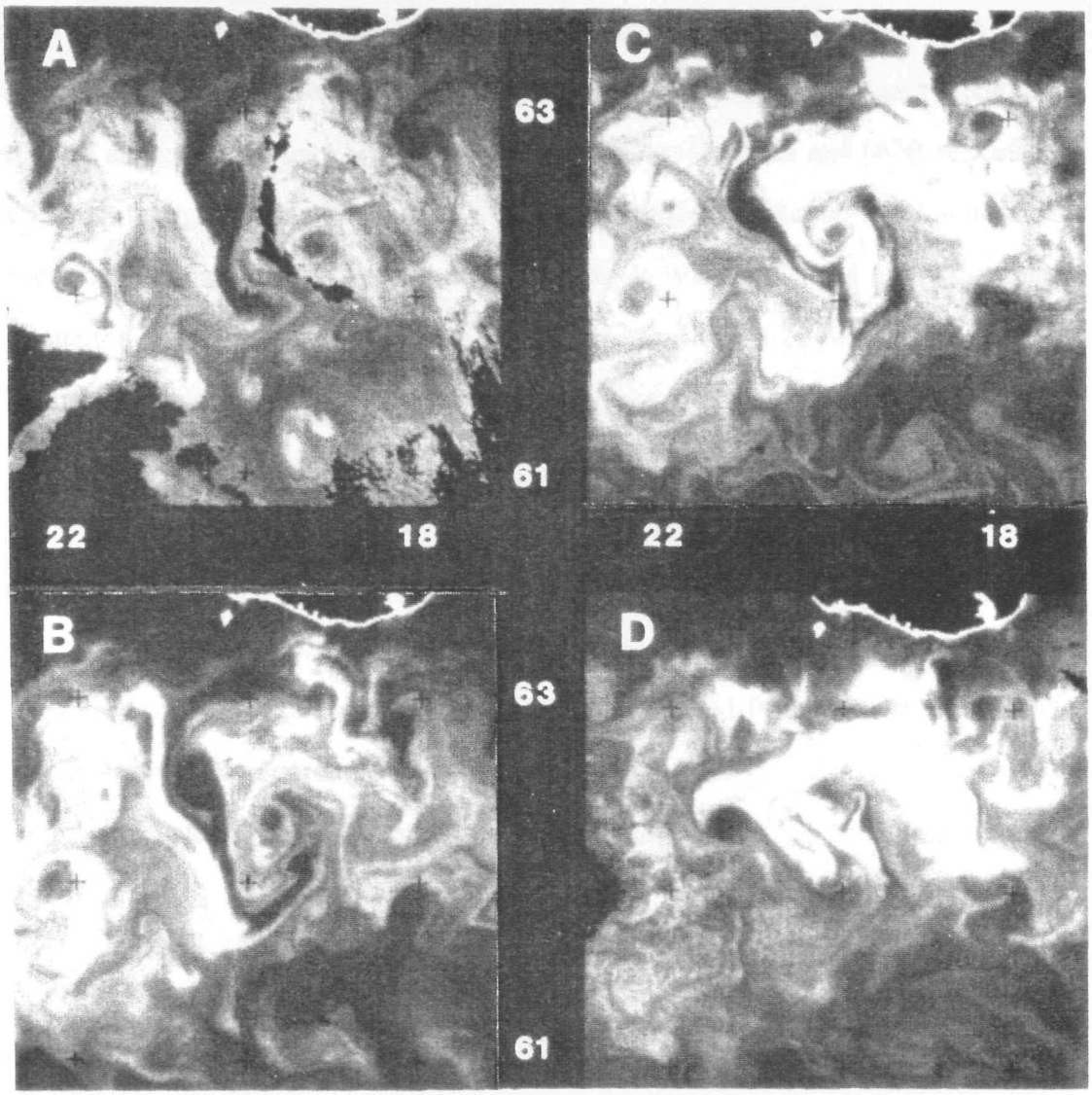

Figure 2.4 Satellite visible images (AVHRR) of the central area of the 1991 *E.huxleyi* bloom in the North Atlantic for A) June 15, B) June 17, C) June 19 and D) June 21. Advection towards the north east within the North Atlantic Drift is apparent south of 61°N, whereas north of this latitude the overall movement is towards the West, though some individual eddies appear to remain almost stationary. (from Holligan *et al.*, 1993a)

Surface coccolith abundance and underway optical values (light scattering (b) at 660nm) were first found to be correlated during a coccolithophore investigation in the North Atlantic in 1987 (Holligan and Balch, 1991); the scattering estimates needed however the input of *in situ* concentration of chlorophyll *a* to correct the direct measurements of red beam attenuation coefficient (660nm). The same study also reported an agreement between along-track AVHRR reflectance and UOR reflectance at 550nm, though it was of a qualitative nature. Recently, a better correlation has been reported (Holligan *et al.*, 1993a) between AVHRR reflectance and underway beam attenuation coefficient at 532nm (c532). The sensitivity threshold of the visible channel of the AVHRR appeared to be equivalent to a c532 value of about $0.8m^{-1}$, which was thought to approximate to a coccolith density of ~20,000 coccoliths/ml. In future, this type of investigations should probably include more direct relationships between surface coccolith abundance, AVHRR reflectance and underway optical measurements. The relationships between these parameters and the vertical attenuation of light should also be investigated. The need for vertical measurements in coccolithophore blooms is clear when considering the potential influence of the bloom attenuated light structure for the survival of the phytoplankton species underneath.

The reflectance response of CZCS bands 1 (443nm) and 3 (550nm) have been recently modelled as a function of the concentration of detached coccoliths and the ratio of coccoliths-to-*E.huxleyi* cells (Balch *et al.*, 1991). These authors used the expressions of Gordon *et al.* (1975 and 1988) relating below water reflectance (R), vertical attenuation coefficient (K) and values of backscattering (b_b) and absorption (a) (using the approximation $K = a + b_b$):

(i) $R = 0.110Q\,[b_b/(a + b_b)]$ (Gordon *et al.*, 1988b)

(ii) $R = 0.3244\,X + 0.1425\,X^2 + 0.1308\,X^3$,

$X = b_b/(a+b_b)$ (Gordon *et al.*, 1975)

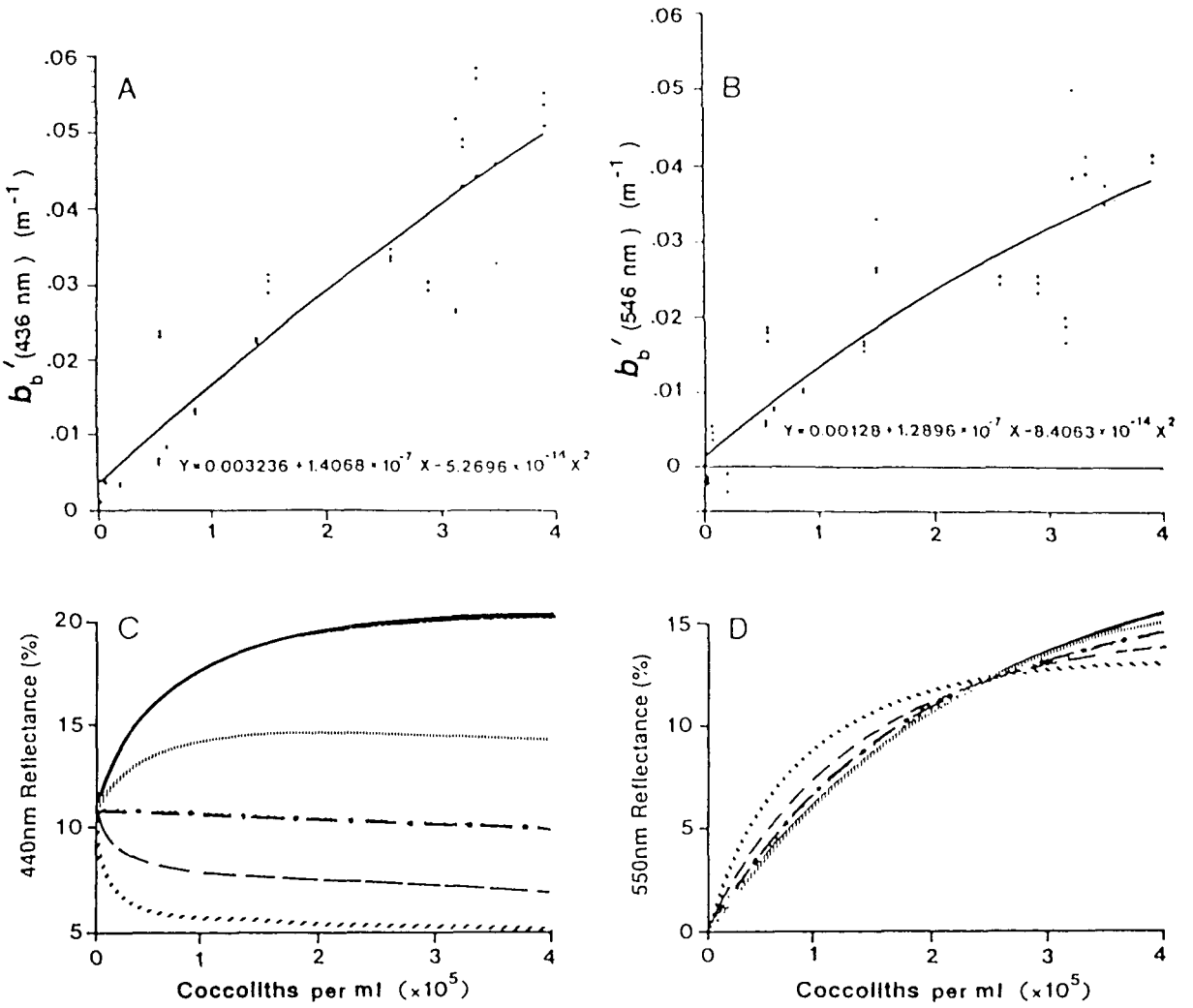

Figure 2.5 Coccolith backscattering at A) 436nm *vs.* coccolith concentration. The equation represents a best-fit polynomial to the data. (85% of the residual variance about the mean is explained). B) As panel A but with 546nm light (89% of the residuals about the mean is explained). For the coccolith concentrations shown here, however, the polynomial fit is not significantly better than a linear fit. C) Results of the reflectance model for blue light (436nm). Different lines represent different ratios of coccoliths to cells: hatched line 20 coccoliths/cell; dashed line, 50 coccoliths/cell; dash-dot line, 100 coccoliths/cell; striped line, 200 coccoliths/cell; solid line, 400 coccoliths/cell; line for 1,000 coccoliths /cell is covered by solid line. D) As panel C, but for green (546nm) light. (from Balch *et al.*, 1991)

The upwelling radiance was expected to be much more evenly distributed in coccolithophore waters than in oceanic clear waters (Austin, 1974; Q=5) and a Q factor of π was assumed in the expression of Gordon *et al.* (1988b). The equations were applied to the particular case of *Emiliania huxleyi* incorporating *in situ*-derived values of *E.huxleyi*-specific absorption and backscattering, and *in situ* polynomial functions relating coccolith abundance and backscattering (Figures 2.5A and B; Balch *et al.*, 1991). The resulting reflectance model at 443nm (~CZCS band 1) (Figure 2.5C; Balch *et al.*, 1991) shows that the coccolith increments will only increase surface water reflectance with coccolith-to-cell ratios >100; with smaller ratios by contrast, the surface reflectance signal will be dominated by absorption of cells. The model at 550nm (~CZCS band 3) (Figure 2.5D; Balch *et al.*, 1991) highlights the existence of a relationship between reflectance and concentration of detached coccoliths almost unrelated to the ratio of coccoliths to absorbing *E.huxleyi* cells. These later results still require testing using measurements of bloom reflectance independent of those used to derive the *E.huxleyi* specific backscattering and absorption coefficients. Another potential extension of the work would be the development of an algorithm to retrieve *E.huxleyi* cell concentration using the reduction of reflectance at 443nm by cell absorption.

B. *EMILIANIA HUXLEYI*

Geological and geographical distribution

Emiliania huxleyi (Lohm) Hay et Moller became the dominant coccolithophore in marine sediments 80,000 years ago (Thierstein *et al.*, 1977) and is still today the most abundant coccolithophore in the world's oceans (Honjo, 1976). The species is thought to have first appeared in the tropics about 280,000 years ago from the *Gephyrocapsa* stock (Thierstein *et al.*, 1977) and to have extended to temperate and subpolar latitudes with the northward retreat of the polar fronts during interglacial periods (McIntyre *et al.*, 1972; Rudiman *et al.*, 1980, Rudiman and McIntyre, 1981). The flooding of today's continental shelves also created shallow water areas where *E.huxleyi* is now the only coccolithophore regularly abundant and which have been compared (Holligan and Balch, 1991) with the major Jurassic and Cretaceous sites of coccolithophore deposition (Gallois *et al.*, 1976).

Studies with sediment traps and phytoplankton samples (Okada and McIntyre, 1977; 1979) have shown a widespread distribution of *E.huxleyi* from tropical to subpolar latitudes and from oceanic to inshore regions, thus exhibiting among the coccolithophores the greatest tolerance to environmental changes. From the global composites of the Coastal Zone Colour Scanner (Figure 2.6; Brown and Yoder, 1994a), waters with the satellite signature of *E.huxleyi* blooms appear to cover an annual averaged area of 1.4×10^6 km^2. The largest annual bloom surface has been observed in the North Atlantic (6.3×10^5 km^2), which in conjunction with the North Pacific and the Southern Ocean (>1 x10^5 Km^2) concentrates approximately 70% of the global bloom extent at temperate and subpolar regions (>40^{o}N,S). At lower latitudes the *E.huxleyi*-classified blooms seem to be restricted to the shelf regions

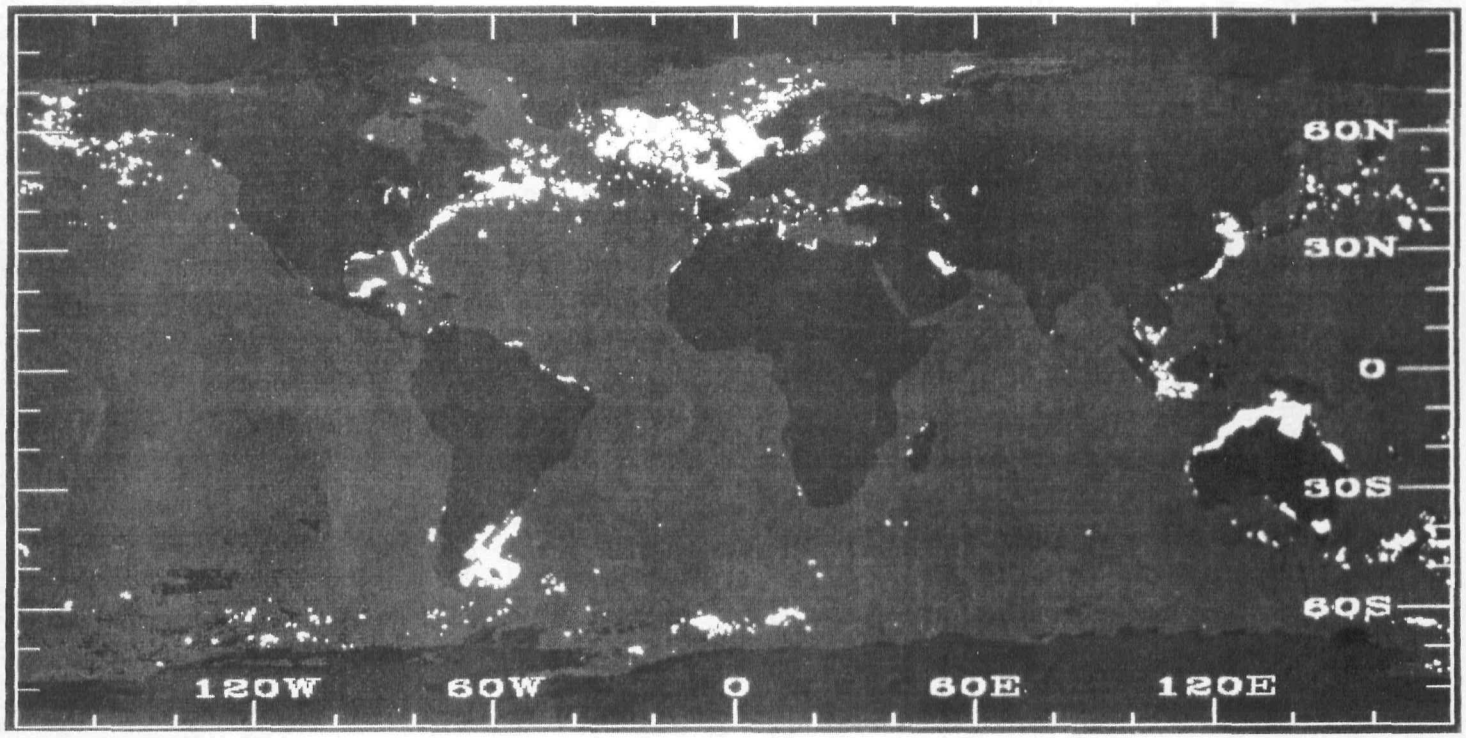

Figure 2.6 Global climatology of classified coccolithophore blooms (measuring >4,800km^2) in Coastal Zone Colour Scanner imagery from November 1978 to June 1986. The maximum extent of the blooms detected during this period is displayed in white shades. (from Brown and Yoder, 1994a)

of the Gulf of Mexico, Northern Australia, and the Yellow and East Chinese Seas; recent sea-truth observations in Australian waters (Blackburn and Cresswell, 1993) appear however to indicate that *Gephyrocapsa oceanica* is the detected coccolithophore. This possible broad zonation of two coccolithophore blooming species, is consistent with the blooms of low and temperate-subpolar latitudes occurring respectively during the early spring and summer months of each hemisphere (Brown and Yoder, 1994a).

Biogeochemical significance

The interest in *Emiliania huxleyi* has increased recently due to the important role of this species in the global carbon and sulphur cycles (Figures 2.7A and B; Westbroek *et al.*, 1993) (see also a review in Holligan and Balch, 1991) . Models of production (Taylor *et al.*, 1991) and *in situ* bloom measurements (Holligan *et al.*, 1993a; Robertson *et al.*, 1994) have shown that calcification by *Emiliania huxleyi* (probably the most abundant calcifying living organism on Earth, Westbroek *et al.*, 1985) can modify significantly the capacity of the surface ocean to store carbon dioxide from the atmosphere according to the equation:

$$Ca^{++} + 2HCO_3^- \longleftrightarrow CaCO_3 + CO_2 + H_2O$$

Coccolith synthesis leads to a relative increase of the partial pressure of CO_2 (pCO_2) but also produces an additional decrement of alkalinity that displaces the equilibrium of calcification in the direction of CO_2. During the 1991 North Atlantic bloom (Holligan *et al.*, 1993a; Robertson *et al.*, 1994) the air-sea gradient of CO_2 was observed to be reduced about 10-40μatm with respect to non-coccolithophore waters. This represented a ~17% reduction of the seasonal drawdown of the CO_2 caused by the spring diatom bloom.

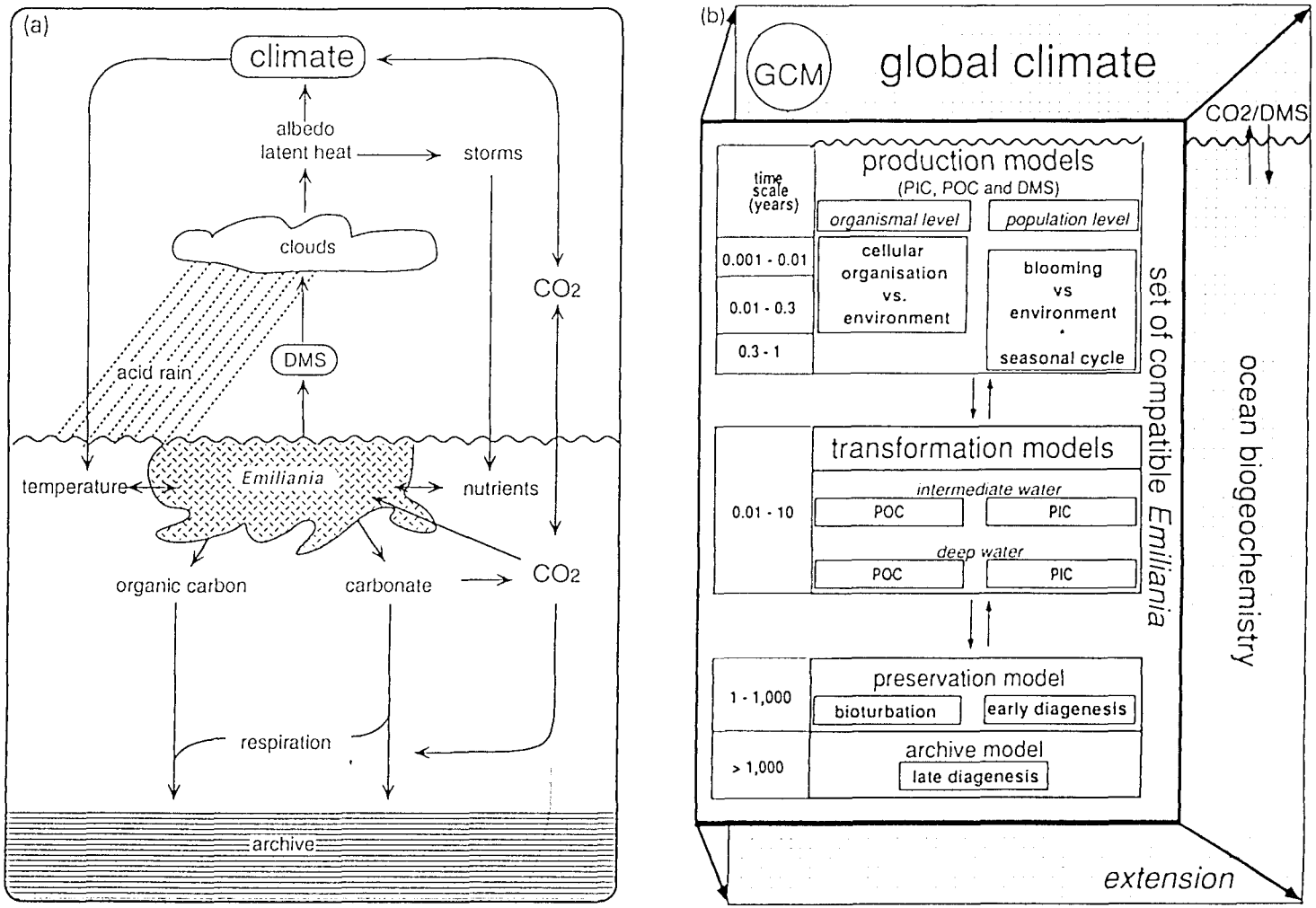

Figure 2.7 A) Overview of major oceanic and atmospheric processes associated with *Emiliania huxleyi*. B) Strategy for modelling *Emiliania huxleyi* in the GEM (Global Emiliania Modelling) and EHUX (Emiliania HUXleyi) research programmes. (from Westbroek *et al.*, 1993)

Coccolithophores including *E.huxleyi* and other Prymnesiophyceae also contain large amounts of the osmoregulator dimethylsulphoniopropionate (DMSP). This sulphur compound after cleavage to dimethylsulphide (DMS) (Vairavamurthy *et al.*, 1985; Turner *et al.*, 1988; Keller *et al.*, 1989) is thought to play a major role in the formation of cloud condensation nuclei and to contribute to the acidity of rainfall (Charlson *et al.*, 1987; Andreae, 1990). Field measurements (Malin *et al.*, 1992; Matrai and Keller, 1993) have shown that the concentrations of DMSP (and to a lesser extent DMS) during bloom episodes of *E.huxleyi* far exceed the average ocean levels. The pathway from phytoplankton to DMS-derived clouds has yet to be further investigated but reports of a covariation between the distributions of chlorophyll and low cloud albedo in the North Atlantic (Falkowski *et al.*, 1992) support a relationship between a higher degree of cloudiness and the presence of sulphate aerosols derived from coccolithophore blooms

Life cycle and morphotypes

The complex life cycle of *Emiliania huxleyi* in laboratory cultures (Figure 2.8; Klaveness, 1972) includes a non-motile phase (the C-cell) with external plates of calcium carbonate or coccoliths (∅:2-4μm), and a free-swimming flagellate form (the S-cell) lacking the specific intracellular system to produce coccoliths. An intermediate *E.huxleyi* stage (the N-cell), morphologically very similar to C-cells, but without calcification ability (Klaveness and Paasche, 1971) has also been described. N-cells and S-cells appear regularly from pure cultures of C-cells in a senescent stage and can be maintained in pure cultures for many years reproducing their own cell kind by binary fission. The transition to S-cells reorganises several of the *E.huxleyi* cytoplasmic components; the coccolith-forming apparatus disappears, a flagellar apparatus is formed and the cell acquires the ability to make uncalcified organic scales lacking in the other phases. The plated and non motile form (C-cell) is the

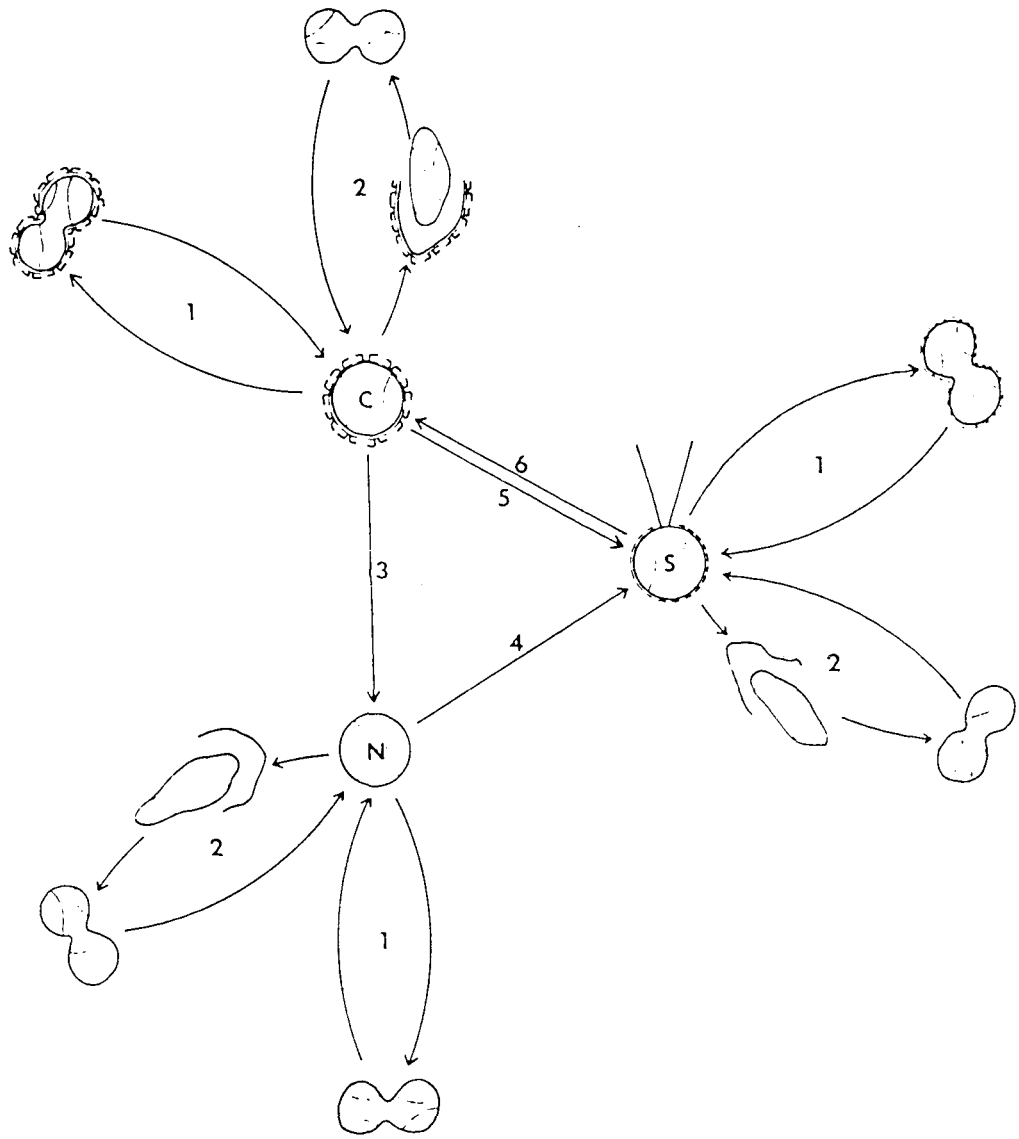

Figure 2.8 The life history of *E.huxleyi* as interpreted from observations of laboratory cultures. 1) Normal vegetative propagation. 2) Aberrant mode of vegetative propagation. 3) Loss of the ability to make calcified coccoliths, N-cells appear. 4) Flagellated cells appear in pure cultures of N-cells. 5) Flagellated cells appear in pure cultures of C-cells. 6) Coccolith-covered cells appear in pure cultures of S-cells. (from Klaveness, 1972)

stage mainly reported during the *E.huxleyi* blooms at sea though the N-cells may appear in the final bloom stages (Green *et al.*, 1990). Difficulties in identifying by standard microscopy the flagellate form (the S-cell) have so far prevented its observation in natural conditions.

The C-cells of *Emiliania huxleyi* have been known for some time to show variations in coccolith morphology. Further differences have been recently indicated in pigment composition, antibody cross-reactions, growth rates and rates of coccolith calcification (Brand, 1982; Borman *et al.*, 1987; Fisher and Honjo, 1991; Van Bleijswijk *et al.*, 1991). Using electron microscopy, Young and Westbroek (1991) have distinguished four main different morphotypes (A, B and C and var. corona) unable to convert into each other in laboratory cultures. Morphotype A has been found all along the Atlantic ocean from 45°N to 54°S, with the morphotype C being a component cell type in latitudes >50°S (Van Bleijswisk *et al.*, 1991; Westbroek *et al.*, 1993) . Similar results have also been reported in the NE Atlantic between 56°N and 63°N (Holligan *et al.*, 1993a) with type A dominating all samples and morphotype C forming up to 20% of the bloom population. Morphotype B appears to be more characteristic of inshore regions as shown by samples from the African coast (24°S-30°S) (Van Bleijswisk *et al.*, 1991; Westbroek *et al.*, 1993) and the North Sea (Holligan *et al.*, 1993b). The possible genetical diversity of *E.huxleyi* (presently recognised as a single species) may be an explanation to its distribution in waters of different hydrographic properties such as ocean and shelf regions.

Bloom onset and termination

The temporal development of an *E.huxleyi* bloom in natural conditions has not yet been described but the available *in situ* data (Balch *et al.*, 1992b; Fernández et al., 1993a) suggest that coccolithophore populations proceed in a similar way to batch

cultures (Linschooten *et al.*, 1991; Balch *et al.*, 1992; Nimer and Merret, 1992). These studies have usually reported during the early phases of *E.huxleyi* growth cell division rates as high as 1 div./day and corresponding calcification/ photosynthesis ratios <1. For the bloom development, the critical period is the short transient (5-10 days) between this exponential growth phase and the lag phase of declining growth; as more carbon is directed into coccolith production (with calcification/photosynthesis ratios ~1) the coccoliths are detached into the surrounding media at a much higher rate than previously giving the water a very strong white colour (*e.g.* Figure 2.9; Westbroek *et al.*, 1993). This late physiological stage, when the bloom has already become optically apparent with densities of detached coccoliths as high as 350,000 coccoliths/ml, is the one in which to frame the investigations of coccolithophore blooms at sea (Holligan *et al.*, 1983; Holligan *et al.*, 1993a; Balch *et al.*, 1991).

Coccolith formation is thought to have originally appeared (600 million years ago) as a way of avoiding calcium toxicity in an ocean of increasing calcium concentration (Degens and Ittekot, 1986); its present functionality by contrast remains uncertain. Early investigations have hypothesised that the coccolith layer may serve as a light-scattering device, thus protecting the cell from excessive illumination but no experimental evidence for this has been found (Paasche, 1964). More recently, it has been suggested that coccoliths serve as a protective device enabling the entrapment of a stable buffer layer between the cell membrane and the local environment (Manton, 1986). Other hypotheses have been proposed: maintenance of internal levels of CO_2 (Westbroek *et al.*, 1983), enhanced tolerance to low salinity (Sikes and Wilbur, 1982), flotation of the coccolithophore cells (Klaveness and Paasche, 1979) and elimination of excessive photosynthetic energy in conditions of nutrient limitation (Baunman *et al.*, 1978).

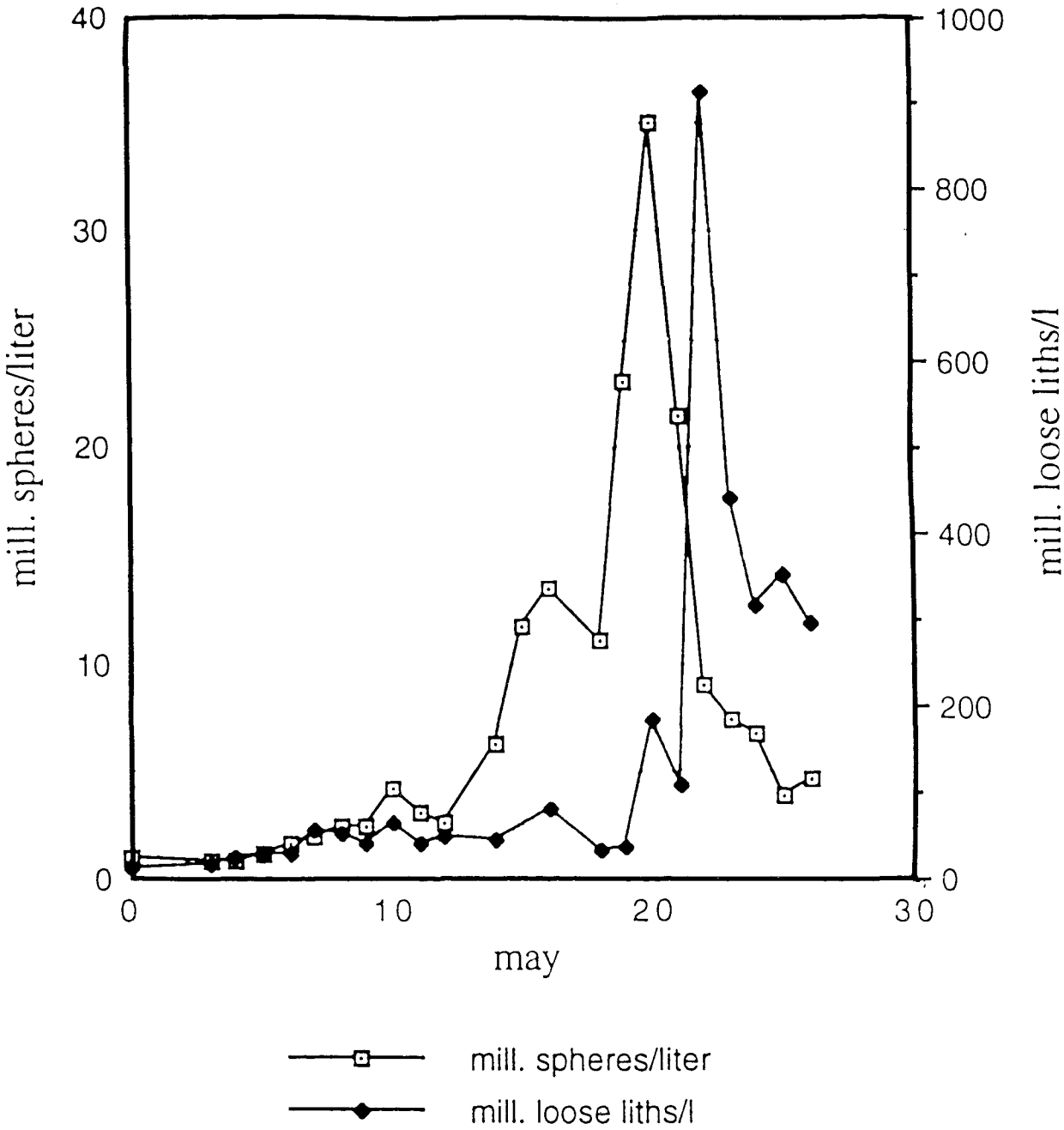

Figure 2.9 Concentration of cells of *Emiliania huxleyi* and detached coccoliths during a bloom in a mesocosm enclosure experiment in Kossfjorden, April 30- May 20, 1992. Note the massive shedding of coccoliths at the end of the bloom. (from Westbroek *et al.*, 1993)

The hydrographic conditions associated with the abundance of *E.huxleyi* at temperate shelf-regions have been thought to conform to conceptual models of phytoplankton succession of Margalef (1978) (Holligan, 1987; Holligan *et al.*, 1993a). Coccolithophores occupy, according to these authors, an ecological niche characterised by low turbulence and depleted concentrations of nitrate or silicate following the decline of the spring diatom bloom. An alternative hypothesis (Holligan *et al.*, 1993b; Westbroek *et al.*, 1993) points to a competitive advantage of *E.huxleyi* with respect to other species by the activation at low phosphate concentration of an alkaline phosphatase that enables the use of dissolved organic phosphorus (Kuenzler and Perras, 1965). The fact that both maximum DOP concentration and NO_3 depletion peaks seasonally after the spring bloom reflects the need for more hydrographic measurements in order to evaluate the role of both potential factors during shelf bloom episodes.

The factors terminating *E.huxleyi* blooms are also uncertain though some external influences have been described. Mesocosm enclosure experiments in Norwegian fjords have shown that *E.huxleyi* can be subject to viral infection and that this may be related to the deficient nutrient status of the cells (Bratbak *et al.*, 1993). Grazing of *Emiliania huxleyi* by large zooplankton (copepods) has also been known for some time (Honjo and Roman, 1978) and recent field experiments (Holligan *et al.*, 1993a) have additionally demonstrated that the species is selectively grazed by microzooplankton (non pigmented flagellates and ciliates); the daily rate of micrograzing (Holligan *et al.*, 1993a) can be as high as 44% for *E.huxleyi* as opposed to 19% for total phytoplankton population. The disappearance of some blooms in satellite images over periods of 1-2 weeks (*e.g.* Brown and Yoder, 1994a), too quick for coccolith sinking, indicates that physical wash out of actively growing cells is an additional factor to be examined.

CHAPTER III. EXPERIMENTAL WORK AND METHODS

A. PLANNING OF THE EXPERIMENT

Remote sensing of *E.huxleyi* blooms

Although blooms of *Emiliania huxleyi* have been studied in Norwegian fjords since early this century (Gran, 1912; Bikernes and Braarud, 1952; Berge, 1962), the investigations only extended to more open regions in the 1980's with the use of satellite sensors in visible wavelengths, mainly CZCS (Holligan *et al.*, 1983) and AVHRR (Groom and Holligan, 1987). Since then, satellite imagery has provided the first global distribution of coccolithophore blooms (Brown and Yoder, 1994a) and identified the North Atlantic as the region where the blooms are most frequent and extensive. Regional CZCS and AVHRR observations have also shown periodic bloom appearances in Iceland (Aiken and Bellan, 1990; Holligan, 1992; Holligan *et al.*, 1993a), Gulf of Maine (Ackleson *et al.*, 1988; Balch *et al.*, 1991), North Sea (Holligan *et al.*, 1989; Holligan *et al.*, 1993b), Norwegian Sea (Trees *et al.*, 1992), Celtic Sea (Holligan *et al.*, 1983; Holligan and Groom, 1986) and Western English Channel (Groom and Holligan, 1987; Grepma, 1988). Given the current lack of *in situ* information of both oceanic (Holligan *et al.*, 1983; Holligan *et al.*, 1993a) and shelf (Balch *et al.*, 1991) blooms, the most powerful application of the satellite data still derives from its processing in near-real time (Groom and Cooper, 1989) on a day-to-day basis in order to detect the phenomenon in an early stage and to plan a subsequent *in situ* survey. This was the approach taken during the present study.

Observational framework

The visible channel (580-680nm wavelength) of the AVHRR sensor onboard the NOAA-11 satellite revealed the presence of a patch of high reflectance water in the mouth of the English Channel near the south coast of Cornwall in June 1992

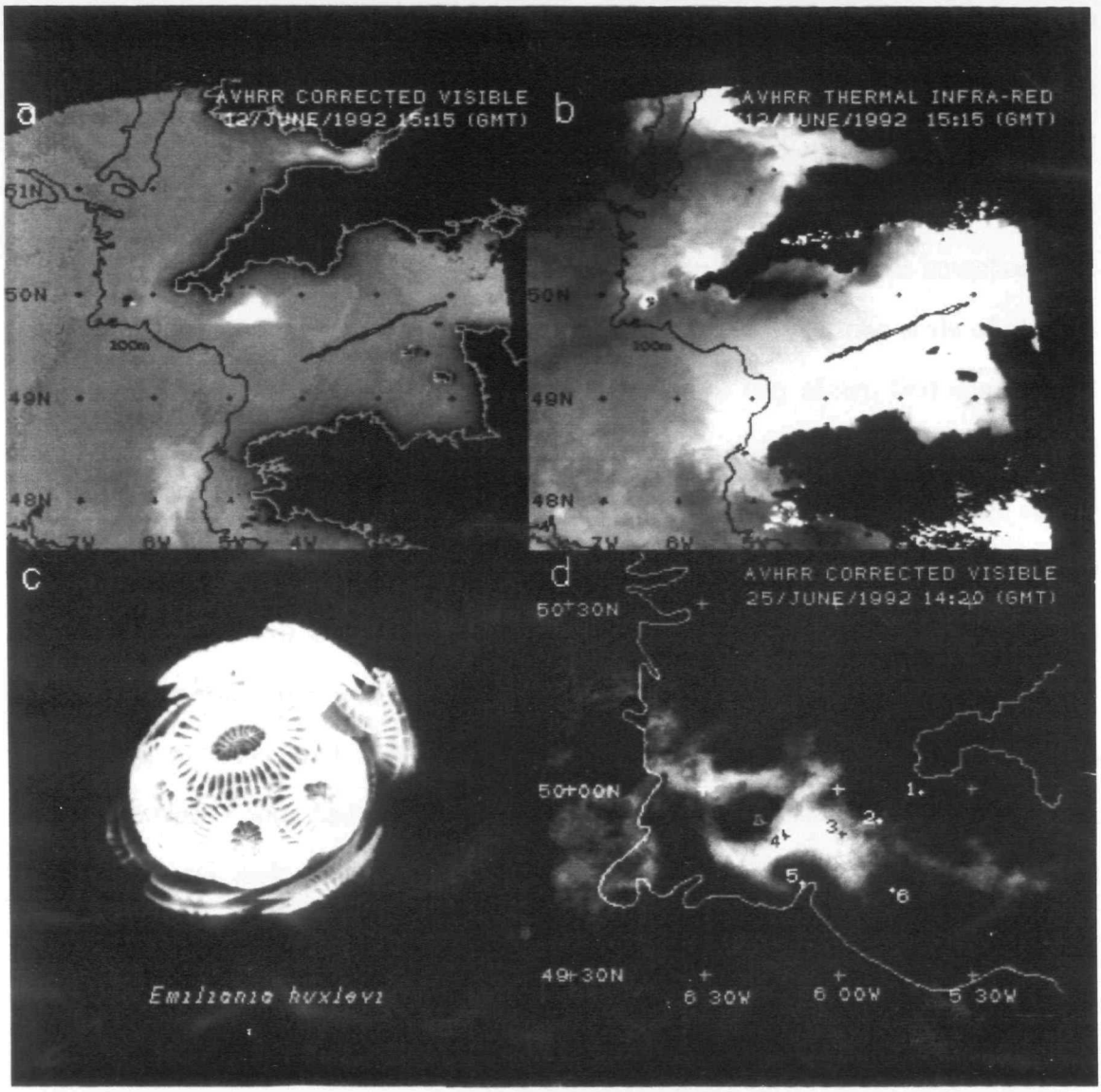

Figure 3.1- A) AVHRR visible satellite image of two coccolithophore blooms observed in the Western English Channel and off Brittany on 12th June 1992, B) corresponding AVHRR infra-red satellite image, C) scanning electron micrograph of the morphotype of *E.huxleyi* cell found in the Western English Channel bloom (morphotype A following the classification by Young and Westbroek (1991)) and D) AVHRR visible satellite image of the Western English Channel bloom on 25th June 1992 with location of sampling stations and 100m water depth contour.

(Figure 3.1A). The patch of *white* water (*i.e.* high AVHRR reflectance) was apparently associated with the southern side of a high surface temperature structure that stretched east-west across Eddystone Bay (Figure 3.1B). A later examination confirmed that this was a coastal bloom of the coccolithophore *Emiliania huxleyi* (Figure 3.1C). A further high reflectance signal, but of larger spatial extent, was also conspicuous off the west coast of Brittany and was situated in the warmer stratified water adjacent to the Ushant front. The Ushant bloom was first noted on 13th May and was now entering a dissipative phase, becoming dispersed and stretched in a north-south direction. It disappeared after 17 June, indicating a time scale of about a month for a coastal bloom of this size. The Eddystone Bay bloom first appeared on 4th June centred near 49°45'N, 4°40'W but advected rapidly west and between 23rd and 24th June started to impact the Isles of Scilly (Figure 3.1D). An airborne survey with the Airborne Thematic Mapper (ATM) sensor was conducted on 23rd June in the coastal boundary of the bloom in response to the satellite observations; the bloom surface fine-structure and spectral variability, not resolved by AVHRR satellite imagery, were analysed. A ship survey was also undertaken during 25th and 26th June between Lands End and the Isles of Scilly; vertical profiles of physical, optical, chemical and biological properties were made at six stations chosen to cover the complete range of bloom surface reflectance (Figure 3.1D).

B. SATELLITE REMOTE SENSING

The evolution of the coccolithophore bloom was examined from an early reflective stage up to the time of the airborne and ship survey by using visible (580-680nm) and thermal infrared (11.5-12.5μm) data from the Advanced Very High Resolution Radiometer (AVHRR) onboard the NOAA series of near-polar satellites.

AVHRR characteristics

The AVHRR scans the Earth with a ±55.4° viewing angle at a nominal altitude of 825km (NOAA-10)/860km (NOAA-11), providing a recording swath of about 2,800km width orthogonal to the direction of travel. The output from the detectors is sampled at a rate so there are 2,048 samples across the swath with a spatial resolution of 1.1 by 1.1km at nadir. The near sun synchronous orbits of the NOAA-series are designed for operating two satellites simultaneously (currently NOAA-10 and 11) enabling each satellite to view the same geographical area twice a day (night and day-time passes) and at approximately the same solar time each day.

BAND	WAVELENGTH RANGE (μm)	SPECTRAL REGION	RADIOMETRIC RESOLUTION
1	0.58-0.68	visible	~0.1%
2	0.72-1.10	near infra-red	~0.1%
3	3.55-3.93	mid infra-red	~0.12degC
4	10.3-11.3	thermal infra-red	~0.12degC
5	11.5-12.5	thermal infra-red	~0.12degC

Table 3.1 AVHRR (NOAA-11) spectral characteristics

The AVHRR onboard NOAA-11 records upwelling radiance in five spectral bands (Table 3.1). The thermal infra-red bands 4 (10.3-11.3μm) and 5 (11.5-12.5μm) are located at spectral ranges, the atmospheric windows, in which the absorption by atmospheric gases is at a minimum. Both bands detect temperature differences of 0.12degC and, when processed for absolute sea surface temperature (SST) (McClain *et al.*, 1985), give an approximate accuracy of ±1°C. The visible band 1 (580-680nm) is located between the wavelength ranges of the bands 3 (540-560nm) and 4 (660-

680nm) of the Coastal Zone Colour Scanner (CZCS; Nimbus-7 satellite). The AVHRR raw data are digitised in a higher number of levels (10-bit; 1,024 digital grey levels) than the CZCS raw data (8-bit; 256 digital grey levels) but the lower AVHRR detector gain (saturating at 100% in AVHRR band 1, 10.8% in CZCS band 3 and 6% in CZCS band 4) reduces the radiometric resolution by a factor 2.3 and 4 with respect to the CZCS bands 3 and 4 (Groom and Holligan, 1987; Grepma, 1988). The permanent operational nature of the AVHRR sensor as part of the dual NOAA system fills the temporal gap between the two colour sensors CZCS (1978-1986) and SeaWiFS (expected to fly in 1995) for the coccolithophore research.

Processing of AVHRR data

The AVHRR raw data were received at the NERC Satellite Receiving Station at Dundee University and transferred as a *quick look* (low resolution image; reduced by a factor of 4) to the NERC Image Analysis Unit at Plymouth University for examination. In the case of potentially useful images, full resolution subscenes (bands 1, 2, 4 and 5) and orbital information for navigation were extracted from the original raw data on the same day. Transfer of the *quick looks* and raw data was performed in near real-time (Groom and Cooper, 1989) over the JANET computer network. Processing of the visible and infra-red data was carried out on a DEC microVAX 3400 with a model 75 I²S image processor with I²S 600 software and AVHRR specific software (Holligan *et al.*, 1989).

The standard atmospheric correction for AVHRR visible data showing coccolithophore blooms (Groom and Holligan, 1987) follows basically the CZCS method of Gordon *et al.* (1983) that treats separately the three different components of the radiance detected by the sensor (L_T^{λ}): the molecular (Rayleigh,Lr^{λ}) and aerosol (Mie, La^{λ}) scattering radiances and the transmitted water radiance ($t^{\lambda}*Lw^{\lambda}$ and t_{oz}^{λ}):

$$L_T^{\lambda} = (L_r^{\lambda} + L_a^{\lambda} + t^{\lambda} * L_w^{\lambda}) * t_{oz}^{\lambda}$$ (Gordon *et al.*, 1983).

NOAA-11 from which most of the daily passes at Dundee were received, has uncertain calibration values in bands 1 and 2 (Kaufman and Holben, 1993) and the above approach cannot be applied. Instead, correction for aerosol (L_a^{λ}) and Rayleigh (L_r^{λ}) scattering was reduced to subtracting from the visible band 1 (exhibiting atmospheric and in-water structures) a fraction (r) of the near infra-red band 2, assumed to contain purely atmospheric variability (Holligan *et al.*, 1993a). Following these authors r was determined as the ratio:

$$r = (\overline{DNvis} - DNw) / \overline{DNnir},$$

where $\overline{DNvis}$ and $\overline{DNnir}$ are respectively the mean digital values of a large coccolithophore-free area surrounding the bloom at the visible and near infra-red bands (bands 1 and 2); DNw represents the theoretical water leaving radiance of pure seawater in AVHRR band 1 calculated using the model of Morel and Prieur (1977).

The aerosol and Rayleigh corrected visible data were converted to reflectances (%) using the preflight calibration coefficient of band 1 ($\gamma = 0.000906$ DN^{-1}; NOAA-11) for sun at zenith (Price, 1988, Kaufman and Holben, 1993). The transmitted water reflectances ($t^{\lambda} * L_w^{\lambda}$) were normalised by the cosine of the solar zenith angle (θ_o) of the different satellite passes, that is function of the latitude, date and time (see Kirk, 1983). Correction for diffuse (t^{λ}) and ozone (t_{oz}^{λ}) transmission was effected using the optical thicknesses of the Rayleigh (τr^{λ}) and ozone (τoz^{λ}) atmosphere and the zenith angles of the pixel-sensor vector (θ) and of the sun (θ_o) (Gordon *et al.*, 1983):

$$t^{\lambda} = \exp\{(-\tau r^{\lambda}/2) * (1/\cos\theta + 1/\cos\theta_o)\}$$

$$t_{oz}^{\lambda} = \exp\{-\tau oz^{\lambda} * (1/\cos\theta + 1/\cos\theta_o)\}$$

To allow comparison between satellite and *in situ* values, the above water reflectance ($R^{\lambda o+}$) were transformed into below water ($R^{\lambda o-}$) reflectances following Austin (1980):

$$R^{\lambda o+} = 0.544 * R^{\lambda o-},$$

The Q factor that converts upwelling radiances into upwelling irradiances was not replaced by the recommended Q=5 (*e.g.* Gordon and Morel, 1983) since the reflectance models of coccolithophore blooms (Balch *et al.*, 1991) hypothesise a Lambertian behaviour of the sea surface.

Thermal infra-red images were processed as brightness temperatures for band 5 (11.5-12.5μm) only since applying the split window technique (McClain *et al.*, 1985) to recover absolute SST would have resulted in a loss of fine spatial variability and a precise delineation of the thermal structures was of interest. Comparable consistency of the satellite time series was preserved by contrast-stretching to the same extent images from the same satellite pass time (14:20-15:20 GMT) and sensor (AVHRR onboard NOAA-11), all of the images being received during a short period of time (3 weeks). A day-time satellite pass was selected to allow the best matching between the thermal and the visible images as the coccolithophore bloom was moving rapidly. As day-time thermal images may show a diurnal thermocline in the top 1 metre (due to solar heating on calm days; Robinson, 1985) the occurrence of the main thermal structures presented for the day satellite passes was tested against thermal images of night satellite passes. Both visible and infra-red images were remapped into a Mercator projection (Snyder, 1982) using a model of the satellite viewing geometries and a ground reference point of precise geographical position (Holligan *et al.*, 1989). Navigation accuracy in the images was tested against a similarly projected coast line contour stored in the image analysis system. Hourly wind data covering the period of observations (from the Isles of Scilly Met Office meteorological station (27m altitude)) and high definition plots of numerical models of the stratification parameter (Pingree and Griffiths, 1978) and wind-induced currents (Pingree and Griffiths, 1980) were used to appraise the movement and structure observed on the satellite images.

C. AIRBORNE REMOTE SENSING

In response to the bloom satellite observations an Airborne Thematic Mapper (ATM) scanner (Daedalus AADS 1268) was flown onboard the NERC Piper aircraft recording 5 flight passes of the eastern bloom region during 23rd June.

BAND	WAVELENGTH RANGE (nm)	SPECTRAL REGION	NOISE EQUIVALENT RADIANCE (12.5scans/s) (1)
1	420-450	visible	<0.10
2™	450-520	visible	<0.02
3™	520-600	visible	<0.015
4	605-625	visible	<0.03
5™	630-690	visible	<0.02
6	695-750	near infra-red	<0.02
7™	760-900	near infra-red	<0.01
8	910-1,050	near infra-red	<0.03
9™	1550-1,750	mid infra-red	<0.015
10™	2,080-2,350	mid infra-red	<0.005
11™'	8,500-13,000	thermal infra-red	<0.2degC (2)

™ Landsat-TM bands

™' The corresponding Landsat band is in the wavelength range 10.4-12.5μm

(1) Noise equivalent radiance (mW/cm^2 μm sr)

(2) Noise equivalent temperature (degC)

Table 3.2 ATM (Daedalus AADS 1268) spectral characteristics

ATM characteristics

The ATM records upwelling radiances at 11 spectral bands, including the 7 bands of the Landsat Thematic Mapper sensor (Table 3.2). The data are digitised in 8-bits allowing a 0-255 range of digital grey levels. The sensor gain can be pre-selected (at each wavelength) among five gain-settings (0.5, 1, 2, 4 and 8) to achieve maximum sensitivity depending on the magnitude of the upwelling radiance. The sensor scans a $\pm 36.86^{o}$ field of view at three different scan rates (12.5, 25 and 50 scans/sec). During the survey, ATM was flown at a height of 3,000m resulting in a swath width of 4.5km and an across-track pixel resolution of 6.3m. The nominal along-track pixel resolution, calculated from the nominal air speed (150 knots) and the preselected scan rate (12.5 scans/sec), was 6.2m. The study focused on the channels at visible wavelengths (bands 2 to 5) as the noise present in the infra-red data (band 11: 8.5-13μ m) was much higher than the sea surface temperature structure. The visible band 1 (420-450nm) has been previously found to be erroneous (Singh, 1988) and was also discarded from the analysis.

ATM processing

The ATM raw data were processed on the same image analysis system as the AVHRR raw data using ATM specific software (Groom *et al.*, 1989). Radiometric calibration of the scanner digital numbers (DN^{λ}) into radiances (L^{λ}) was performed at each wavelength according to Wilson (1986):

$$L^{\lambda} = GAIN^{\lambda} * (DN^{\lambda} - BASE^{\lambda})$$

$$GAIN^{\lambda} = \{[4000 * Lc^{\lambda}] / [256*(V^{\lambda} - V_o^{\lambda})]\} / GAIN\text{-}SETTING$$

$$BASE^{\lambda} = [(256 * V_o^{\lambda}) / 4{,}000] * GAIN\text{-}SETTING$$

Lc^{λ} ($W/cm^2.nm.sr \times 10^{-7}$) represents the calibration source radiance, V_o^{λ} (mV/DN) the

voltage output for zero input radiance, V^{λ} (mV/DN) the sensor voltage output when input radiance is Lc^{λ}, and 4000 the maximum value of Lc^{λ} corresponding to the digital number 256. Calibration values (supplied by NERC Scientific Services) were measured one month before the flight (25th May 1992). ATM radiances (L^{λ}) were converted into irradiance reflectances (R^{λ}) using the solar spectral irradiance at the top of the atmosphere (E_o^{λ}) and the solar zenith angle (θ_o) at the time of the survey (*e.g.* Viollier *et al.*, 1980):

$$R\lambda = (\pi L^{\lambda}) / (E_o^{\lambda} * \cos\theta_o)$$

Atmospheric correction was carried out using a modified form of the CZCS procedure of Gordon *et al.* (1983) developed for ATM data (Groom *et al.*, 1989). The height of the aircraft is allowed for by including in the CZCS equations a factor (f) that specifies the fraction of the Rayleigh scattering atmosphere below the airborne sensor. f (0.31) was calculated from the aircraft height (h=3,000m) and the scale height for the Rayleigh scattering atmosphere (~7.99km) assuming an exponential decrease of the atmospheric constituents with altitude:

$$f = \exp[-h/7.99]$$

Rayleigh scattering reflectance (Rr^{λ}) and the diffuse (t^{λ}) and ozone (t_{oz}^{λ}) transmission terms were calculated assuming single scattering and using the following equations:

$$Rr^{\lambda} = [\tau r^{\lambda} / 4\cos\theta\cos\theta_o] * \{f*[Pr^{\lambda}(\theta-) + Pr^{\lambda}(\theta+)\rho(\theta)] + [Pr^{\lambda}(\theta+)\rho(\theta_o)]\}$$

$$\cos\theta_{\pm} = \pm \cos\theta_o\cos\theta + \sin\theta_o\sin\theta\cos(\phi-\phi_o)$$

$$t^{\lambda} = \exp\{(-\tau r^{\lambda}/2) * (f/\cos\theta + 1/\cos\theta_o)\}$$

$$t_{oz}^{\lambda} = \exp\{-\tau oz^{\lambda} * (1/\cos\theta_o)\}$$

τr^{λ} and $Pr^{\lambda}(\theta_{\pm})$ are respectively the scattering optical thickness and phase function; τoz^{λ} is the optical thickness of the ozone atmosphere; the sensor-pixel-sun geometry is specified by the zenith and azimuth angles of the sun (θ_o,ϕ_o) and of the pixel-sensor vector (θ,ϕ); $\rho(\theta)$ and $\rho(\theta_o)$ represent the Fresnel reflectance for incident angle θ or

θ_o. The term including θ- accounts for the contribution due to the photons that have been backscattered from the atmosphere into the sensor without interacting with the sea surface. The terms including θ+ represents the contribution of photons reflected specularly from the sea surface and that have been scattered in the atmosphere before ($\rho(\theta)$) or after ($\rho(\theta_o)$) the sea surface reflection.

The scattering reflectance due to aerosol (Ra^{λ}) (normally 1-2km in depth) can not be calculated as with Rayleigh scattering since its optical characteristics vary with the aerosol composition and its temporal and spatial distribution. The applied correction (following Gordon *et al.*, 1983) relied on the assumption that despite a possible heterogeneous distribution of the aerosol concentration, the ratio of aerosol reflectances at two wavelengths is constant ($\varepsilon_{\lambda 1 \lambda 2}$) over the image. If we consider that the aerosol size distribution follows a power law with wavelength, $\varepsilon_{\lambda 1 \lambda 2}$ can then be estimated as follows:

$$Ra^{\lambda 1}/Ra^{\lambda 2} = \varepsilon_{\lambda 1 \lambda 2} = (\lambda_1/\lambda_2)^{-n} \quad (n = \text{Angstrom exponent}).$$

Using this equation, the Angstrom exponent (0.4) was retrieved from the slope of log-log regression of Rayleigh corrected near infra-red reflectances (bands 6 to 10) in coccolithophore clear-waters (where the sea is assumed to be black; Lw=0) *vs.* the corresponding band wavelengths. The aerosol scattering in visible bands 2 to 5 was calculated using in the above expression the Angstrom exponent and the Rayleigh corrected near infra-red data at band 6 (containing only aerosol scattering radiance).

The atmospherically corrected images still exhibited systematic differences in reflectance approximately orthogonal to the direction of flight. To remove this across track shading (probably due to residual atmospheric and scanner effects), an empirical shade normalisation was applied for each wavelength assuming that shading was absent at nadir (Donaghue and Hook, 1986). Above water reflectances were

transformed to below water reflectances (Austin, 1980) to allow comparison with the *in situ* reflectance values taken during the ship sampling. Navigation of the data was performed by using the flight geolocations and track characteristics and tested against a ground control point (Wolf Rock). Table 3.3 documents the beginning and end points of the 5 flight passes, the times at which data recording started and ended and the bearing of the plane for each pass.

LIGHT LINE	START TIME (GMT)	END TIME (GMT)	INITIAL POSITION	FINAL POSITION	BEARING
1	11:16	11:21	49° 54' 51" N 5° 49'30" E	49° 47' 18" N 5° 38' 54" E	145.0°
2	11:24	11:29	49° 47' 57" N 5° 35'30" E	49° 57' 54" N 5° 51' 30" E	313.5°
3	11:32	11:36	49° 59' 48"N 5° 48' 42" E	49° 48' 00" N 5° 34' 24" E	148.0°
4	11:40	11:46	49° 47' 12" N 5° 27' 48" E	49° 58' 27" N 5° 45' 24" E	321.0°
5	11:49	11:54	49° 59' 42" N 5° 42' 24" E	49° 47' 42" N 5° 28' 00" E	141.5°

Table 3.3 Airborne survey flight lines

The georeferenced ATM runs were smoothed into 20 x 20 pixel bins to remove high frequency noise and possible structure discrepancies of the run overlapping areas (due to a different recording time). This resulted in a horizontal resolution of ~120m, still much higher than the satellite imagery. The runs were finally merged together and contoured using the UNIRAS package.

D. *IN SITU* MEASUREMENTS

The bloom was surveyed by R/V Squilla on 25th and 26th June at six vertical stations (Table 3.4).

STATION (DEPTH)	DAY (JUNE 92)	TIME (GMT)	POSITION	TIDAL CORRECTED POSITION *
1 (67m)	25	9:26	49° 59' 23" N 5° 44' 15" E	49° 59' 35" N 5° 40' 50" E
2 (75m)	25	11:23	49° 55' 37" N 5° 52' 57" E	49° 55' 07" N 5° 50' 35" E
3 (81m)	25	13:06	49° 53' 18" N 6° 00' 06" E	49° 52' 54" N 5° 58' 50" E
4 (81m)	25	14:48	49° 52' 26" N 6° 11' 48" E	49° 52' 26" N 6° 11' 48" E
5 (96m)	26	9:53	49° 44' 15" N 6° 11' 00" E	49° 45' 03" N 6° 07' 35" E
6 (93m)	26	12:30	49° 43' 58" N 5° 50' 15" E	49° 43' 43" N 5° 47' 35" E

* Stations positions corrected for a tidal displacement based on the difference between the time of the AVHRR satellite pass on 25th June (14:20 GMT) or 26th June (14:09 GMT) and the actual time of station sampling; the position correction was calculated from tidal currents of the nearest tidal stream diamond.

Table 3.4 *In situ* sampling stations

Continuous underway measurements (3m depth) of temperature, chlorophyll *a* fluorescence and red beam attenuation coefficient (660nm) were made along the ship track. Vertical profiles (0-60m depth) of temperature, chlorophyll *a* fluorescence and upwelling and downwelling irradiance (415, 443, 490, 554, 632nm and PAR) were

registered at the station positions. Water samples were also drawn with a Niskin bottle (10l) at discrete depths between the surface and 60m for subsequent analysis ashore of phytoplankton carbon standing stocks (chlorophyll *a*, particulate C and N, particulate Ca and species identification and counting) and inorganic nutrients (nitrate and phosphate). Two drogued Argos buoys were deployed on 25th June in the centre of the patch (near station 4) to monitor the movement of the bloom water in the possible absence of further cloud free satellite images.

Physical and optical measurements

Underway temperature was measured with an STD system carrying a platinum resistance thermometer (Hytech; 0.01degC) (Pingree and Mardell, 1976). Beam attenuation coefficient was recorded along the ship track with a 0.25m pathlength transmissometer operating at a peak wavelength of 660nm (Sea Tech; $0.0025m^{-1}$) (Bartz *et al.*, 1978). Underway measurements of chlorophyll *a* fluorescence were carried out with an Aquatracka fluorometer (Chelsea instruments) (Pingree and Harris, 1988). Calibration of the chlorophyll *a* fluorescence was effected by comparison with discrete chlorophyll *a* samples determined fluorometrically. At each station the transmissometer lenses were cleaned and the transmissometer lowered for *in situ* measurements. Beam attenuation coefficient (c) was calculated from transmission (T) with the expression

$$T = \exp(-c*r),$$

where r represents the pathlength of the sensor.

Vertical profiles (0-60m depth) of temperature, chlorophyll *a* fluorescence and upwelling and downwelling scalar irradiance were registered with the Undulating Oceanographic recorder in vertical mode (UOR; Aiken and Bellan, 1990). The

sensors for depth, temperature and fluorescence were respectively of potentiometric type (Vernitron model 3000; 0.5m), a thermistor (YSI 44030; 0.1degC) and an in-house constructed fluorometer (Aiken, 1981; 0.1 mg Chl*a*/m^3). Downwelling and upwelling irradiance were measured with irradiance sensors with cosine collectors (Holligan *et al.*, 1993a). Data was logged *in situ* with a microprocessor controlled solid-state data-logger (SSDL) with capacity for 64,000 measurements and transferred in the laboratory to an IBM PC for data processing and analysis. The profiles of chlorophyll *a* fluorescence were calibrated against *in situ* chlorophyll *a* measurements from samples taken at discrete depths. PAR diffuse attenuation coefficient was calculated as the derivative of the logarithm of PAR downwelling irradiance (Ed(PAR)) with depth (Jerlov, 1976; Kirk, 1983):

$$K(PAR) = d[LnEd(PAR)]/dz$$

Surface irradiance reflectances and vertical irradiance reflectance profiles were estimated at each depth from the ratio of upwelling to downwelling irradiances (Jerlov, 1976; Kirk, 1983):

$$R^{\lambda} = Eu^{\lambda}/Ed^{\lambda}$$

The Argos drifting buoys used during the study were of the Moonraker 112A type, equipped with sensors for sea surface temperature (0.05degC), battery voltage monitoring and drogue loss indication. The buoys were fitted with battery packs to give an expected life of 6 months at a transmit repetition rate of 90s. Before deployment and immediately on deployment each buoy was monitored using an Argos Gonio 400 portable receiver to verify correct functioning. The buoys were drogued at 20m depth, near the bottom of the bloom. Temperature and position data were transmitted to the Argos central computer via the standard Argos frequency of 401.650 ±0.004 MHz, and extracted at PML over the PSS/Transpac JANET communications link.

Phytoplankton carbon stocks

Living cells, empty coccospheres and detached coccoliths of *Emiliania huxleyi* were identified and counted in water samples preserved with buffered formalin solution (~1% formalin in the sample). The non-coccolithophore species were examined in samples preserved with acidic Lugol's iodine. Identification and counting were carried out with a Wild (M20) inverted microscope using the Uthermöl (1958) method. This technique is based on the settlement of the phytoplankton cells or particles on a sedimentation chamber (50ml) during a sufficiently long period of time (24h). The phytoplankton concentration of the sample (C; cell/ml) was determined from areal cell counts (Cn; cells) at the bottom of the chamber following the simple relation:

$$C = (Cn * A)/ V$$

V represents the volume of the subsample sedimented (50ml) and A a dimensionless factor relating the total number of microscopic grids (at the bottom surface of the sedimentation chamber) and the number of grids counted. Depending on the cell abundance every second or fourth transect of grids was examined; the counting of flagellates was carried out along a diameter of grids (A=150/1).

Chlorophyll *a* concentration was determined by fluorometric assay (Yentsch and Menzel, 1963 and Holm-Hansen *et al.*, 1965; see Parsons *et al.*, 1984). Onboard the ship, 100ml water samples were filtered on GF/F glass fibre filters and the filters stored immediately deep frozen (-20°C). A suspension of magnesium carbonate was added while filtering to prevent descomposition of chlorophyll *a* into phaeophytin pigments by the acidity of the filter. At the laboratory, pigment was extracted on a 90% acetone (v/v) solution over 24h at 4°C and subsequently centrifuged (3000rpm for 5 minutes). The fluorometric analysis was performed using a Turner Designs

fluorometer and the chlorophyll *a* concentration of the sample was calculated from the expression:

$$mgChl a/m^3 = F * f * (R_1-R_2) * (T/T-1);\ T = R_1/R_2$$

R_1 represents the first fluorometer reading, R_2 a second reading after acidification of the sample tube (2 drops of 5% (V/V) hydrochloric acid), f the ratio of the acetone extract volume to the sample volume and F the calibration factor with a standard of pure chlorophyll *a* (Sigma). The chlorophyll *a* concentration of the standard was determined in a spectrophotometer (Perkin Elmer Lambda 2 UV/VIS) following the equations of Parsons *et al.* (1984).

Total particulate carbon (TPC) and nitrogen (TPN) were measured by dry combustion in oxygen with a CHN analyser (Carlo-Erba 1500 series 2) using an acetanilide standard. Seawater samples of 500ml volume were filtered during the survey on pre-treated (450°C for 24h) Whatman GF/F filters. A controlled vacuum (about 100kPa) was used while filtering to avoid breaking of phytoplankton cells. The filters were manipulated by steel forceps to minimise contamination and, after filtering, kept deep frozen (-20°C) folded in aluminium foil. Particulate inorganic carbon (PIC) was estimated (following Fernández *et al.*, 1993a) from the measured calcium content of the material collected on GF/F filters (500ml samples). It was assumed that all the particulate calcium was present as calcium carbonate. Calcium concentration was determined by flame atomic absorption spectrometry using an air-acetylene flame at 422.7nm. Particulate organic carbon (POC) was calculated by subtracting particulate inorganic carbon from TPC.

Inorganic nutrients

Concentration of phosphate and nitrate were measured in seawater samples kept frozen (-20°C) during the survey, and analysed at the laboratory in an autoanalyser

Technicon AAII in conjunction with known standard concentrations. The method for the determination of inorganic phosphate (Murphy and Riley, 1962; Kirwood, 1989) was based on the reaction of the ions with an acidified molibdate reagent (sulphuric acid, ammonium molibdate and potassium antimony tartrate) which yields a phosphomolibdate complex. The complex was then reduced with ascorbic acid to give a blue compound containing antimony in a 1:1 atomic ratio to phosphorus. The final reaction pH was kept <1 in order to avoid a competitive reaction from silicate.

The nitrate analysis was based on the reduction of nitrate to nitrite that was then estimated via the formation of a coloured azo dye. The final nitrate concentration was obtained by subtracting from the total nitrate plus nitrite concentration the nitrite concentration of the seawater (same procedure without reduction). The automated reduction of nitrate to nitrite was carried out in a reductor column filled with copper-coated cadmium granules (Grassoff, 1976; 1983) and using a solution of ammonium chloride as a buffer. After the reduction step, the nitrite determination (Grassoff, 1976; 1983) was based on the reaction of the ions with an aromatic amine (sulphanilamide hydrochloride) leading to the formation of a diazonium compound. This compound was then coupled with a second aromatic amine (N-1-naphthyl-ethylendiamine-dihydrochloride) to form a final azo dye the concentration of which is proportional to the initial amount of nitrite over a wide range of concentrations (0-10 $\mu M\ NO_2$).

CHAPTER IV. OBSERVATIONS

A. EVOLUTION OF THE BLOOM

Development

The *E.huxleyi* bloom was first observed in satellite imagery on June 4th off Eddystone Bay (49°45'N, 4°40'W) remaining centred near this position till 12th June (Figure 4.1A and B). Maximum AVHRR reflectance and area during this period increased rapidly from 0.7% and 245km^2 to the maximum values of 3.8% and 1,200km^2. The bloom was associated with the southern boundary of a warm area that covered most of the Bay and that matched the region of the highest values for the English Channel (2-3.2) of the stratification parameter (S) (Figure 4.1C). S measures the tendency of the water column to stratify under the influence of a surface heat flux in the presence of tidal mixing (Pingree and Griffiths, 1978). The tidally mixed regions off Start Point (SP), Lizard Point (LP), Isles of Scilly (IS) and Lands End (LE), defined in the numerical model by stratification parameter values ≤ 1, were similarly seen in the thermal images as surface cool waters. The satellite signature in the coastal region of Eddystone Bay was cooler than expected from the S distribution, maybe as a result of wind-induced vertical mixing in shallow waters, or coastal flow of cooler waters from the east. A wave-like structure (~25km wavelength), characteristic of thermal fronts, was observed at the southern edge of the bloom.

Advection

The most conspicuous aspect of the evolution of the bloom was advection from Eddystone Bay on June 13 to the Isles of Scilly on June 24 (Figures 4.2A to C). Combined visible-thermal images on June 17 and 20 showed the warm water of Eddystone Bay being driven westwards around the Lands End Peninsula and carrying within it the patch of coccoliths, now stretched out by the field of flow.

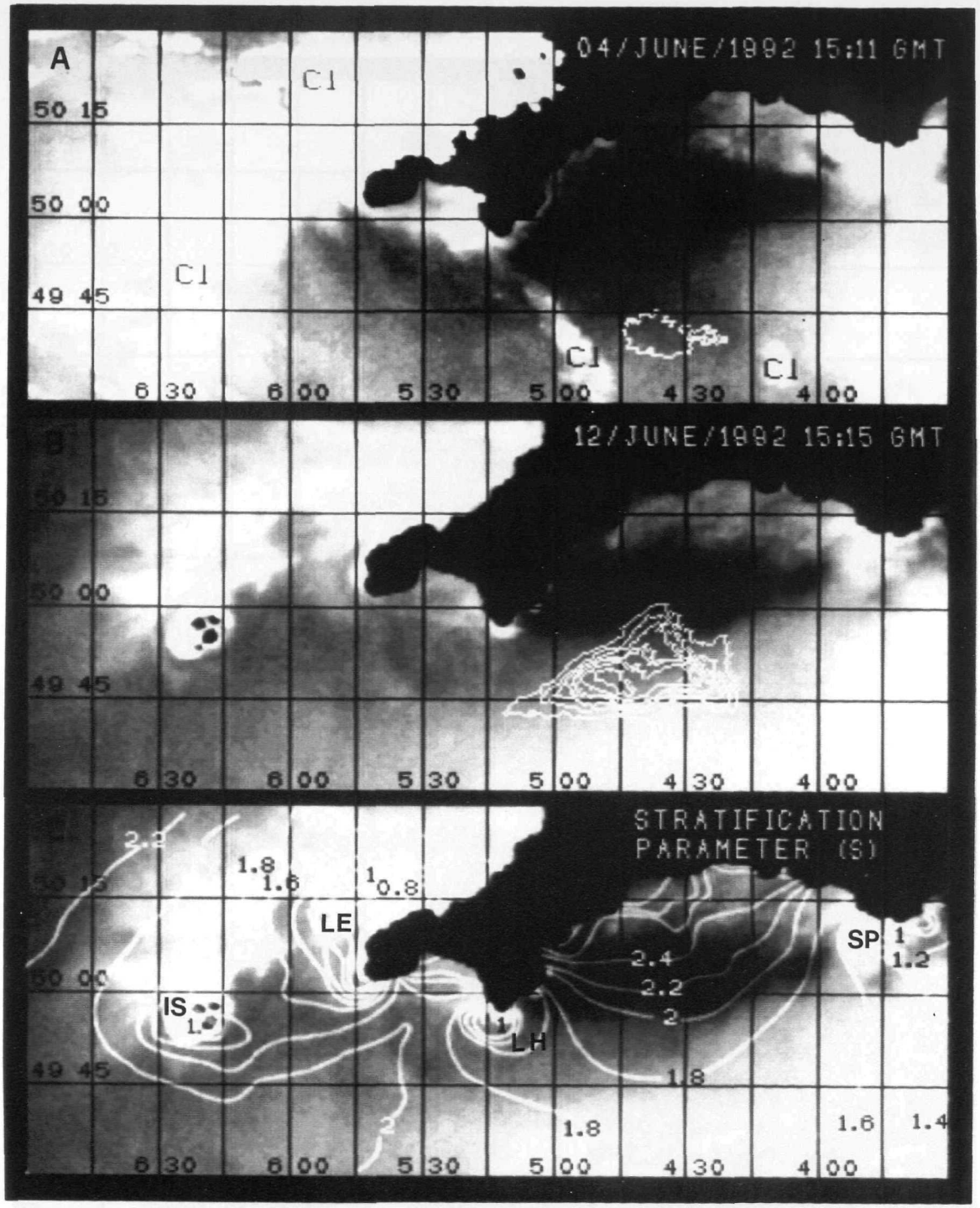

Figure 4.1 Combined AVHRR satellite reflectance (white contours) and thermal (background) images on A) 4th and B) 12th June 1992. A minimum reflectance contour of 0.6% with increments of 0.6% has been plotted. Warm waters are shown as dark shades and cool waters as white shades. "Cl" denotes regions covered by clouds. C) Stratification parameter (S) contours (high definition plot of numerical model by Pingree and Griffiths (1978)) overlaying Figure 4.1B. The tidal mixing areas of the region ($S \leq 1$) are identified with initials: Start Point (SP), Lizard Head (LH), Isles of Scilly (IS) and Lands End (LE).

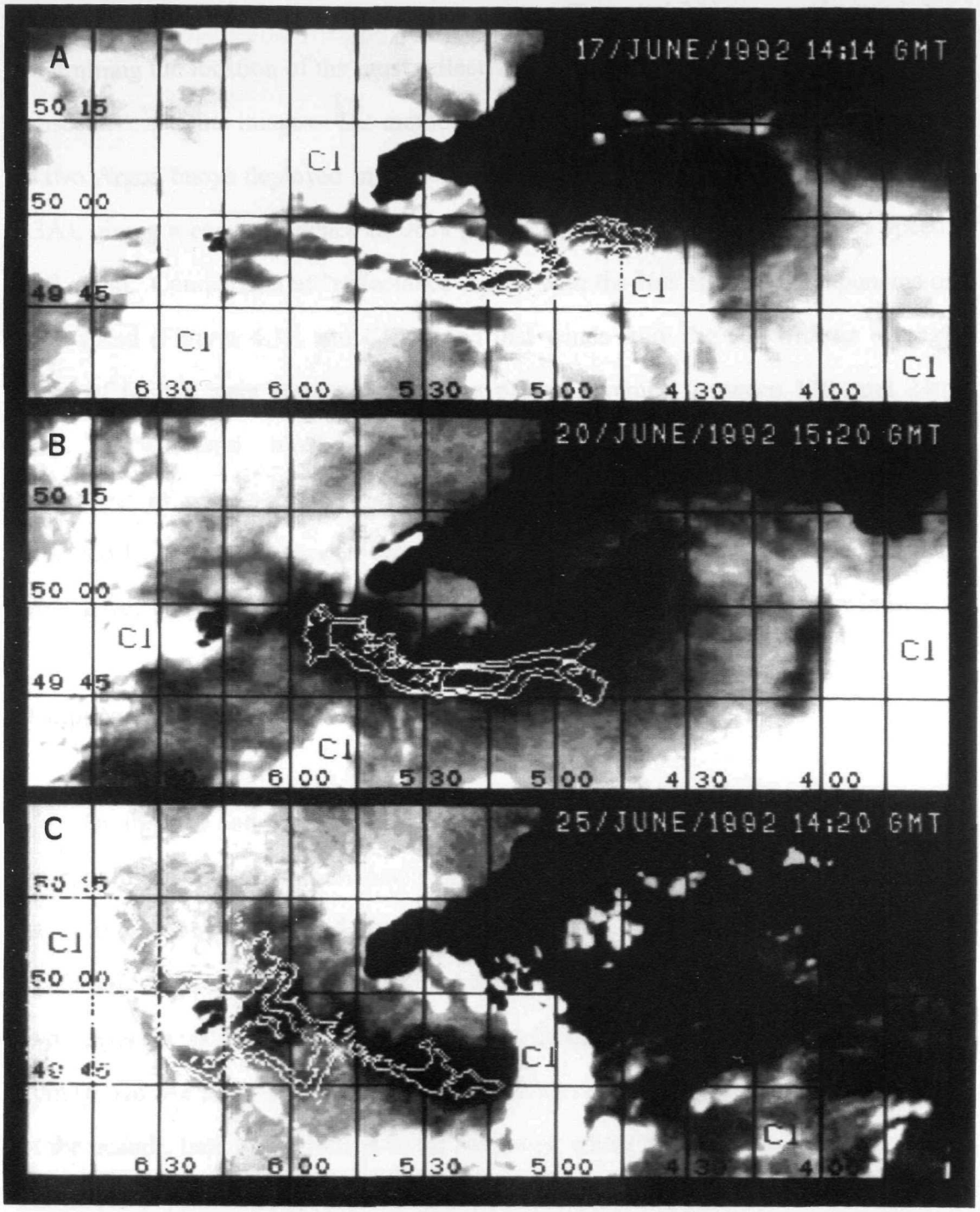

Figure 4.2 Combined AVHRR satellite reflectance (white contours) and thermal (background) images on A) 17th, B) 20th and C) 25th June 1992. A minimum reflectance contour of 0.6% with increments of 0.6% has been plotted. Warm waters are shown as dark shades and cool waters as white shades. "Cl" denotes regions covered by clouds.

The velocity of the patch against time (Figure 4.3A) was calculated by determining the location of the most reflective centre of the coccolithophore bloom in consecutive satellite images. The method was tested against the 24h averaged velocity of two Argos buoys deployed in the patch centre on June 25 (shaded area in Figure 4.3A), giving a correspondence of 96% ("reflectance" speed: 11.3cm/s; buoys speed: 10.9 cm/s). Comparison of "reflectance" speed with the N/S and E/W components of wind speed (Figures 4.3B and C) showed that winds from the NE with an average speed of 6.6m/s were responsible for the patch movement between 13th and 24th June. The westward bloom movement seemed to be more related to the south component of wind velocity than to the west component, as has been previously indicated by numerical models (Pingree and Griffiths; 1980) which predict stronger wind driven currents around Lizard Head with NE winds rather than with E winds.

Disappearance

On days 25 and 26 (Figures 4.4A and B), when the field study was conducted, the core of the coccolithophore patch was already first starting to be incorporated into the anticyclonic tidal circulation surrounding the Isles of Scilly (Pingree and Maddock, 1985; Pingree and Mardell, 1986). The water movement was tracked by two Argos buoys deployed on June 25 in the bloom core and drogued at a depth of 20m (broad line overlapped on the images). After moving clockwise around the south of the Islands, both buoys moved to the northwest where their path diverged into north and south branches of the flow. A similar northwest flow past the Isles of Scilly is sometimes evident in infra-red satellite images where it appears as a cool plume of water emanating from the Islands. The buoy in the north branch of the flow moved northwest at a speed of ~7cm/s. The buoy that took the south branch moved northwest more slowly (~2cm/s). The satellite coccolith reflectance images on June

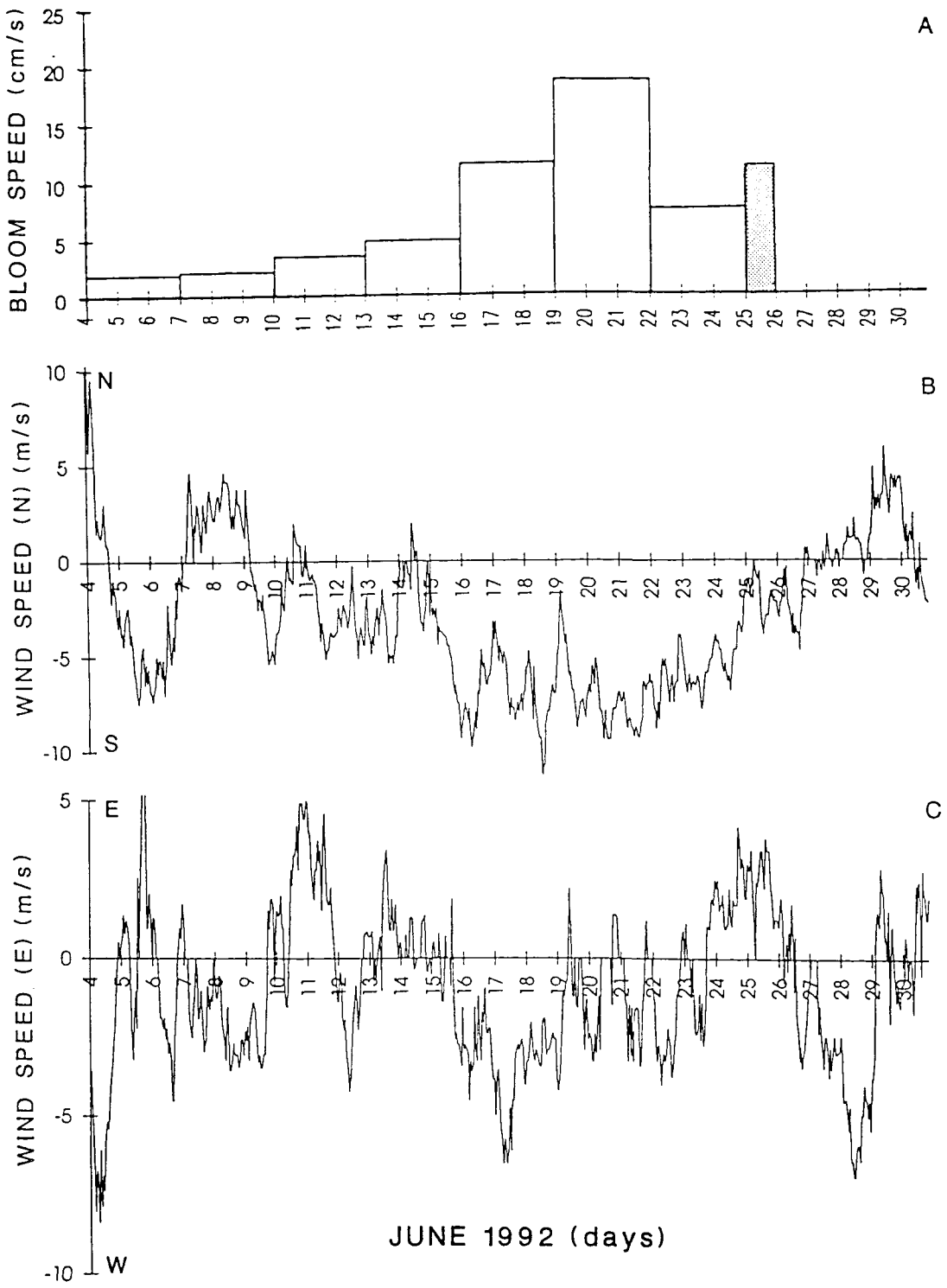

Figure 4.3 A) Time series of 3-days averaged "AVHRR reflectance" speed or coccolithophore bloom speed (cm/s) calculated from satellite reflectance images during the period 4th June-24th June. The method has been tested between days 25th and 26th June against the 24h averaged velocity (shaded area) of two drifting buoys deployed in the core of the coccolithophore bloom. B) Time series of N component of wind speed (m/s) and C) E component of wind speed (m/s) covering the period 4th June-1st July 1992.

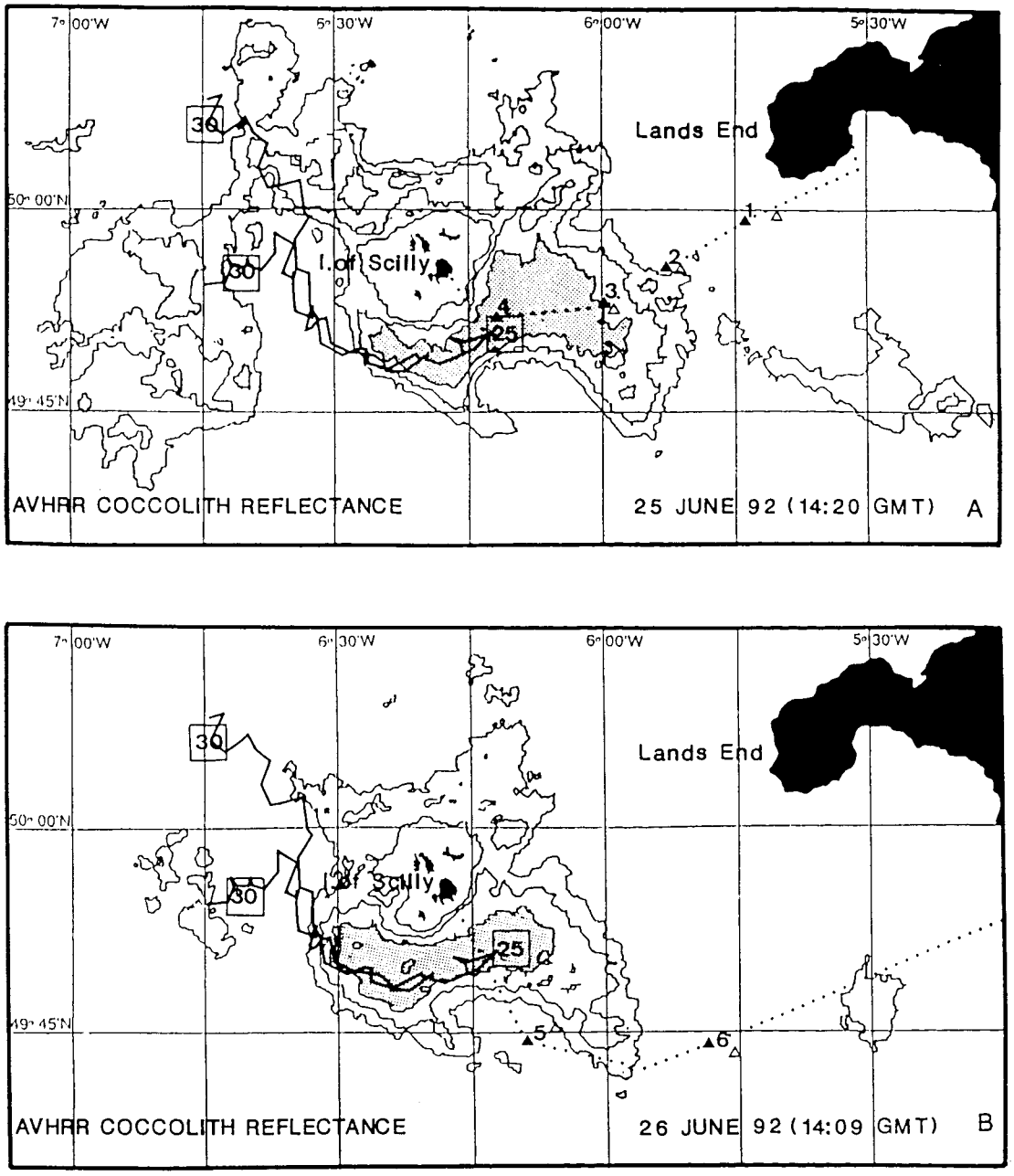

Figure 4.4 AVHRR satellite reflectance contours for the sampling days A) 25th and B) 26th June 1992 (minimum reflectance contour: 0.6%; reflectance increments 0.4%). Also shown the ship's track (dotted line), the location of the stations (black triangles), the tidally corrected positions (white triangles) and the 5 days track (25th-30th June) of two Argos buoys deployed in the core of the coccolith patch (broad line). Note that on the second sampling day (26th June) the ship's track cut features that were changed little from the day before: a wave-like structure on the southern edge of the bloom and a detached reflective area at approximately 49° 50'N 5° 30'W.

25th and 26th showed some bloom structure to the west of the Islands and a suggestion of similar northward and southward branches. There was no evidence of the coccolithophore patch on July 7th, the first cloud-free satellite image of the area following 26th June, indicating a 3-4 weeks life time for this bloom (similar to that of the bloom observed earlier off Brittany, see Methods).

B. PHYSICAL AND BIOLOGICAL STRUCTURE OF THE BLOOM

Surface structure

Underway temperature measurements (Figure 4.5A) recorded the warm water mass confining the reflective bloom (see also satellite image on the sampling day, Figure 4.2C). Warmest bloom waters (>17.2°C) were located in an eastern detached area of the coccolithophore patch, showing a suggestion of the westward warm flow observed in the satellite images. The main reflective signature of the bloom occurred within a large structure defined by the 16.0°C -16.2°C isotherms and was bounded to the NE and W with the cooler (<15.4°C) tidally mixed regions. To the south, where the warm coccolithophore waters bounded cooler (<15.4°C) offshore waters, the outcropping isotherms 15.4-16°C were observed to be associated with the wave-like edge of the reflective bloom.

Surface chlorophyll *a* values (Figure 4.5B) lower than 0.50mg/m^3 were observed inside the reflective coccolithophore waters. The 0.50mg Chl*a*/m^3 contour defined a surface boundary with the surrounding tidal fronts at about 15.5-16°C (see Figure 4.5A). A surface chlorophyll *a* limit between the bloom and offshore waters (<0.50mg Chl*a*/m^3) was not observed, with the exception of a tongue of slightly higher chlorophyll *a* values (>0.5mg/m^3) intruding into the coccolithophore patch at its southern edge. A minimum value of less than 0.25 mg Chl*a*/m^3 occurred at the eastern region of the bloom.

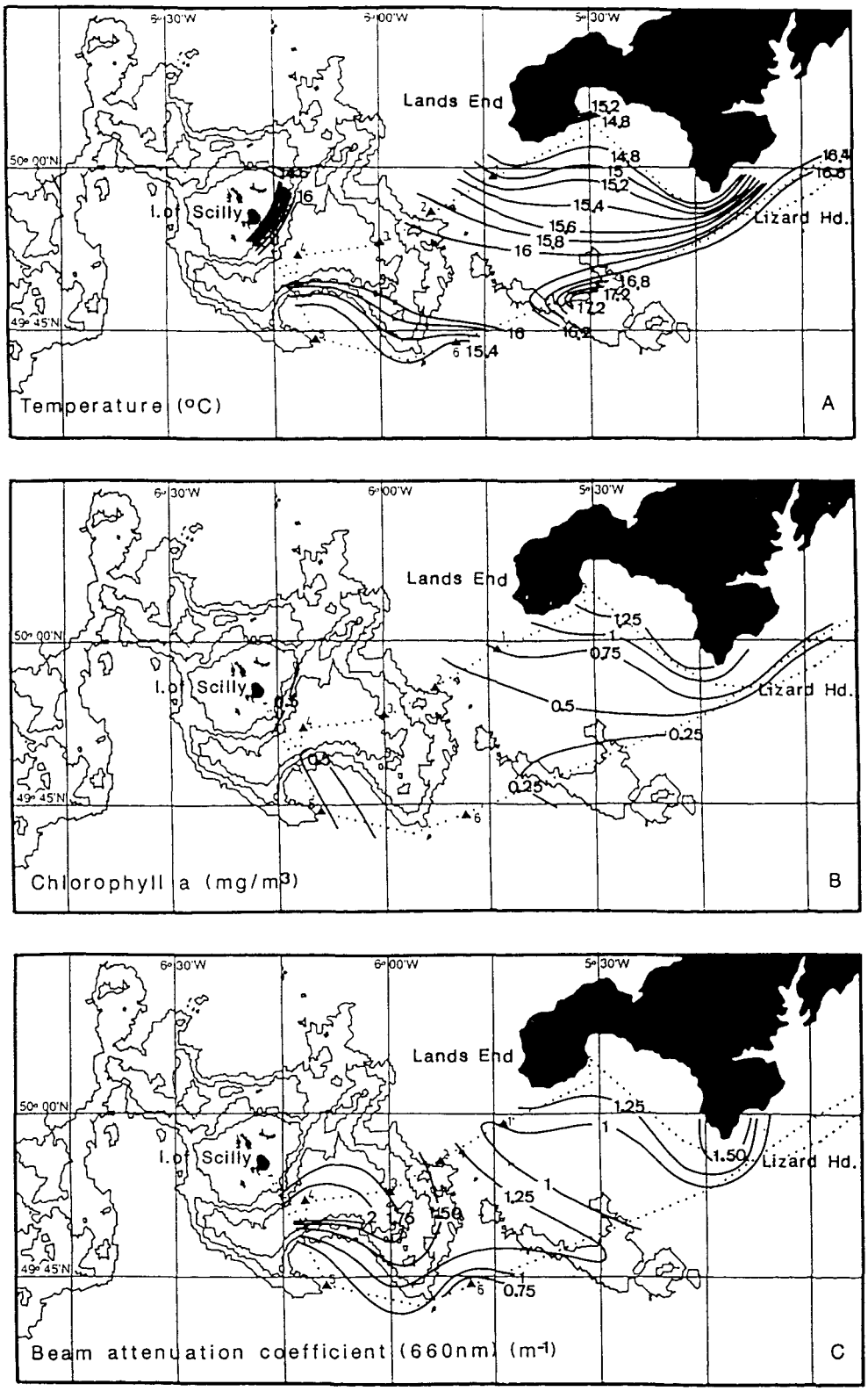

Figure 4.5 Surface distribution of A) temperature (°C), B) chlorophyll *a* (mg/m^3) and C) beam attenuation coefficient at 660nm (m^{-1}) along the cruise track (dotted line). The contours are an interpretation of the along-track values based on the background AVHRR reflectance image on 25th June (from Figure 4.4A).

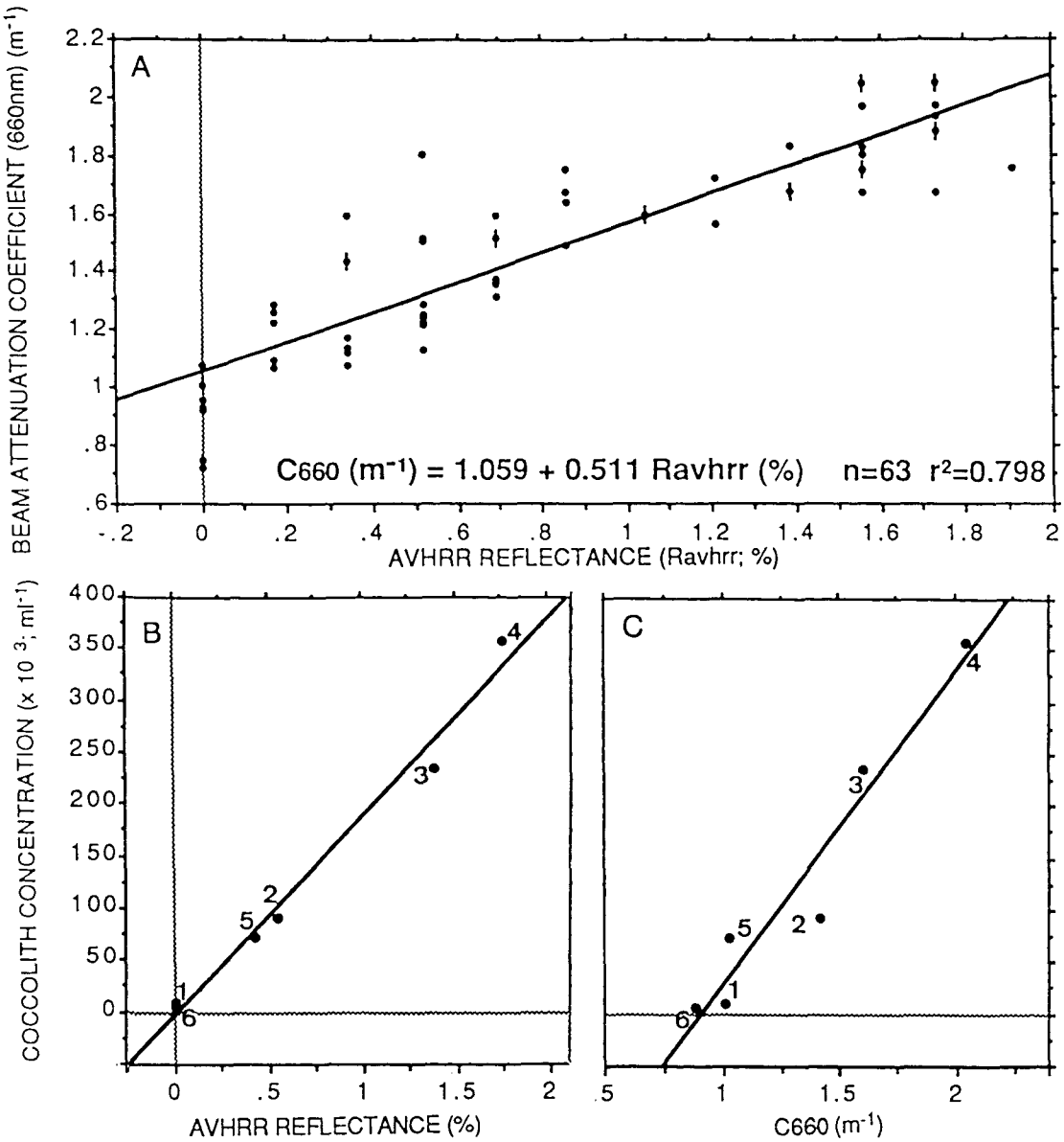

Figure 4.6 Empirical relationships between A) beam attenuation coefficient at 660nm (m^{-1}) and AVHRR reflectance (%) (AVHRR discrete reflectance increments of ~0.165 correspond to the sensor sensitivity using the onboard calibration values); B) AVHRR reflectance (%; 3x3 pixels averages) and concentration of coccoliths (coccoliths/ml) (numbers 1 to 6 indicate sampling stations); and C) beam attenuation coefficient at 660nm (m^{-1}) and concentration of coccoliths (coccoliths/ml).

Beam attenuation coefficient at 660nm (c660) (Figure 4.5C) mapped the surface structure of the bloom well. The coccolithophore-dominated waters were confined within beam attenuation coefficient values higher than 1.25m^{-1} that progressively increased towards the most reflective centre (c660>2m^{-1}). Surface values of c660 also registered the wave-like feature of the southern edge of the bloom (0.75-1.75m^{-1}). The range of values within the coccolithophore patch (1.25-2m^{-1}) was typically higher than that observed in the region of strongest tidal mixing off the Lands End Peninsula (1.25->1.50m^{-1}). The empirical relationships between satellite reflectance, coccolith density and c660 (Figures 4.6A to C) indicated that each 1% of AVHRR bloom reflectance or an equivalent increase of about 200,000 coccoliths/ml was detected underway by beam attenuation coefficient increments of ~ 0.5m^{-1}.

Vertical hydrographic structure

Temperature profiles at the sampling stations (Figure 4.7A) identified the relatively mixed waters near the Lands End Peninsula (station 1) and the stratified waters offshore (station 6). The warm reflective waters (stations 2 to 4) exhibited a characteristic pool-like section with a pronounced seasonal thermocline having a central maximum depth (station 3) of about 25m. The warm pool was defined by temperatures between 15°C and 16°C, with the 16°C isotherm (extending from 5°W to 6°15'W; see Figure 4.5A) within 5m of the surface. At the boundaries of the warm pool (stations 1/2 and 4/5) the isotherms outcropped at the surface giving rise to the thermal fronts observed in the surface distribution of temperature (see Figure 4.5A).

The section of chlorophyll *a* (Figure 4.7B) characterised the three distinct hydrographic environments observed in the temperature profiles. Chlorophyll *a* values higher than 0.75mg/m^3 extended from surface to 30m depth in the highly

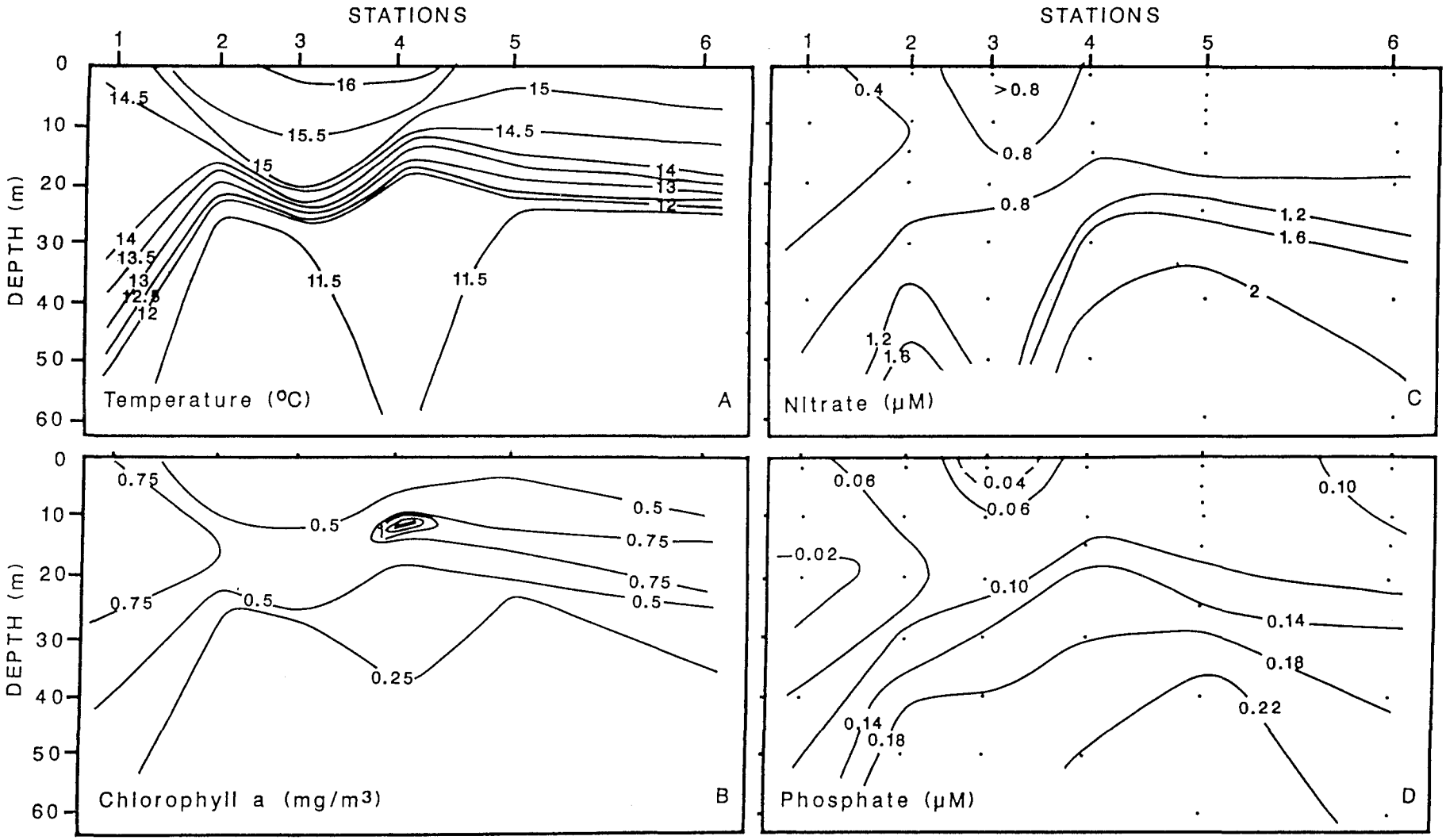

Figure 4.7 Vertical distribution of A) temperature (°C), B) chlorophyll *a* (mg/m³), C) nitrate concentration (µM) and D) phosphate concentration (µM).

productive tidally mixed area (station 1). The stratified offshore waters were characterised by a chlorophyll *a* maximum (>0.75mg/m^3) in the thermocline. The pool of warm water showed a much broader subsurface chlorophyll *a* maximum (from 15m to 25m depth at the centre of the pool) with a typical chlorophyll *a* concentration of 0.50mg/m^3. Both bloom and offshore waters exhibited similar low surface values (<0.50mg Chl*a*/m^3). The highest chlorophyll *a* levels (1.70 mg/m^3) were located in the thermocline below the offshore outcropping isotherms. A depression of the 0.25 mg Chl*a*/m^3 contour from 20m to 35m depth was noticeable at station 4 that followed the same pattern as the 11.5°C isotherm.

The distributions of nitrate and phosphate (Figures 4.7C and D) followed patterns similar to the temperature section. The 0.10μM PO_4 and 0.8μM NO_3 contours were placed at about the thermocline level and deepened between station 4 and 3 following the pool-like structure. In the tidally mixed station 1, nutrient values < 0.4μM NO_3 and < 0.06μM PO_4 were found to be associated with the region of relatively high chlorophyll *a* biomass (>0.75mg/m^3). In the non tidally-mixed waters above the thermocline, nutrient concentrations were typically at postspring bloom levels (<1μM NO_3 and <0.10μM PO_4) and showed a distinct NO_3 maximum (>0.8μM) and PO_4 minimum (<0.04 μM) in the surface core of the warm pool.

E.huxleyi standing stocks

The distribution of *E.huxleyi* cells (Figure 4.8A) was relatively widespread across the surface pool of warm waters. The detached coccoliths (Figure 4.8B), that largely outnumbered the concentration of cells (>175 coccoliths/cell at surface station

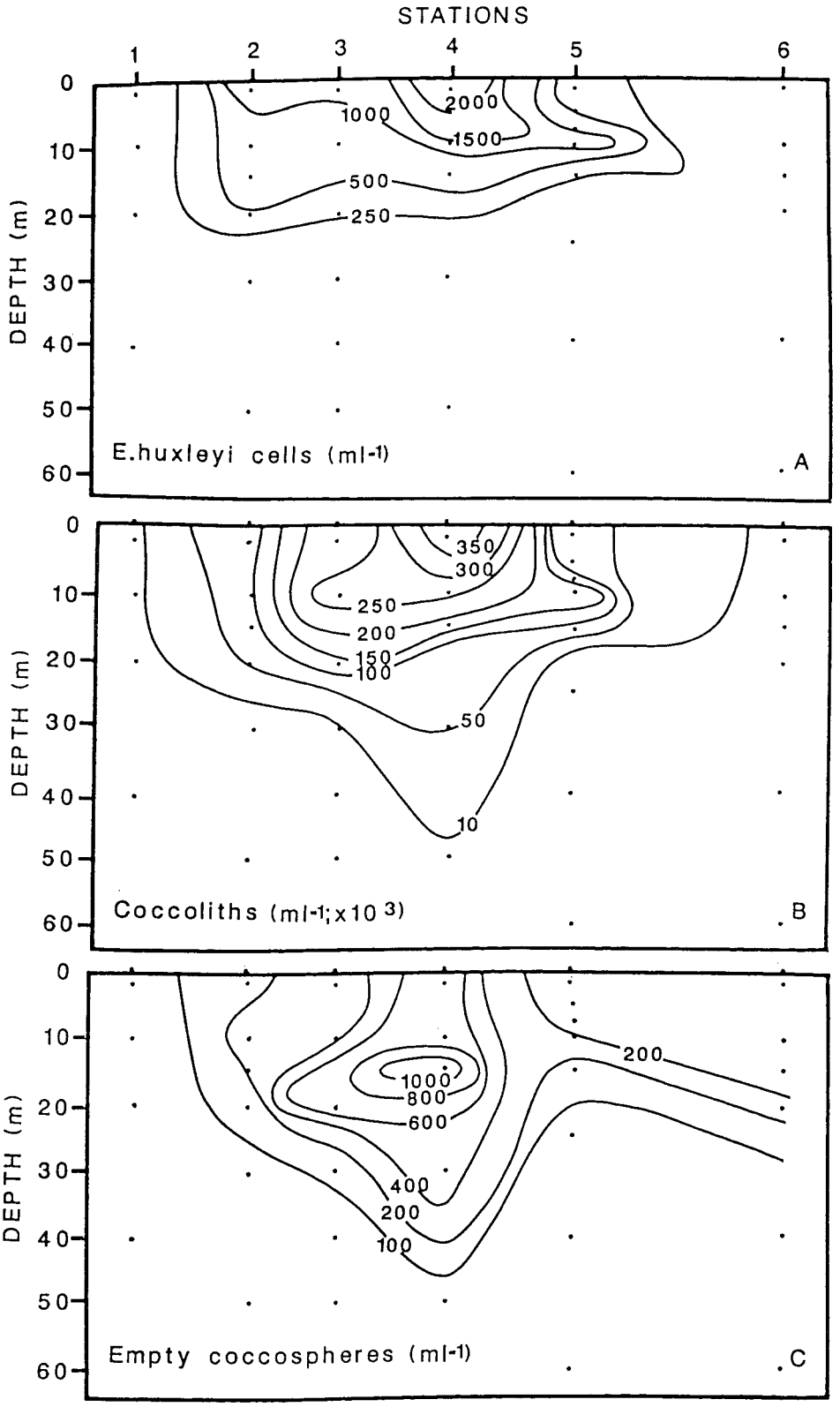

Figure 4.8 Vertical distribution of A) concentration of *E.huxleyi* cells (cells/ml), B) concentration of detached coccoliths (coccoliths/ml x 10^3) and C) concentration of empty coccospheres (coccospheres/ml).

4), were clearly confined within the warm pool structure (see Figure 4.7A). Cells and coccoliths presented densities higher than 2,000 cells/ml and 350,000 coccoliths/ml in a surface core at station 4. The core suggested a stronger surface flow of water moving past the Isles of Scilly to the south. Both distributions extended to station 5 as a subsurface extension of the southern edge of the bloom between 10 and 15m depth. The 1,000 cells/ml contour spread across the surface to stations 1 and 2 where the influence of the Lands End tidal mixing fronts was encountered. Comparison with the chlorophyll *a* distribution (see Figure 4.7B) showed that the densest region of *E.huxleyi* cells (1,000->2,000 cell/ml) exhibited values of chlorophyll *a* typically $<0.50 mg/m^3$.

The highest concentration of empty coccospheres (>1,000/ml; Figure 4.8C) was positively correlated with the bulk of living cells but concentrated at deeper depths (ca. 15m) and showing a sinking pattern. From the depth of maximum coccosphere concentration (15m) and the period of the decaying phase of the bloom (from 12th June) a sinking rate of ≥1.1m/day was estimated, very close to the 1.5m/day value reported for *E.huxleyi* in laboratory experiments (Smayda, 1970). At the central station 4, the deepest fractions of empty coccospheres (<600 coccospheres/ml) and coccoliths (<100,000 coccoliths/ml) were depressed to 50m depth, as was also the 11.5°C isotherm (see Figure 4.7A). The width reduction (~60%) of the most reflective bloom core that occurred as the bloom was incorporated into the clockwise circulation of the Isles of Scilly (see Figures 4.4A and B) may have broadened the deepest and weakest part of the thermocline bringing down associated coccoliths and coccospheres to this level.

Non-coccolithophore photosynthetic phytoplankton

A sinking population of the small diatom *Nitzschia delicatissima* (Figure 4.9A; shaded section), was observed inside the coccolithophore bloom. The diatom patch was located within coccolith densities higher than 25,000-50,000 coccoliths/ml or densities of empty coccospheres higher than 100-200 coccospheres/ml but excluded from the core of >300,000 coccolith/ml. The development of this population possibly took place before the occurrence of the coccolithophore bloom as suggested by the consecutive vertical location of the sinking cores of empty coccospheres and *Nitzschia* cells, despite the smaller size of the diatoms. The vertical shape of the population of *Nitzschia* followed the descending pattern of coccoliths and coccospheres at station 4 down to 35m. At this depth, this species matched the 0.25mg Ch*la*/m^3 contour, distributed similarly. At the subsurface levels (30m) where *Nitzschia* was most abundant (>120cells/ml), the chlorophyll *a* values were as low as those associated with the *E.huxleyi* cells (<0.5mg/m^3).

A subsurface (10-15m depth) population of the dinoflagellate *Gyrodinium aureolum* (Figure 14.9B; shaded section) was observed below the densest core of coccoliths (>300,000 coccoliths/ml). The observed intermediate cell abundance (>250 cells/ml) was characteristic of June, larger bloom densities tending to appear during July and August (Holligan and Harbour, 1977; Simpson *et al.*, 1982). This species was associated with the outcropping of the 15°C-16°C isotherms at the southern thermal front and accounted for the relatively high chlorophyll *a* values (>1.7mg/m^3) observed at station 4 at 10-15m depth.

Relatively high concentrations of small photosynthetic flagellates (from 4,000 cell/ml up to 7,000 cells/ml) (Figure 4.9C) made up the bulk of phytoplankton abundance outside the bloom (stations 2, 5 and 6). The coccolithophore waters

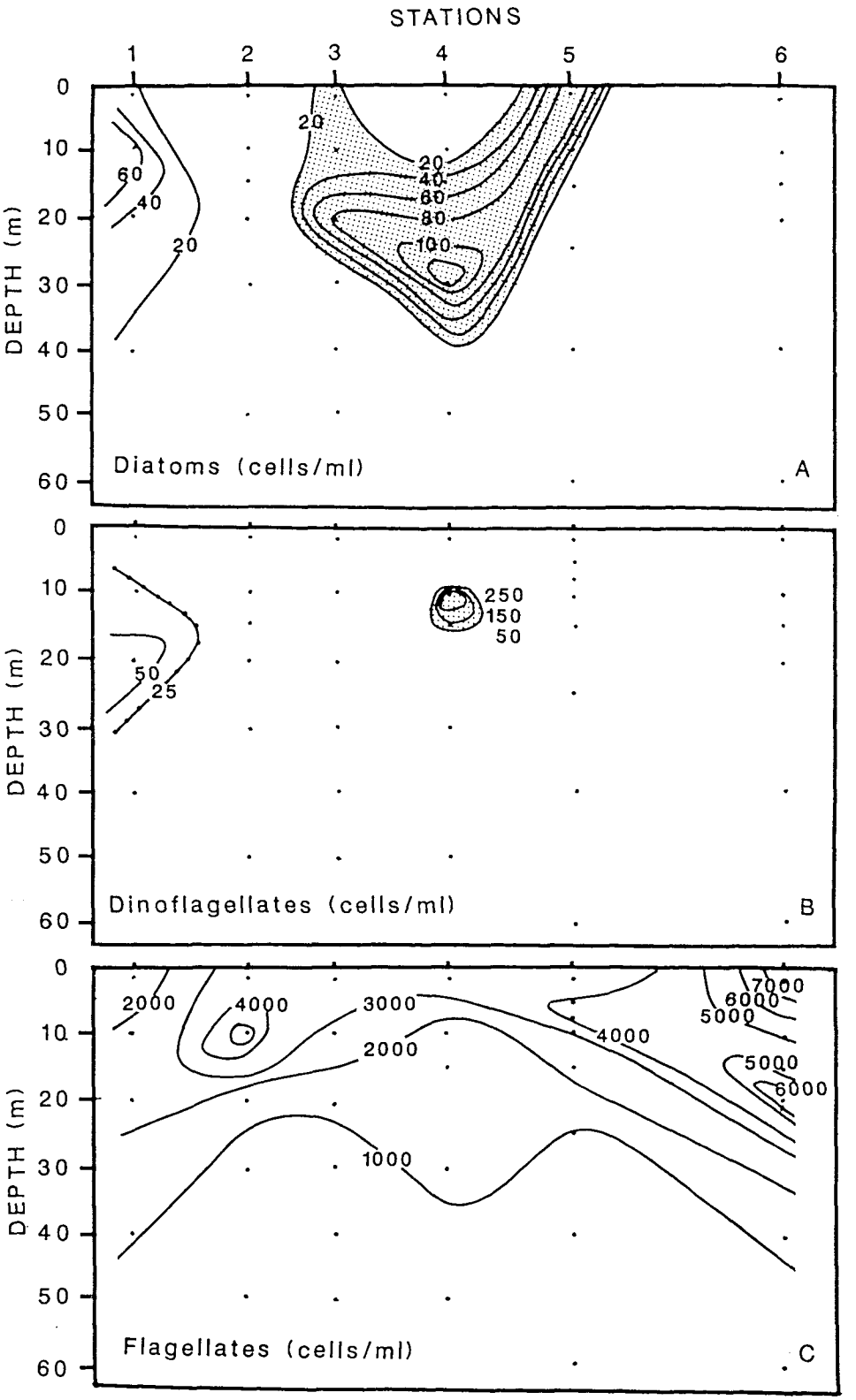

Figure 4.9 Vertical distribution of non coccolithophore photosynthetic phytoplankton (cell/ml): A) diatoms (shaded section: *Nitzschia delicatissima*), B) dinoflagellates (shaded section: *Gyrodinium aureolum*) and C) flagellates.

(stations 3 and 4) typically exhibited flagellate densities lower than 3,000 cell/ml with the 1,000cell/ml contour dropping characteristically to 35m depth at station 4. The phytoplankton assemblage of the tidally mixed area was dominated by large and medium-sized diatoms of the genus *Leptocylindrus* (see also Simpson *et al.*, 1982), *Rhizosolenia* and *Thalassiosira* (Figure 4.9A, unshaded section; up to 60 cells/ml), species characteristic of turbulent environments, and the small dinoflagellate *Gymnodinium* sp. (Figure 4.9B, unshaded section; up to 40 cells/ml).

Particulate carbon

Particulate inorganic carbon (PIC) (Figure 4.10A) was the property that best resolved the vertical structure of the abundant detached coccoliths (LITH) (see Figure 8A). Both distributions covaried according to the following equation:

$$PIC\ (mgC/m^3) = 22.33 + 0.000868 * LITH\ (coccoliths/ml) \qquad r^2=0.92;\ n=30.$$

The relationship gave an average coccolith carbon content of 0.868 pgC/coccolith and an average calcite-C concentration in non coccolithophore waters of 22.33 mgC/m^3. Maximum PIC values of about 300mgC/m^3 were found in the coccolith surface core (station 4). At the edges of the pool of coccoliths, the contribution of PIC to the total particulate carbon content decreased sharply from 80 to 20%.

The distribution of particulate organic carbon (POC) (Figure 4.10B) followed the inverse spatial trend of the distribution of particulate inorganic carbon (PIC) with values (>50 mgC/m^3) 2 times lower within the bloom than outside. The bloom PIC increments (5-6 times higher values inside the bloom than outside) were comparatively higher than the POC decrements and resulted in a C/N vertical section (Figure 4.10C) quite similar to the distributions of PIC and detached coccoliths. The C/N ratio, ranging from 10 to 18 atC/atN in the coccolithophore waters, resolved the high surface values at stations 3 and 4 and the subsurface extension at station 5.

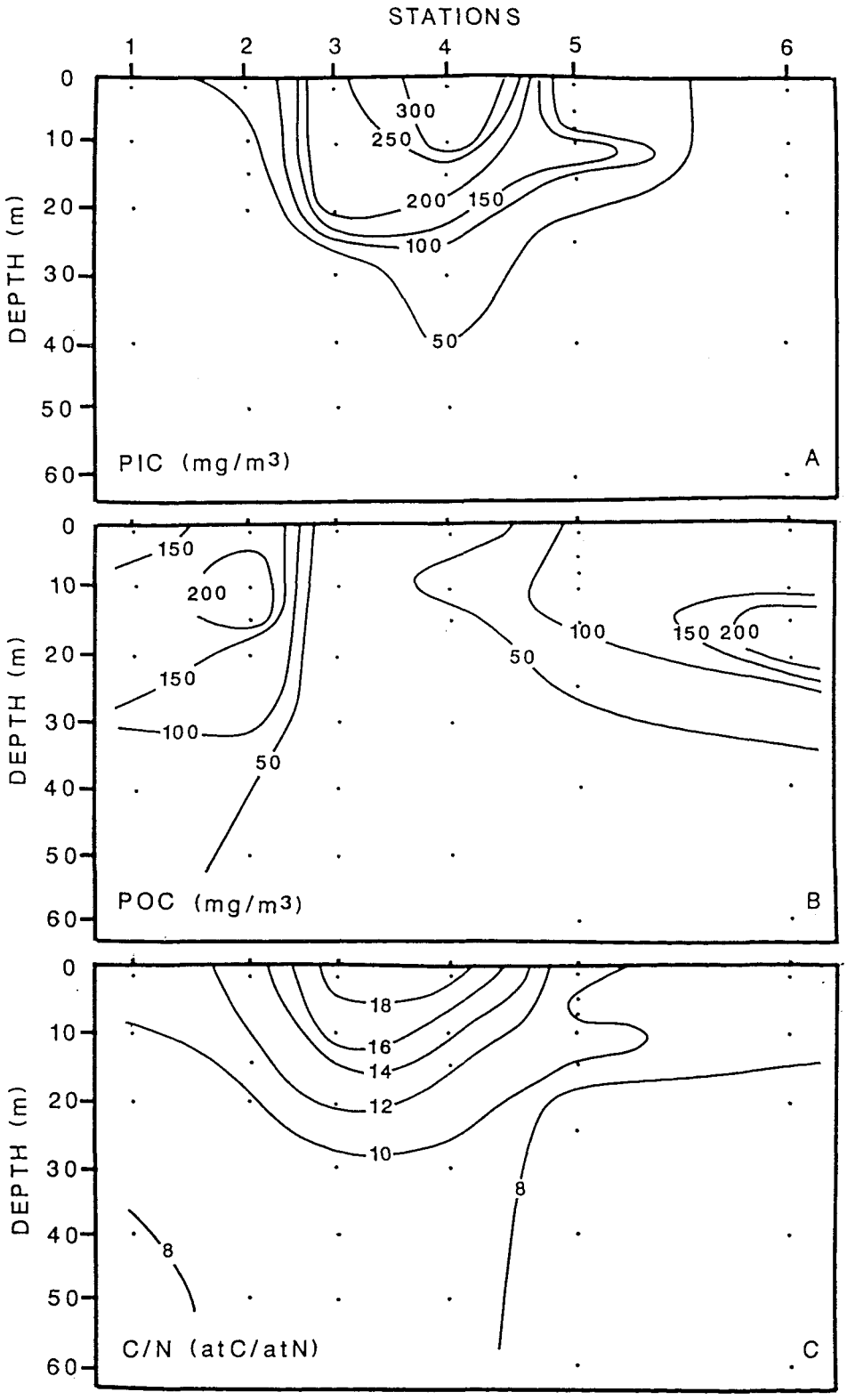

Figure 4.10 Vertical distribution of A) particulate inorganic carbon (PIC; mgC/m^3), B) particulate organic carbon (POC; mgC/m^3), C) C/N ratio (by atoms).

C. OPTICAL PROPERTIES OF THE BLOOM

PAR diffuse attenuation coefficient

The distribution of PAR vertical extinction coefficient (K(PAR); Figure 4.11A) correlated well with the distribution of the detached coccoliths (see Figure 4.8A). The bloom was defined by values higher than $0.15m^{-1}$ increasing towards the densest coccolith centre ($>0.3m^{-1}$). The K(PAR) defined patch was shaped as the pool-like structure of the coccoliths and was similarly placed on top of a steep vertical gradient, here defined at the bottom by the $0.10m^{-1}$ contour. The empirical regressions of K(PAR) (m^{-1}) with coccolith density (coccoliths/ml) and AVHRR reflectance (%) (Figures 4.11B and C) showed that an increment of 200,000 coccoliths/ml or the equivalent 1% AVHRR reflectance increment (see Figure 4.6B) increased K(PAR) $\sim 0.1\ m^{-1}$.

PAR diffuse attenuation coefficient and beam attenuation coefficient at 660nm showed a relationship (Figure 4.11D; continuous line) no different from that described in the Western English Channel waters (broken line). The values of Secchi disk depth were however 2.6 times shallower within the bloom (Figure 4.11E; continuous line) than in the Western English Channel waters (broken line) for a given c660 value. The shift resulted from the almost white light scattering of the coccoliths that reduced the contrast of the white Secchi disk. The result invalidates a direct use of the empirical formula relating K to Secchi disk depth (KD~ 1.7 for the English Channel, Poole and Atkins, 1929; see also Højerslev, 1982 in the North Sea) whenever coccoliths are abundant (>10,000 coccoliths/ml; see line crossing point near the outside bloom stations 1 and 6 in Figure 4.11E) .

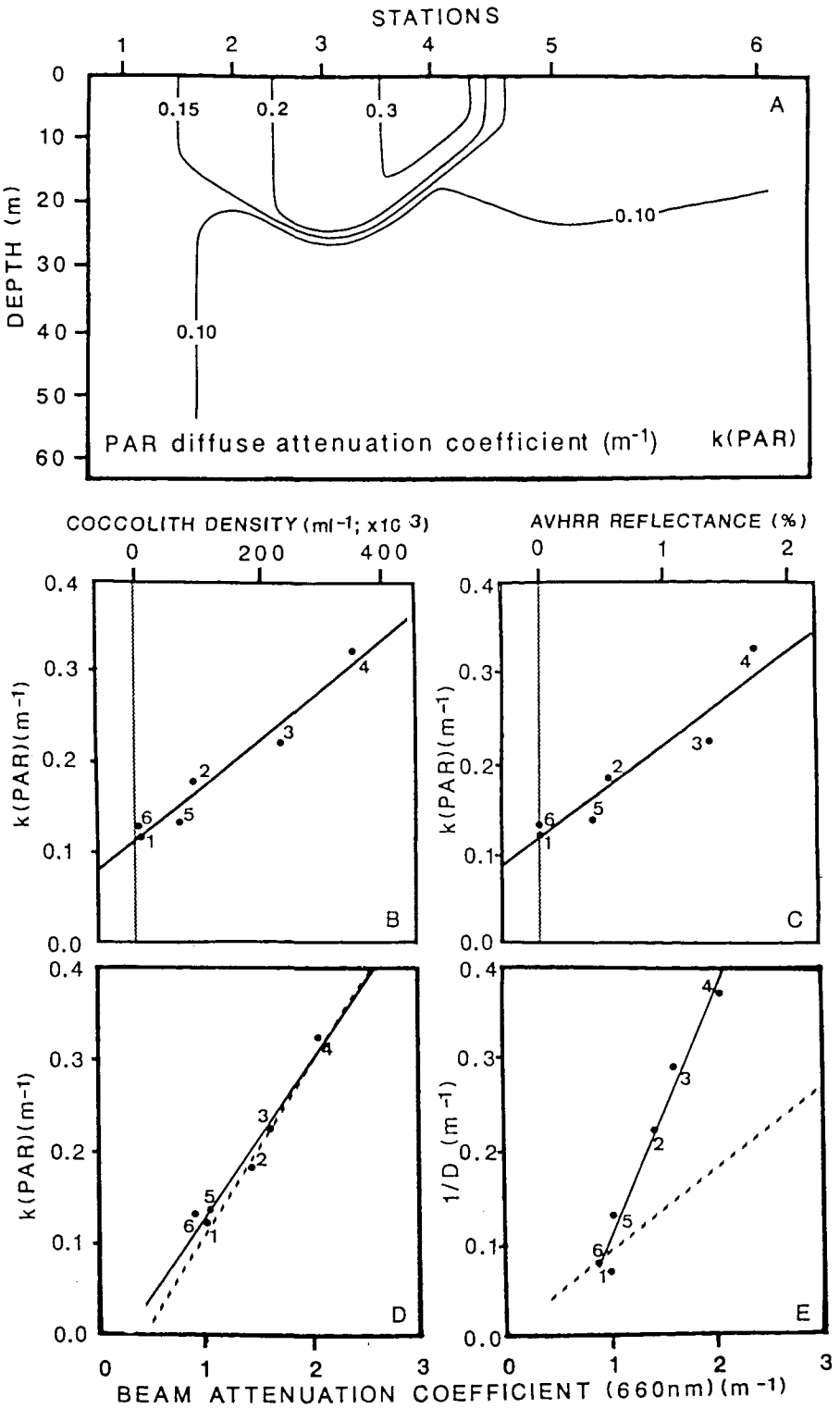

Figure 4.11 A) Vertical distribution of PAR diffuse attenuation coefficient (k(PAR); m^{-1}), B) empirical relationship between k(PAR) (m^{-1}) and surface concentration of coccoliths (coccoliths/ml x 10^3), C) empirical relationship between k(PAR) (m^{-1}) and AVHRR satellite reflectance (%), D) empirical relationship between k(PAR) (m^{-1}) and red beam attenuation coefficient (660nm; m^{-1}) in the coccolithophore bloom compared with the same relationship for the English Channel waters in winter (broken line; R.D.Pingree, unpublished data) and E) empirical relationship between the inverse of Secchi disk depth (m^{-1}) and beam attenuation coefficient (m^{-1}) compared with the same relationship described in the English Channel waters in winter (broken line; Pingree *et al.*, 1986).

In situ reflectance

The surface reflectance spectrum, 415-660nm, (Figure 4.12) characterised the coccolithophore dominated waters. The reflectance signature within the bloom was always higher than in the surrounding regions (stations 1 and 6), and increased from the coccolith patch edges to the coccolith patch centre. The less reflective outside stations also showed the 550nm peak typical of waters with sediments in suspension (Kirk, 1983); higher in the tidal mixed region (station 1) than in the open shelf (station 6). The reflectivity of the bloom was stronger between 415 and 554nm and decreased rapidly in the upper wavelength region of the spectrum where the absorption by pure water increases sharply (Kirk, 1983). The reflectances at 632nm and at 554nm were well correlated by a ratio ~2 (Figure 4.13A and B). There was also a good relationship between *in situ* reflectance at 632nm and satellite AVHRR reflectance (630nm mean wavelength; broadband 580-680nm). The ratio ~2.7 of this empirical regression resulted from the direct use of the onboard calibration values of the satellite sensor (see Methods, Chapter III). A vertical section of reflectance contours at 554nm (Figure 4.13C), near the wavelength of minimum *E.huxleyi* absorption (see absorption spectrum as broken line in Figure 4.12), correlated well with the vertical distribution of detached coccoliths (see Figure 4.8B).

Airborne ATM reflectance

The reflectance fine-structure of the eastern region of the bloom on day 23 (Figure 4.14A: AVHRR image, x4 bilinearly zoomed) was well resolved by the airborne ATM scanner (120 x 120m) at the visible bands 2 (450- 520nm; blue), 3 (520-620nm; green), 4 (605-625nm; yellow) and 5 (630-690nm; red) (Figures 4.14B to E).

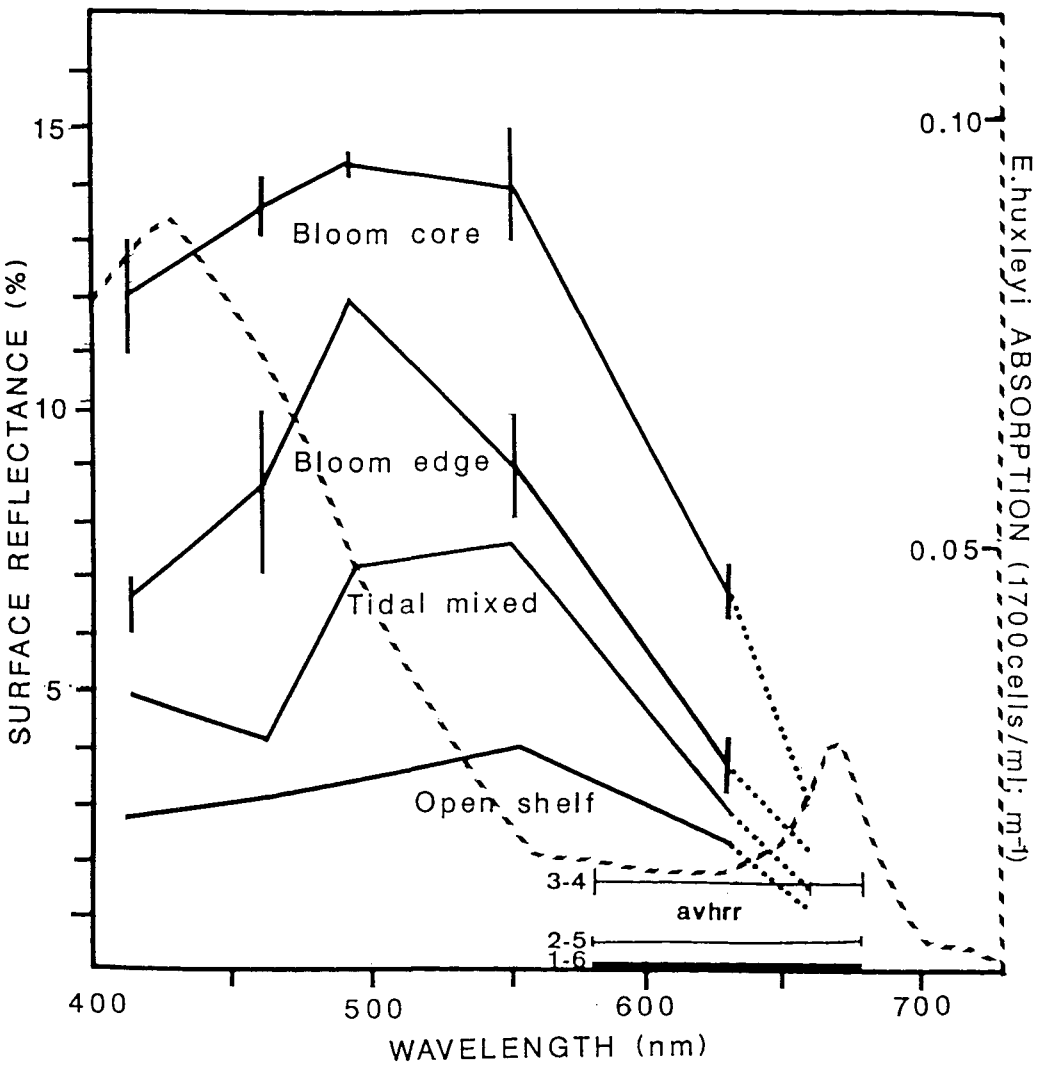

Figure 4.12 Spectrum of *in situ* surface reflectance (%) in the range of wavelengths 415-660nm at the coccolith patch core (stations 3 and 4), coccolith patch edges (stations 2 and 5), tidally mixed region (station 1) and open shelf waters (station 6). Vertical lines indicate the range of averaged values (stations 3/4 and 2/5). Dotted line (from 632 to 660nm) indicates an indirect calculation (Kirk, 1981) of the reflectance at 660nm from the beam attenuation coefficient value at this wavelength (c660) and using as absorption c660~0.4 for clear waters. Thin horizontal line from 580nm to 680nm shows AVHRR reflectance values. Also shown for reference the absorption spectrum (m^{-1}) of a similar coastal *E.huxleyi* bloom in the Gulf of Maine (Balch *et al.*, 1991) (broken line).

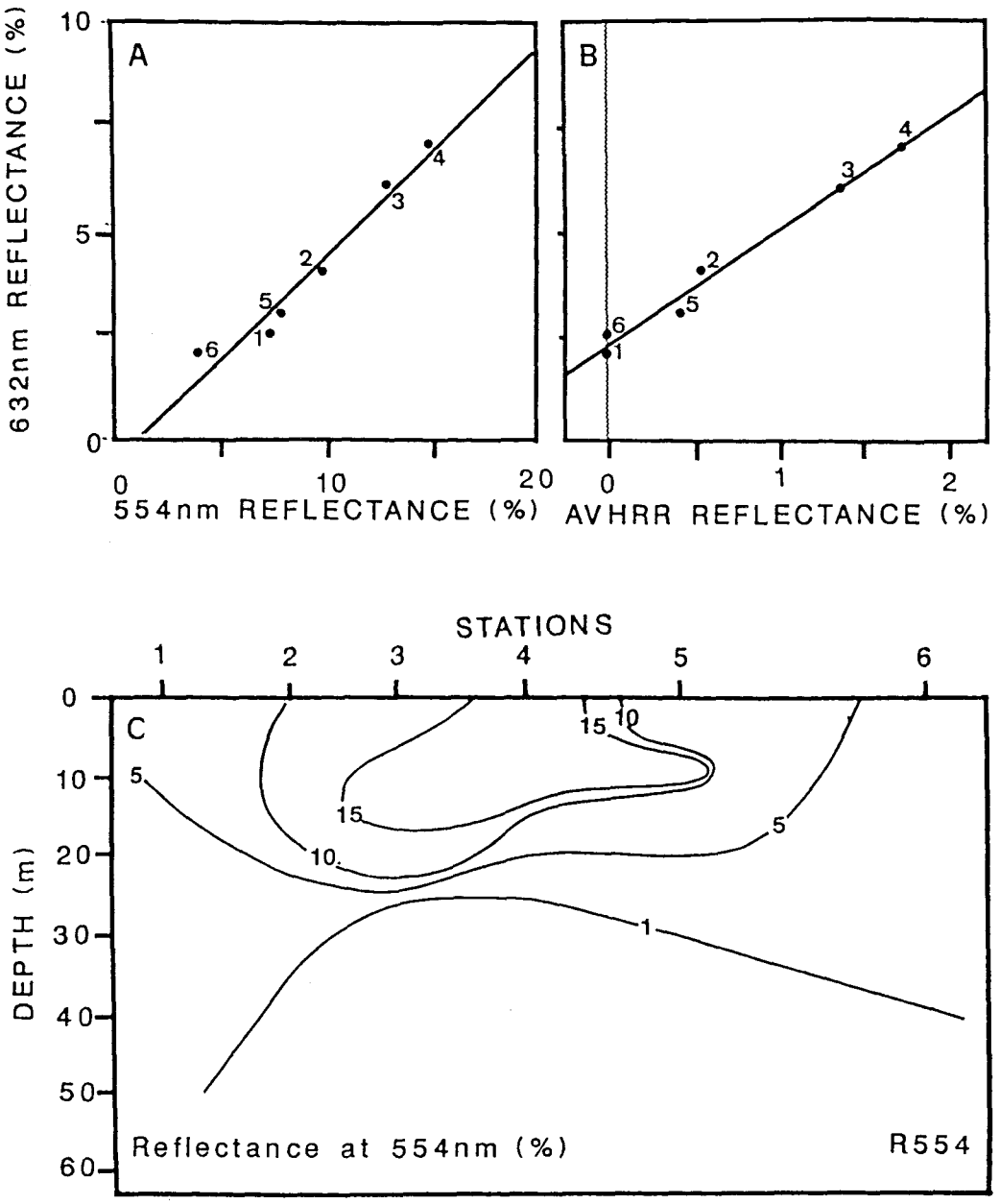

Figure 4.13 A) Empirical relationship between reflectance at 632nm and at 554nm. B) Empirical relationship between *in situ* reflectance at 632nm and satellite AVHRR reflectance (630nm mean-wavelength; broadband 580-680nm). C) Vertical distribution of *in situ* reflectance at 554nm.

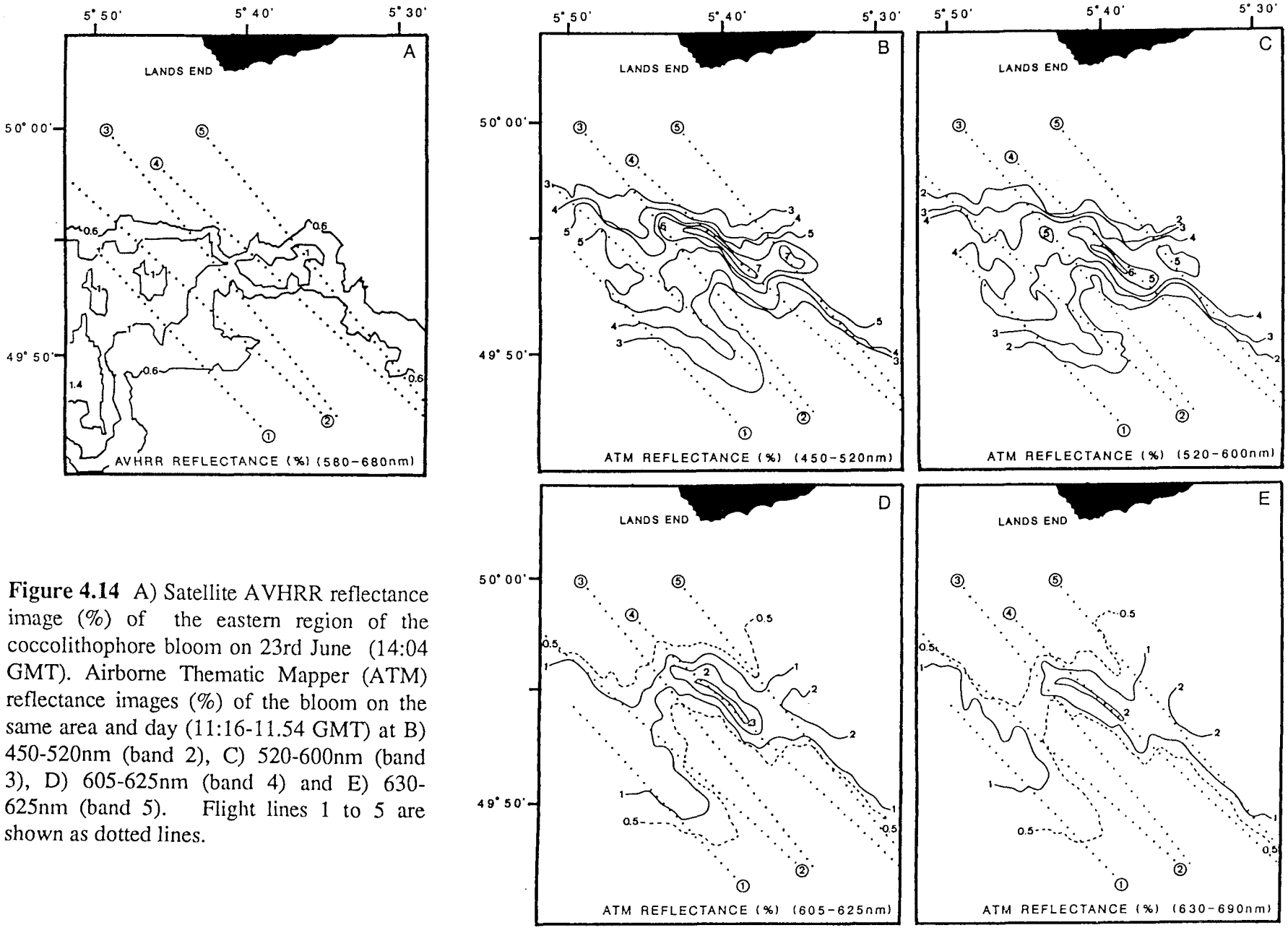

Figure 4.14 A) Satellite AVHRR reflectance image (%) of the eastern region of the coccolithophore bloom on 23rd June (14:04 GMT). Airborne Thematic Mapper (ATM) reflectance images (%) of the bloom on the same area and day (11:16-11.54 GMT) at B) 450-520nm (band 2), C) 520-600nm (band 3), D) 605-625nm (band 4) and E) 630-625nm (band 5). Flight lines 1 to 5 are shown as dotted lines.

Satellite (Figure 4.14A) and airborne (Figures 4.14B to E) images were recorded less than 3h apart (AVHRR: 14:04 GMT; ATM: 11:16-11:54 GMT) and therefore presented a number of highly comparable spatial features. The southern edge of the bloom showed an eastern bloom tail at flight line 5, a large bloom convolution between flight lines 5 and 2 and a bloom appendix between flight lines 2 and 1. The featureless northern bloom edge was similarly shaped in the AVHRR and ATM data, with the exception of the most eastern region not covered by the ATM along-path width. Some common structure was also observed inside the bloom: a highly reflective coccolith core between flight lines 5 and 3 (at about 49° 54'N) and an area of relatively low reflectance (<5% at ATM band 2 and <4% at ATM band 3 and <1% with AVHRR) centred at 49°53'N 5°46'W. The comparison of both data sets overall demonstrated the ATM ability to define the abrupt and convoluted reflectance transition at the bloom edges and the marked meanderings and flow structures within the bloom core.

Comparison between ATM images at the four visible bands showed significantly higher reflectances at bands 2 (485nm 3->7%) and 3 (560nm; 2->6%) (Figures 4.14B and C) than at the lower frequency wavelengths (band 4: 615nm, 0.5->3%; band 5: 660nm, 0.5->2%) (Figures 4.14D and E); this was similar to what had been observed in the *in situ* reflectance spectrum (see Figure 4.12). Band 2 reflectances were on average ~ 1% above the same reflectances at band 3; the core of maximum reflectance values was additionally slightly shifted towards the bloom edge in band 2 with respect to band 3 (maybe due to changing coccolith/cell ratios). The maximum reflectances at the low reflective bands 4 (605-625nm; >3%) and 5 (630-690; >2%) were 2-3 times higher than the corresponding maximum AVHRR (580-680nm) values (>1%), confirming the ~2.7 factor necessary to calibrate AVHRR (see Figure 4.13B).

CHAPTER V. DISCUSSION AND CONCLUSIONS

Physical processes

The evolution of a coastal bloom of the coccolithophore *Emiliania huxleyi* has been studied in the Western English Channel in June 1993 from an early reflective stage to a mature and dissipative phase (3-4 weeks). The time series of combined visible and thermal satellite images in conjunction with the predictions of a numerical model of the stratification parameter (Figure 4.1) indicates that *E.huxleyi* first appeared and developed in an area of relatively high stratification where the tidal currents are weak. The effectively zero resultant wind conditions during this 8-days initial period also seem to have favoured bloom development by minimising cell and coccolith dispersion by wind effects. The subsequent bloom evolution was also strongly determined by meteorological conditions. Strengthening NE winds advected the stratified warm water within which the bloom developed over a distance up to 100km (from Eddystone Bay to the Isles of Scilly) at a maximum speed of 20 cm/s (Figures 4.2 and 4.3). The disappearance of the bloom occurred after its incorporation into the anticyclonic tidal circulation surrounding the Isles of Scilly (Figure 4.4). The divergence of the flow west of the Islands into southward and northward branches suggests bloom removal by dispersion.

The coastal current driving the bloom has been shown to be an important mechanism for regional redistribution not only of heat (Figures 4.5A and 4.7B) and coccolithophores (Figures 4.5A and 4.8) but also of associated chemical and biological properties and other component phytoplankton species. The reduction of particulate organic carbon (POC) in the extremely calcified coccolithophore environment (Figures 4.10A and B) evidences how the bloom waters, arriving in the

area only one day before sampling, replaced the previously established POC-enriched shelf waters, now confined to the bloom boundaries. The dominant influence of the advective field on the chemical distribution is also observed in the C/N ratios (Figure 4.10C), relatively close to the Redfield ratio (*e.g.* Harris, 1986) outside the bloom and markedly increasing (up to 18) within the patch of coccoliths. Distinctly low flagellate densities (1,000- <4,000 cell/ml) (Figure 4.9C) at the coccolithophore stations similarly point to the substitution of the previous flagellate-dominated shelf water mass by a coccolithophore water mass (Figure 4.8B and A) containing additionally a population of *Nitzschia delicatissima* (Figure 4.9A, shaded section). The subsurface chlorophyll *a* maximum (SCM) associated with both populations of *Nitzschia delicatissima* and *Emiliania huxleyi* (Figure 4.7B) (much broader and with a much lower chlorophyll *a* concentration than the SCM outside the bloom) also reflects the biological change brought to the area by advection.

The physical processes not only influenced the temporal evolution of the bloom but also various scales of its spatial structure. The strong thermal front at the southern edge of the coccolithophore bloom (Figures 4.5A and 4.7A) limited offshore patch spreading, thus probably determining a more pronounced growth of the *E.huxleyi* cells towards the coastal zone (Figures 4.8A and B). The meandering shape of this frontal feature (Figure 4.5A) also imposed a distinct spatial dimension (~25km wavelength) (Figures 4.4A and B) within which the distribution of open shelf and bloom water properties covaried (Figure 4.5C). As opposed to the motionless periods, the bloom width was strongly narrowed during the phases of rapid advection around Lizard Head (Figures 4.2A and B) and around the Isles of Scilly (Figures 4.4A and B). In addition to this horizontal compression of the bloom core (Figure 4.4 A and B) the tidal circulation of Isles of Scilly was also probably responsible for deepening to 40-50m depth some fractions of the pools of coccoliths (Figure 4.8B; see

also calcite distribution in Figure 4.10A), *E.huxleyi* empty coccospheres (Figure 4.8C) and cells of *Nitzschia delicatissima*, a component species of the bloom (Figure 4.9A, shaded section ; see also chlorophyll *a* distribution in Figure 4.7B).

E.huxleyi life history strategy

For the first time in a satellite time series, it has been possible to identify the short transitional period of rapid coccolith detachment described in laboratory (Balch *et al.*, 1992b) and mesocosm experiments (Westbroek *et al.*, 1993). This stage was observed to occur (Figures 4.1A and B) as an initial phase (4-12th June) of rapid increase of bloom reflectance and area from minimum (0.7% and 245km^2) to maximum values (3.6% and 1,200km^2). The slowly decreasing reflectance values during the subsequent period of satellite observations (13-26th June) are similarly consistent with the experimental descriptions of *E.huxleyi* in a stationary growth phase. The high coccolith/cell ratios in the bloom core (>170; Figures 4.8A and B) and the presence of supercalcified *E.huxleyi* cells (showing multiple layers of coccoliths; *e.g.* Figure 3.1C) indicates that the bloom was effectively sampled at the final stage of the non-motile *E.huxleyi* phase (Balch *et al.*, 1991) and that the cell division was almost ceasing (Fernández *et al.*, 1993a). The high percentage of empty coccospheres (~30% of the total number of living and dead cells; Figures 4.8C and A) could similarly be explained by cellular lysis and probable release of naked flagellate *E.huxleyi* cells, which represent the subsequent *E.huxleyi* life stage in culture conditions (Klaveness, 1972; Green *et al.*, 1990).

The comparison of particulate carbon and coccolithophore standing stocks of the present bloom with those reported in the last decade shows marked similarities and differences between blooms of shelf and oceanic regions. Maximum *E.huxleyi* cell abundances vary between shelves (2,000 cells/ml; Balch *et al.*, 1991, this work) and

ocean (8,000-10,000 cells/ml; Holligan *et al.*, 1983; Fernández *et al.*, 1993a); by contrast the upper coccolith concentrations show a maximum production stock of about 300,000- 350,000 coccoliths/ml independent of the region in which the bloom develops. *In situ* measurements of particulate inorganic carbon in shelf (Figure 4.9A) and oceanic (Fernández *et al.*, 1993a) conditions similarly point to the existence of an upper threshold of calcite-C production with a value of about 5-6 g/m^2. The observation in the Western English Channel of a morphotype (A) (Figure 3.1C) also reported for oceanic regions (Holligan *et al.*, 1983; Fernández *et al.*, 1993a) indicates that in this area the difference in maximum concentration of *E.huxleyi* cells with respect to the ocean was due to an external factor rather than to genotype diversity. A possible explanation could be higher nitrate concentrations in the ocean (up to 5μM; Holligan *et al.*; 1983; Fernández *et al.*, 1993a) than in shelf waters (<1μM; Figure 4.7C; Balch *et al.*, 1991), thus increasing the photosynthetic efficiency (α^c) and the maximum potential photosynthetic rate (P_m^c) of the oceanic *E.huxleyi* cells (Fernández *et al.*, 1993a; Balch *et al.*, 1992).

The high ratios of dissolved nitrate-to-phosphate (N/P) associated with the coccolithophore waters (up to 13, Figures 4.7C and D) are consistent with the activation by *E.huxleyi* of the facultative alkaline phosphatase that hydrolyses dissolved organic phosphorus (DOP) (Kuenzler and Perras, 1965; Holligan *et al.*, 1993b; Westbroek *et al.*, 1993). A similar conclusion is suggested by the distinct appearance inside the bloom of the small diatom *Nitzschia delicatissima* (Figures 4.8B and 4.9A), a characteristic species of waters that have a high content of dissolved organic compounds (D.H.Harbour pers.com.). The effect of phosphate starvation on organic growth can probably be discarded as the observed N/P ratio (below the Redfield ratio of 16) indicates that a potential nutrient limitation would have been related to nitrate rather than to phosphate concentrations. One possible explanation

relating the phosphatase mechanism and the bloom occurrence could be cleavage of DOP compounds known to inhibit calcite growth (Klaveness and Paasche, 1979), thus enhancing coccolith production.

Biogeochemical significance

The total calcite production of the bloom in June 1992 has been calculated from the bloom area (1,200km^2) on the day of maximum development (12th June) and the value of particulate inorganic carbon (PIC) integrated over the bloom depth during the sampling days 25 and 26 (6gC/m^2). Since the sinking of PIC out of the mixed layer was negligible (Figure 4.10A) the coccolithophore bloom production can be estimated as 60,000 tonnes of calcite or 7,200 tonnes of calcite-C. For comparison, the organic carbon production of the spring diatom bloom in an area of the same extent has been calculated as 18,000 tonnes C, using an average daily production rate of 1.5gC/m^2.day during the spring diatom bloom in the Western English Channel (Jordan and Joint, 1984) and assuming an average bloom life of 10 days. The bloom of coccolithophores studied in the present work represented, in inorganic carbon alone, 40% of the carbon production per unit area of the spring bloom of the Western English Channel. Assuming that 50-75% of the organic carbon produced during the spring diatom bloom is recycled within the euphotic zone (Falkowski *et al.*, 1988; Walsh, 1989), it can be concluded that the presence of this coccolithophore bloom exporting its calcite-C to the sediments had in the local C export budget the equivalent effect of a second spring bloom, the most important annual bloom at temperate latitudes.

The standing stock of DMS during the 1992 bloom has been estimated from the mean concentration of *E.huxleyi* cells in the upper 30m at the time of sampling (773 cells/ml) and an average cell-specific DMSP value of 3.8pg measured in a similar shelf bloom at the Gulf of Maine (Matrai and Keller, 1993). Assuming a DMSP-to-

DMS mole conversion, the concentration of organic sulphur potentially released into the bloom waters was 21.9 nmol DMS-S/l. This value represents a 7 fold increase with respect to the mean level in the global oceans (3.1nmol DMS-sulphur/l; Andreae, 1986), underlying the importance of the blooms for sulphur cycling. Assuming that the DMS concentration in air is negligible in comparison with bloom surface waters and using a sea-to-air DMS transfer velocity of 2.90 m/day (global and year-round average for shelf regions; Andreae, 1986), the calculated DMS-S concentration of the bloom yields a maximum flux of DMS-S to the atmosphere of 6.35nmol S/cm^2.day. A more accurate estimate of the evasion of DMS to the atmosphere will however have to include factors affecting DMSP-DMS conversion such as bacterial (Kiene and Bates, 1990) and chemical degradation (Brimblecombe and Shooter, 1986).

Optical properties

The extent to which the coccolithophore bloom changed the optical properties of the water column has been examined. An *in situ* reflectance spectrum (Figure 4.12) was shown to characterise the coccolithophore bloom environment and the surrounding stratified and tidally mixed waters. The study has also provided a first approach to determining the relationships between density of coccoliths, satellite AVHRR reflectance (Ravhrr) and optical properties such as red beam attenuation coefficient (c660), PAR diffuse attenuation coefficient (K(PAR)) and Secchi disk depth (Figures 4.6A, B and C and Figures 4.11B, C and D) (see Holligan *et al.* (1993a) for Ravhrr-c536 relationship). The relationship between AVHRR (580-680nm) and *in situ* (632nm) reflectance (Figure 4.13B) will enable for subsequent studies a straightforward calibration of band 1 of the AVHRR (NOAA-11). Of particular importance was the application of the coccolith related optical properties to the underway mapping of the surface bloom distribution (*i.e.* surface measurements of red beam attenuation coefficient; Figure 4.5C) and to the resolution of the meandering

fine-structure (120 x 120m) at the bloom core and edges (*i.e.* airborne survey with the ATM multispectral scanner, Figures 4.14B to E).

Reduction of the light available for photosynthesis below the surface layer occupied by the coccolithophores was probably a major factor inhibiting the development of the thermocline chlorophyll maximum (see Figures 4.7A and B). Coccolith backscattering reflecting light out of the bloom water (Figure 4.12) meant that 10-15% less of the incoming solar radiation (400-600nm) was available for subsurface phytoplankton growth. Further shading of the thermocline was due to extreme coccolith densities (up to 300,000 coccoliths/ml) attenuating the vertical distribution of PAR light up to 0.3 m^{-1} (Figure 4.11A and B). The coccolith-induced light field may have also favoured the growth of phytoplankton species able to grow under low light levels. It is noted in this context that *Gyrodinium aureolum*, observed below the densest coccolith layer (>300,000 coccoliths/ml) (Figures 4.8B and 4.9B), adapts to low light levels by increasing significantly the chlorophyll content per cell (Garcia and Purdie, 1992), can form its own blooms despite autoshading (Holligan, 1987) and develops in Norway as late in the year as mid November when the surface irradiation is very reduced (Tangen, 1979). The higher degree of monospecificity reported for coccolithophore blooms with respect to the surrounding non-coccolithophore waters (*e.g.* Holligan *et al.*, 1983; Holligan *et al.*, 1993a) is also consistent with this potential selection of component phytoplankton species by the bloom light environment.

The joint location of the densest cores of *E.huxleyi* cells (>2,000 cells/ml) and coccoliths (>300,000 coccoliths/ml) (Figures 4.8A and B) indicates that *Emiliania huxleyi* by detaching coccoliths was also shading progressively its own light for photosynthetic absorption. This self-shading mechanism, that reduces the assimilation number (P_m^B) of *E.huxleyi* cells (Fernández *et al.*, 1993a), could proceed through

coccolith-related extinction coefficient increments (Figures 4.11A and B) and also through increased coccolith reflectances (up to 12%) in the wavelength region of maximum *E.huxleyi* absorption (Figure 4.12). It is plausible to hypothesise that after an initial and intense coccolith detachment, the core of the growing cells is progressively displaced from the coccolith patch centre to the edges where the light is less restricted and a higher potential maximum growth can take place. The relatively high density of cells occurring at the bloom boundary station 2 (>1,000 cells/ml; 70 coccoliths/cell *cf.* >170 coccoliths/cell at station 4; Figures 4.8A and B) and different locations of the cell core (*i.e.* at the centre of the coccolith patch and at the coccolith patch edges in other studies, Balch *et al.*, (1991), Fernández *et al.*, (1993a)) are consistent with this hypothesis.

Coccolithophore reflectance algorithms

The semianalytical optical model of Balch *et al.* (1991) that expresses surface reflectance at 546nm (R_{546}) as a function of coccolith concentration (NL) and the coccolith/cell ratio (NL/NC) (see Literature Review, Chapter II) has been simplified into a concise algorithm and compared with the distribution of sea-truth results (Figure 5.1A; cf. Figure 2.5D).

The salient features of the conversion of the model into a simple expression can be summarized as follows: (i) the straightforward relation $R=0.35\ b_b/(a+b_b)$ of Gordon *et al.* (1988) (b_b: backscattering; a: absorption; with a π angular distribution function) was used instead of the complex polynomial function of Gordon *et al.* (1975) applied by Balch *et al.* (1991); (ii) the coccolith-specific backscattering used in this study (b_{bL546}: 1.2896×10^{-13} m^2/coccolith) was the first order value of the original polynomial relationship coccolith concentration *vs.* coccolith backscattering (see Figure 2.5B; note that Balch *et al.*(1991) did not observe a significant difference

between their polynomial relationships and straight lines); (iii) the backscattering due to 10 coccoliths was added to the cell-specific backscattering of Balch *et al.* (1991) (b_{bc546}: 0.540 x 10^{-11} m^2/cell) that corresponded to unplated cells, (iv) similarly to the original model, the *E.huxley*i cell-specific absorption (a_{c546}) was 1.17 x 10^{-11} m^2/cell, the absorption by coccoliths was considered negligible and the values of backscattering (b_{bw546}) and absorption (a_{w546}) of pure sea water were taken from Smith and Baker (1981); (v) in the final numerical model, R_{546} remained highly independent of NL/NC (as stated by Balch *et al.*, 1991) and a simple algorithm was formulated fixing NL/NC to an intermediate value of 100 coccoliths/cell (young bloom: 50 coccoliths/cell; old bloom: 150 coccoliths/cell).

$$NL = \frac{(b_{bL546} + b_{bw546}) \times REF_{546} - a_{w546}}{NC/NL \times [a_{c546} - (b_{bc546} \times REF_{546})]} \times 10^{6}$$

$$REF_{546} = \frac{35 - R_{546}}{R_{546}}$$

NL:	coccolith concentration (coccoliths/ml)
NC/NL:	ratio of *E.huxleyi* cells to coccoliths
R_{546}:	surface reflectance at 546nm (%)
b_{bL546}:	coccolith-specific backscattering at 546nm (m^2/coccolith)
b_{bc546}:	cell-specific backscattering at 546nm (m^2/cell)
b_{bw546}:	backscattering of pure sea water at 546nm (m^{-1})
a_{c546}:	cell-specific absorption at 546nm (m^2/cell)
a_{w546}:	absorption of pure sea water at 546nm (m^{-1})

Comparison between the algorithm (Figure 5.1A; lines) and the *in situ* data (white triangles) showed a reflectance shift of ~1% with respect to a best position in the theoretical curve (black triangles) but a general good agreement of both distributions. Assuming no error in the *in situ* measurements, in the model of Balch *et al.* (1991) and in the simplifications of this model applied here, the best fit between the the sea-truth data and the theoretical predictions would correspond to a model

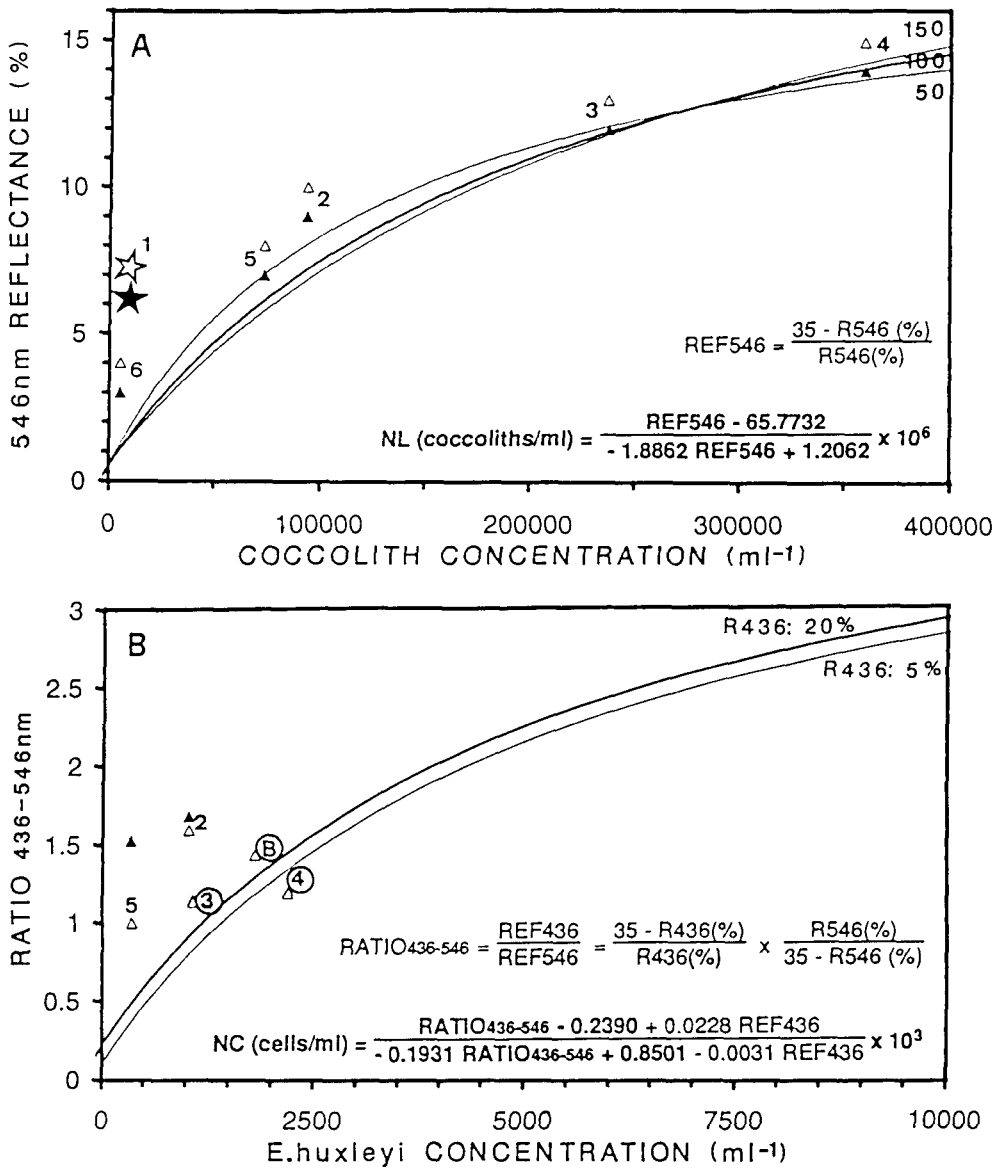

Figure 5.1 A) Simplified reflectance model, derived from Balch *et al.* (1991), relating surface reflectance at 546nm (R_{546}, %) and coccolith concentration (coccoliths/ml). The model was formulated for three bloom coccolith/cell ratios 50: (young bloom, upper thin line), 150 (old bloom; lower thin line) and 100 (broad line). The numerical expression in the figure was derived from the intermediate 100 coccoliths/cell ratio. The marks in the figure show the observed distribution of *in situ* surface reflectance against *in situ* coccolith concentration overlaid on the modelling distribution. Numbers 1 to 6 indicates the coccolithophore bloom stations. White triangles represent direct measurements; black triangles indicate a better approximation of the latter values to the modelling curve after subtracting a reflectance shift of ~1% reflectance. The tidally mixed station 1 is shown as a large star and highlights the limitation of the model in regions with high loads of sediments in suspension. B) Theoretical relationship (lines) between *E.huxleyi* cell concentration (NC; cells/ml) and a reflectance ratio $RATIO_{436\text{-}546}$ derived from the two single band reflectance models (436 and 550nm) of Balch *et al.* (1991). The model was formulated for two distinct values of 436nm reflectance (R_{436}): 5% (low R_{436}; thin line) and 20% (high R_{436}, broad line). The distribution of *in situ* data (cell concentration *vs.* $RATIO_{436\text{-}546}$) was overlaid on the modelling distribution and marked and annotated as in the previous figure. B denotes *in situ* data from Table 1 of Balch *et al.* (1991) corresponding to a shelf *E.huxleyi* bloom in the Gulf of Maine on June 1988.

with a Q value of 3.8, relatively close to the isotropic distribution of light ($Q=\pi$). The limitation of the model was apparent at the tidally mixed station 1 (large star) where characteristic high loads of sediments in suspension gave strong ~550nm reflectance (Kirk, 1983).

The concentration of *E.huxleyi* cells (NC) has also been related, on theoretical grounds, to a reflectance ratio ($RATIO_{546-436}$) between two wavelengths (546nm and 436nm) in the regions of minimum and maximum cell absorption. The relation of Gordon *et al.*(1988b) was developed for each wavelength as in the previous algorithm for coccolith concentration. The coccolith-specific and cell-specific data by Balch *et al.* (1991) were used or modified similarly. Final backscattering and absorption coefficients at 436nm were:

$b_{bL436}= 1.4068 \times 10^{-13}$ m^2/coccolith,

$a_{c436}= 5.62 \times 10^{-11}$ m^2/cell,

$b_{bc436}= 0.750 \times 10^{-11}$ m^2/cell.

Linking both single band expressions by the NL term led to the following equation:

$$NC = \frac{w1RATIO_{436-546}-w2+w3REF_{436}}{-c1RATIO_{436-546}+c2+c3REF_{436}} \times 10^3$$

$$RATIO_{436-546} = \frac{REF_{436}}{REF_{546}} = \frac{35 - R_{436}}{R_{436}} \times \frac{R_{546}}{35 - R_{546}}$$

constants

$w1 = b_{bL436} \times a_{w546}$

$w2 = b_{bL546} \times a_{w436}$

$w3 = (b_{bL546} \times b_{bw436}) - (b_{bL436} \times b_{bw546})$

$c1 = b_{bL436} \times a_{c546}$

$c2 = b_{bL546} \times a_{c436}$

$c3 = -(b_{bL546} \times b_{bc436}) + (b_{bL436} \times b_{bc546})$

where NC represents *E.huxleyi* cell concentration (cell/ml) and the other terminology is specified as in the previous section.

The model, plotted as lines in Figure 5.1B, showed a relationship between *E.huxleyi* cell concentration (NC) and $RATIO_{436-546}$ practically independent of the absolute reflectances at 436nm (R_{436}:20% broad line and R_{436}: 5% thin line); R_{436} could thus be fixed to a constant value in a possible future algorithm. To test the validity of the model in the full range of *E.huxleyi* cell concentrations requires data from an oceanic coccolithophore bloom (up to 10,000cells/ml); some conclusions can however be derived from the measurements of the present shelf study. The applicability of the model seems to be restricted to the inner region of the coccolithophore bloom (triangles at stations 3, 4, and station B from Balch *et al.* 1991). At the bloom edges (triangles at stations 2 and 5), by contrast, the satellite retrieval of *E.huxleyi* cell abundance will be biased by the presence of a high density of flagellates (see Figure 4.9C); these species absorb strongly at 436nm (Morel and Ahn, 1991) and are also a common feature at the edges of oceanic coccolithophore blooms (Fernández *et al.*, 1993a).

Further research work on *E.huxleyi* blooms

An immediate remote sensing extension of the present research derives from the recent development of a classifying methodology (Brown and Yoder, 1994a; b) to retrieve the interannual mean location, duration and size of coccolithophore blooms from the NASA CZCS data set (Feldman *et al.*, 1989). This approach is relevant to our coccolithophore study as it could allow us to test the observed relationship between bloom occurrence and high values of the stratification parameter (Pingree and Griffiths, 1978) over averaged areas of frequent bloom development. A large regional characterisation of the temporal and spatial distribution of coccolithophore blooms would additionally permit assessment of the impact of the blooms on the variability of inorganic carbon and organic sulphur production. Three major problems will have to

be overcome when developing this work: the presence of suspended sediments displaying a similar reflectance pattern to that of the blooms, the occurrence of heavy cloud cover in particular years (biasing the variation of bloom timing and size), and the detection of the classified blooms in a very late development stage due to the strong reflectance decision boundaries of the method of Brown and Yoder (1994a; b).

The wider significance of the Thesis derives from the imminent availability of data from the multispectral colour scanner SeaWiFS (General Science Corporation, 1991). The use of band 4 (545-565nm) of this new colour sensor and a single band algorithm similar to that analysed in this work (Figure 5.1A), will allow coccolith related properties to be directly monitored from space. This will be particularly relevant to investigation of calcite build-up during the early bloom stages (see Figure 4.1A). A SeaWiFS reflectance $RATIO_{490\text{-}555}$ (band 3: 480-500nm and band 4: 545-565nm), comparable in structure to that presented in this study (Figure 5.1B), may also enable *E.huxleyi* cell distributions to be remotely sensed. The SeaWiFS band 3 would take advantage of the very low absorption at 490nm by the flagellates (Morel and Ahn, 1991) and the distinct *E.huxleyi* pigment 19' hexanoyloxylfucoxanthine (absorption maximum at 520nm and up to 85% of the total *E.huxleyi* carotenoids (Haxo, 1985)). Studies of bloom ageing dynamics and the spatial variability of the core of growing cells (Figures 4.8A and B), processes associated with the proportion of cells to coccoliths, could benefit from this approach.

Summary of achievements

I. AVHRR satellite imagery (visible and thermal bands) in conjunction with ship and airborne surveys has been used to investigate the physical factors associated with the development, advection and disappearance (3-4 weeks life time) of a shelf bloom of the coccolithophore *Emiliania huxleyi* in the Western English Channel in June 1992. The physical processes that appeared important in patch evolution and structure are, differential stratification in an area of weak tidal currents, initial zero wind conditions (allowing local development), later strengthening NE winds (driving a coastal warm surface current), entrainment of the bloom water into the anticyclonic tidal circulation around the Isles of Scilly and finally bloom dispersal by mixing and flow divergence.

II. The short transitional period of rapid coccolith detachment described in laboratory and mesocosm experiments has been first identified for the first time in a satellite time series as an initial phase of rapid increase of bloom reflectance and area. The stationary *E.huxleyi* growth phase described in laboratory batch cultures had also a correspondence in a subsequent longer period of steady bloom AVHRR reflectances. Observations during the ship survey of high coccolith/cell ratios in the bloom core and supercalcified *E.huxleyi* cells indicates that the bloom was effectively sampled at a final phase when the cell division was almost ceasing. The high percentage of empty coccospheres could be similarly explained by cellular lysis and release of flagellate *E.huxleyi* cells which represent the subsequent life stage in culture conditions.

III. The extent to which the bloom changed the local optical structure (red beam attenuation coefficient, PAR diffuse attenuation coefficient, *in situ* reflectance spectra (415-660nm) and Airborne Thematic Mapper reflectance) has been investigated. The bloom optical properties were used to map the surface bloom distribution and to resolve from aircraft the meandering fine-structure of the bloom; they were also correlated with coccolith concentrations in order to quantify future optical estimates.

The coccolith-induced light field appeared to be associated with three main biological effects: inhibition of the chlorophyll maximum development by shading of the thermocline, possible selection of phytoplankton species able to grow under low light levels (*Gyrodimium aureolum*) and progressive self-shading of the *E.huxleyi* population.

IV. A semianalytical optical model relating surface reflectance at 546nm and coccolith concentrations (Balch *et al.*, 1991) has been simplified into a concise algorithm for remote sensing. Comparison of the algorithm with sea-truth data has shown a reasonably good agreement between both distributions in the full range of coccolith concentrations (0-400,000 coccoliths/ml). The algorithm can not be applied to tidally mixed areas as a result of characteristic high loads of suspended sediments giving a strong reflectance at 550nm. The concentration of *E.huxleyi* cells has also been related, on theoretical grounds, to a reflectance ratio, respectively in the regions of minimum (546nm) and maximum (446nm) pigment absorption. The potential applicability of the relationship would be limited to the inner region of the coccolithophore bloom, that has relatively low densities of flagellates (species absorbing strongly at 446nm). The use in future of the SeaWiFS band 3 (480-500nm) could overcome this limitation and take additional advantage of the distinct *E.huxleyi* pigment 19'hexanoyloxyfucoxanthin.

The combined results of satellite, airborne and ship-based observations of this Thesis are relevant to future investigations of large-scale blooms of coccolithophores such as those observed by CZCS in the Bay of Biscay (Figure 5.2). The use of ocean colour remote sensing from future satellites will allow extrapolation of the local biological observations from ships to the whole bloom extent. The success of these studies will ultimately be dependent on combining the field survey with historic and real-time remote sensing as has been demonstrated on a smaller scale in thisThesis.

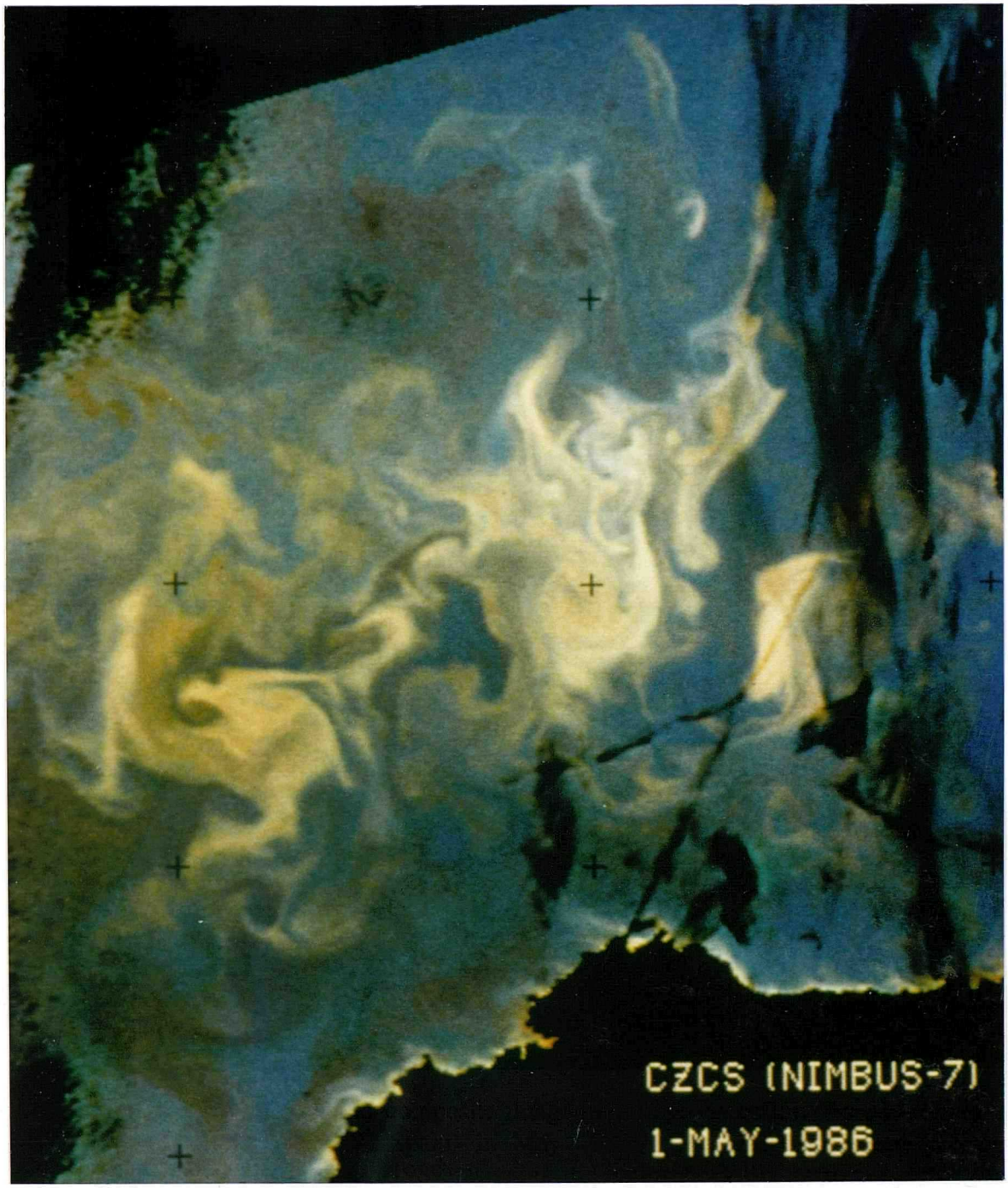

Figure 5.2 CZCS colour composite image of a large coccolithophore bloom in the Bay of Biscay (off NW Spain) in May 1986. The image has been produced (following Holligan *et al.*, 1989) asigning the atmospherically corrected reflectances for band 1 (blue), 2 (green) and 3 (yellow) to blue, green and red colours in the image thereby giving a seminatural colour image. Clear high salinity water appears blue as a result of the lower absorption of blue light by sea water. The combined effects of backscattering and absorption give rise to intermediate colour patterns of the different phytoplankton populations. Coccolithophores appear as white reflectances due to backscattering in all three visible bands. It is remarkable in the image the spatial scale of the bloom and the eddy-like finestructure how the bloom edges are evolving.

REFERENCES

Abbot,M.R., Carder,K., Brown,O.B., Evans,O.B., Gordon,H.R., Muller-Karger,F.E. and Esaias,W.E. (1994) Ocean colour in the 21st century: A strategy for a 20-year time series. *NASA Tech. Mem. 104566*, vol. 17, 20 pp.

Ackleson,S., Balch,W.M. and Holligan,P.M. (1988) White waters of the Gulf of Maine. *Oceanography*, 1, 18-22.

Aiken,J. (1981) A chlorophyll sensor for automatic remote operation in the marine environment. *Mar. Ecol. Prog. Ser.*, 4, 235-239.

Aiken,J. and Bellan,I. (1990) Optical oceanography: an assessment of a towed method. *In* Herring,P.J., Campbell,A.K., Whitfield,M. and Maddock,L. (eds.), Light and life in the sea. Cambridge University Press, Cambridge, pp. 39-57.

Andreae,M.O. (1986) The ocean as a source of atmospheric sulphur compounds. *In* Buat-Menard,P. (ed.), The role of air-sea exchange in geochemical cycling. Reidel, Dordrecht, pp. 331-362.

Andreae,M.O. (1990) Ocean-atmosphere interactions in the global biogeochemical sulphur cycle. *Mar. Chem.*, 30, 1-29 .

Arias,E., Manriquez,P., Caldentey,P. and Sousa,J.M. (1980) Hidrografia de la plataforma costera de Vizcaya y Guipuzcoa (Febrero a Diciembre de 1976). *Inv. Pesq.*, 44, 13-34.

Austin,R.W. (1974) The remote sensing of spectral radiance from below the ocean surface. *In* Jerlov,N.G. and Nielsen,E.S. (eds.), Optical aspects of Oceanography. Academic Press, London, pp. 317-344.

Austin,R.W. (1980) Gulf of Mexico ocean colour surface truth measurements. *Boundary-layer Meteorol.*, 18, 269-285.

Austin,R.W. and Petzold,T.J. (1981) The determination of the diffuse attenuation coefficient of sea water using the coastal zone color scanner. *In* Gower,J.R.F. (ed.) Oceanography from Space. Plenum Press , New York, pp. 239-256.

Balch,W.M. (1993) Reply. *J. Geophys. Res.*, 98, 16,585-16,587.

Balch,W.M., Abbott,M.R. and Eppley,R.W. (1989) Remote sensing of primary production I: A comparison of empirical and semianalytical algorithms. *Deep-Sea Res.*, 36, 281-295.

Balch,W.M., Evans,R.E., Brown,J., Feldman,G., McClain,C. and Esaias,W. (1992a) The remote sensing of ocean primary productivity: Use of a new data compilation to test satellite algorithms. *J. Geophys. Res.*, 97, 2,279-2,293.

Balch,W.M., Holligan,P.M., Acklesson,S.G. and Voss,K.J. (1991) Biological and optical properties of mesoscale coccolithophore blooms in the Gulf of Maine. *Limnol. Oceanogr.*, 36, 629-643.

Balch,W.M., Holligan,P.M. and Kilpatrick,K.A. (1992b) Calcification, photosynthesis and growth of the bloom-forming coccolithophore *Emiliania huxleyi. Cont. Shelf. Res.*, 12, 1353- 1374.

Bannister,T.T. (1974) Production equations in terms of chlorophyll concentration, quantum yield and upper limit to production. *Limnol. Oceanogr.*, 19, 1-12.

Banse,K. and Yong,M. (1990) Sources of variability in satellite-derived estimates of phytoplankton production in the Eastern Tropical Pacific. *J. Geophys. Res.*, 95, 7,201-7,215.

Bartz,R.J, Zaneveld,R.V. and Pak,H. (1978) A transmissometer for profiling and moored observations in water. *SPIE (Ocean Opt.)*, 5, 102-108.

Baumann,I.G., Isenberg, H.D., Gennaro,J. (1978) The inverse relationship between nutrient nitrogen concentration and coccolith clasification in cultures of the coccolithophorid *Hymenomonas* sp. *J. Protozool.*, 25,253-256.

Berge,G. (1962) Discoloration of the sea due to *Coccolithus huxleyi* "bloom". *Sarsia*, 6, 27-40.

Bikernes,I. and Braarud,T. (1952) Phytoplankton in the Oslo Fjord during a *Coccolithus huxleyi* summer". *Avh. norske Vidensk. Akad. Oslo*, 1952/2, 1-23.

Bishop,J.K.B. and Marra,J. (1984) Variations in primary production and particulate carbon flux through the base of the euphotic zone at the site of the Sediment Trap Intercomparison Experiment (Panama Basin). *J. Mar. Res.*, 42, 189-206.

Bishop,J.K.B. and Rossow,W.B. (1991) Spatial and temporal variability of surface solar irradiance. *J. Geophys. Res.*, 96, 16,839-16,858.

Blackburn,S.I. and Cresswell,G. (1993) A coccolithophorid bloom in Jervis Bay, Australia. *Aust. J. Mar. Freshwater Res.*, 44, 253-60.

Borman,A.H., De Vrind-De Jong,E.G., Thierry,R., Westbroek,P. and Bosch,L. (1987) Coccolith associated polysaccharides from cells of *Emiliania huxleyi* (Haptophyceae). *J. Phycol.*, 23, 118-123.

Borstad,G.A, Hill,D.A. and Kerr,R.C. (1989) Use of the Compact Airborne Spectroscopy Imager (CASI): Laboratory examples. Proceedings IGARSS'89/12th Canadian Symposium on Remote Sensing, IEEE, 4, 2,081-2,084.

Brand,L.E. (1982) Genetic varability and spatial patterns of genetic differentation in reproductive rates of the marine coccolithophores *Emiliania huxleyi* and *Gephyrocapsa oceanica*. *Limnol. Oceanogr.*, 27, 236-245.

Bratbak,G., Egge, J.K. and Heldal, M. (1993) Viral mortality of the marine alga *Emiliania huxleyi* (Haptophyceae) and termination of algal blooms. *Mar. Ecol. Prog. Ser.*, 93, 39-48.

Bricaud,A. and Morel,A. (1987) Atmospheric corrections and interpretation of marine radiances in CZCS imagery: Use of a reflectance model. *Oceanol. Acta*, SP(6), 33-50.

Brimblecombe,P. and Shooter,D. (1986) Photo-oxidation of dimethyl sulphide in aqueous solution. *Mar. Chem.*, 19, 343-353.

Brown,C.W. and Yoder,J.A. (1994a) Coccolithophorid blooms in the global ocean. *J. Geophys. Res.*, 99, 467-482.

Brown,C.W. and Yoder,J.A. (1994b) Distribution pattern of coccolithophorid blooms in the NW Atlantic ocean. *Cont. Shelf Res.*, 14, 175-194.

Brown,O.B., Evans,R.H., Brown,J.W., Gordon,H.R., Smith,R.C. and Baker,K.S. (1985) Phytoplankton blooming off the U.S. East coast: A satellite description. *Science*, 229, 163-167.

Campbell,J.W. and O'Reilly,J.E. (1988) Role of satellites in estimating primary production on the NW Atlantic continental shelf. *Cont Shelf Res.*, 8, 179-204.

Carder,K.L. and Steward,R.G. (1985) A remote sensing reflectance model of a red-tide dinoflagellate off west Florida. *Limnol. Oceanogr.*, 30, 268-298.

Charlson,R.J., Lovelock,J.E., Andreae,M.O. and Warren,S.G. (1987) Oceanic phytoplankton, atmospheric sulphur, cloud albedo and climate. *Nature*, 326, 655-661.

Cornillon,P, Evans,D., Brown,O.B., Evans,R., Eden,P. and Brown,J. (1988) Processing, compression and transmission of satellite IR data for near real-time use at sea. *J. Atmos. Ocean Tech.*, 5, 321- 327.

Degens,E.T. and Ittekot,V. (1986) Ca^{++} stress, biological response and particle aggregation in the aquatic habitat. *Neth. J. Sea Res.*, 20, 109-116.

Donoghue,D.N.M. and Hook,S.J. (1986) Pre-processing of airborne multispectral data: A necessity for quantitative remote sensing. *In* Proceedings of the NERC 1985 Airborne Campaign Workshop. NERC, Swindon, E13-E17.

Emery,W.J, Thomas,A.C., Collins,M.J., Crawford,W.R. and Maklas,D.L. (1986) An objective method for computing advective surface velocities from sequential infra-red satellite images. *J. Geophys. Res.*, 91, 12,865-12,878.

Eppley,R.W., Stewart,E., Abbot,M.R. and Heyman,U. (1985) Estimating ocean primary production from satellite chlorophyll: Introduction to regional differences and statistics for the Southern California Bight. *J. Plankton Res.*, 7, 57-70.

Eppley,R.W., Stewart,E., Abbot,M.R. and Owen,R.W. (1987) Estimating primary production from satellite-derived chlorophyll: Insights from the Eastropac data set. *Oceanol. Acta*, SP(6), 109- 113.

Esaias,W.E., Feldman,G., McClain,C.R. and Elrod,J.A. (1986) Satellite observations of oceanic primary productivity. *EOS*, 67, 835-837.

Falkowski,P.G., Flagg,C.N., Rowe,G.T., Smith,S.L., Whitledge,T.E., and Wirick,C.D. (1988) The fate of the spring diatom bloom: export or oxidation? *Cont. Shelf Res.*, 8, 457-484.

Falkowski,P.G., Kim,Y., Kolber,C., Wilson,C., Wrick,C. and Cess,R. (1992) Natural *versus* anthropogenic factors affecting low-level cloud albedo over the North Atlantic. *Science*, 256, 1,311-1,313.

Feldman,G., Kuring,N., Ng,C., Esaias,W., McClain,C., Elrod,N., Maynard,D., Endres,D., Evans,R. , Browns,J., Walsh,S., Carle,M. and Podesta,G. (1989) Ocean color: Availability of the global data set. *EOS*, 70, 634-635.

Fernández,E., Boyd,P., Holligan,P.M. and Harbour,D.S. (1993a) Production of organic and inorganic carbon within a mesoscale coccolithophore bloom in the NE Atlantic. *Mar. Ecol. Prog. Ser.*, 97, 271-285.

Fernández,E., Cabal,J., Bode,J.L., Botas,A. and Garcia-Soto,C. (1993b) Plankton distributions across a slope-current induced front in the Southern Bay of Biscay. *J. Plankton Res.*, 15, 619- 641.

Fisher,N.S. and Honjo,S. (1991) Intraspecific differences in temperature and salinity responses in the coccolithophore *Emiliania huxleyi*. *Biol. Oceanogr.*, 6, 335-361.

Fraga,F. (1981) Upwelling off the Galician coast, NW Spain. *In* Richards,F.A. (ed.), Coastal upwelling. American Geophysical Union, Washington D.C., pp.176-182.

Frouin,R., Fiuza,A.F.G., Ambar,I. and Boyd, T. (1990) Observations of a poleward surface current off the coasts of Portugal and Spain during winter. *J. Geophys. Res.*, 95, 679-691.

Gallois,R.W. (1986) Coccolith blooms in Kimmeridge Clay and the origin of the North Sea oil. *Nature*, 259, 473-475.

Garcia,C.A.E. and Robinson,I.S. (1991) Chlorophyll *a* mapping using Airborne Thematic Mapper in the Bristol Channel (South Gower coastline). *Int. J. Remote Sensing*, 12, 2,073-2,086.

Garcia,C.A.E. and Robinson,I.S. (1989) Sea surface velocities in shallow seas extracted from sequential CZCS satellite data. *J. Geophys. Res.*, 94, 12,681-12,692.

Garcia,V.M.T and Purdie,D.A. (1992) The influence of irradiance on growth, photosynthesis and respiration of *Gyrodinium* cf. *aureolum*. *J. Plankton Res.*, 14, 1,251-1,265.

Garcia-Soto,C., Halliday,N.C.H., Groom,S.B., Lavin,A. and Coombs,S.H. (1991) Satellite imagery, hydrography and plankton distribution off the NW coast of Spain in April 1991. *Cons. int. Explor. Mer* (CM Papers and Reports), C:17.

Garcia-Soto,C. and Madariaga,I. de (1994) Spring phytoplankton bloom in the SE Bay of Biscay during April 1991. *Kobie*, 22 (in press).

Garcia-Soto,C., Madariaga,I. de, Villate,F. and Orive,E. (1990) Day-to-day variability in the plankton community of a coastal shallow embayment in response to changes in river runoff and water turbulence. *Estuar. coast. Shelf. Sci.*, 31, 217-229.

General Science Corporation (1991) SeaWiFS science data and information system architecture report. General Sciences Corporation, Laurel, 133 pp.

Gordon,H.R. (1978) Removal of atmospheric effects from satellite imagery of the oceans. *Appl. Opt.*, 17, 1,631-1,636.

Gordon,H.R. (1981) A preliminary assesment of the NIMBUS-7 CZCS atmospheric correction algorithm in a horizontally homogeneous atmosphere. *In* Gower,J.F.R. (ed.) Oceanography from Space. Plenum Press, New York, pp. 257-265.

Gordon, H.R., Austin,R.W., Clark,D.C., Hovis,W.A and Yentsch, C.S. (1985) Ocean colour measurements. *Adv. Geophys.*, 27, 297- 333.

Gordon,H.R., Brown,J.W. and Evans,R.H. (1988a) Exact Rayleigh scattering calculations for use with the Nimbus-7 Coastal Zone Colour Scanner. *Appl. Opt.*, 14, 417-427.

Gordon,H.R., Brown,O.B., Evans,R.H., Brown,J.W., Smith,R.C., Baker,K.S and clark,D.K. (1988b) A semianalytical radiance model of ocean color. *J. Geophys. Res.*, 93, 10,909-10,904.

Gordon,H.R., Brown,O.B. and Jacobs,M.M. (1975) Computed relationships between the inherent and apparent optical properties of a flat homogeneous ocean. *Appl. Opt.*, 14, 417-427.

Gordon,H.R. and Clark,D.K. (1980) Remote sensing optical properties of a stratified ocean: An improved interpretation. *Appl. Opt.*, 18, 3,428-3,430.

Gordon,H.R., Clark,D., Brown,J., Brown,O., Evans,R. and Broenkow,W. (1983) Phytoplankton pigment concentration in the Middle Atlantic Bight: Comparison of ship determinations and CZCS estimates. *Appl. Opt.*, 22, 20-36.

Gordon,H.R. and McCluney,W.R. (1975) Estimation of the depth of sunlight penetration in the sea for remote sensing. *Appl. Opt.* 14, 413-416.

Gordon,H.R. and Morel,A. (1983) Remote assessment of ocean colour for interpretation of satelite visible imagery: a review. Springer-Verlag, New York, 114 pp.

Gower,J.F.R and Borstad,G.A (1981) Use of the *in vivo* fluorescence line at 685nm for remote sensing surveys of chlorophyll *a.* *In* Gower,J.F.R (ed.), Oceanography from space. Plenum Press, London, 329-338.

Gower,J.F.R, Borstad,G.A., Gray,L.H. and Edel,H.R. (1987) The Fluorescence Line Imager: Imaging spectroscopy over water and land. Proceedings of the 11th Canadian Symposium on Remote Sensing, Waterloo, 689-697.

Gran,H.H. (1912) Pelagic plant life. *In* Murray,J.and Hjort,J. (eds.), The depths of the ocean. MacMillan and Co., London, pp. 307-386.

Grashoff,K. (1976) Methods of seawater analysis. Verlag-Chemie, Weinheim, 317 pp.

Grashoff,K. Ehrhardt,M. and Kremling,K. (1983) Methods of seawater analysis, 2nd edition. Verlag-Chemie, Weinheim, 419 pp.

Green,J.C., Perch-Nielsen,K. and Westbroek,P. (1990) Prymnesiophyta. *In* Margulis,L., Corliss,J.O., Melkonian,M. and Chapman,D.J. (eds.), Handbook of Protoctics. Jones and Barlett, Boston, pp. 293-317.

Grepma (1988) Satellite (AVHRR/NOAA-9) and ship studies of a coccolithophore bloom in the Western English Channel. *Mar. Nature*, 1, 1-14.

Groom,S.B. and Cooper,E. (1989) Real-time satellite processing for transmission to NERC ships. *NERC Computing,* 47, 47-51.

Groom,S.B., Moore,G.F., Aiken,J. and Allen,C.M. (1989) Aircraft and ship observations of coastal waters off the North Yorkshire coast. *In* Proceedings of the NERC 1988 Airborne Campaign Workshop. NERC, Swindon, 155-186.

Groom,S.B. and Holligan,P.M. (1987) Remote sensing of coccolithophore blooms. *Adv. Space Res.*, 7, 73-78.

Harris,G.P. (1986) Phytoplankton ecology: Structure, function and fluctuation. Chapman and Hall, London, 384 pp.

Harris,G.P., Haffner,G.D. and Piccinin,B.B. (1980) Physical variability and phytoplankton communities II: Primary productivity by phytoplankton in a physically variable environment. *Arch. Hydrobiol.*, 88, 393-425.

Harrison,W.G. and Platt,T. (1986) Photosynthesis-Irradiance relationships in polar and temperate phytoplankton populations. *Polar Biol.*, 5, 153-164.

Haynes,R. and Barton,E.D. (1990) A poleward flow along the Atlantic coast of the Iberian peninsula. *J. Geophys. Res.*, 95, 11,425-11,441.

Haxo,F.T. (1985) Photosynthetic action spectrum of the coccolithophorid *Emiliania huxleyi* (Haptophyceae): 19' hexanoyloxyfucoxanthin as anthena pigment. *J. Phycol.*, 21, 282- 287.

Hemery,G. and Wald,L. (1986) Etude des fronts de maree et des deplacements des masses d'eau sur les cotes atlantiques francaises et en Manche occidentale. Rapport final de Convention. C.R.B.P.O./M.E.R., Paris, 17 pp.

Højerslev,N.K., (1982) Bio-optical properties of the Fladen Ground: "Meteor"-FLEX-75 and FLEX-76. *J. Cons int. Explor. Mer*, 40, 272-290.

Holligan,P.M. (1987) The physical environment of exceptional phytoplankton bloom in the NE Atlantic. *Rapp. P.-V. Reun.*, 187, 9-18.

Holligan,P.M. (1992) Do marine phytoplankton influence global climate? *In* Falkowski,P.G., Woodhead,A.D. (eds.), Primary productivity and biogeochemical cycles in the sea. Plenum Press, New York, pp. 487-501.

Holligan,P.M., Aarup,T. and Groom,S.B. (1989) The North Sea satellite colour atlas. *Cont. Shelf Res.*, 9, 667-765.

Holligan.P.M. and Balch,W.M. (1991) From oceans to cells: Coccolithophore optics and biogeochemistry. *In* Demers,S. (ed.) Particle analysis in Oceanography. Springer-Verlag, Berlin, pp. 301-324.

Holligan,P.M., Fernández,E., Aiken,J., Balch,W.M., Boyd,P., Burkill,P.H., Finch,M., Groom,S.B., Malin,G., Muller,K., Purdie,D.A., Robinson,C., Trees,C., Turner,S.M. and Van der Waal,P.A. (1993a) A biogeochemical study of the coccolithophore *Emiliania huxleyi* in the N Atlantic. *Global Biogeochem. Cycles*, 7, 879-900.

Holligan,P.M. and Groom,S.B. (1986) Phytoplankton distributions along the Shelf Break. *Proc. R. Soc. Edinb. (B)*, 88, 239-263.

Holligan,P.M., Groom,S.B. and Harbour, D.S. (1993b) What controls the distribution of the coccolithophore *Emiliania huxleyi* in the North Sea? *Fish. Oceanogr.*, 2, 175-183.

Holligan,P.M. and Harbour,D.S. (1977) The vertical distribution and succession of phytoplankton in the Western English Channel. *J. mar. biol. Ass. U.K.*, 57, 1,075-1,093.

Holligan,P.M., Viollier,M., Harbour,D.S., Camus,P. and Champagne-Philippe,M. (1983) Satellite and ship studies of coccolithophore production along a continental shelf-edge. *Nature*, 304, 339-342.

Holm-Hansen,O., Lorenzen,C.J., Holmes,R.W. and Strickland,J.D.H. (1965) Fluorimetric determination of chlorophyll. *J. Cons. int. Explor. Mer*, 30, 3-15.

Honjo,S. (1976) Coccoliths: Production, transportation and sedimentation. *Mar. Micropaleontol.*, 1, 65-79.

Honjo,S. and Roman,M.R. (1978) Marine copepod faecal pellets: Production, preservation and sedimentation. *J. mar. Res.*, 36, 45-57.

Hooker,S.B., Esaias,W.E., Feldman,G.C., Gregg,W.W. and McClain,C.R. (1992) An overview of SeaWiFS ocean colour. *NASA Tech. Mem. 104566*, vol.1, 24 pp.

Hovis, W.A., Clark,D.K., Anderson,F., Austin,R.W., Wilson,W.H., Baker,E.T., Ball,D., Gordon,H.R., Mueller,J.L., El Sayed,S.W., Sturm,B., Wrigley,R.C. and Yentsch,C.S. (1980) Nimbus-7 Coastal Zone Colour Scanner: system description and initial imagery. *Science,* 210, 60-63.

Jain,A.K. (1989) Fundamentals of digital image processing. Prentice-Hall, Englewood Cliffs, 569 pp.

Jassby,A.T. and Platt,T. (1976) Mathematical formulation of the relationship between photosynthesis and light for phytoplankton. *Limnol. Oceanogr.*, 21, 540-547.

Jerlov,N.G. (1976) Marine optics. Elsevier, Amsterdam, 231 pp.

Jordan,M.B. and Joint,I.R. (1984) Studies on phytoplankton distribution and primary production in the Western English Channel in 1980 and 1981. *Cont. Shelf Res.*, 3, 25-34.

Kaufman,Y.J. and Holben,B.N. (1993) Calibration of the AVHRR visible and near IR bands for atmospheric scattering, ocean glint and desert reflection. *Int. J. Remote Sensing*, 14, 21-52.

Keller,M.D., Bellows,W.K. and Guillard,R.R.L. (1989) Dimethyl sulphide production in marine phytoplankton. *In* Saltzman,E.S. and Cooper,W.J. (eds.), Biogenic sulphur in the marine enviroment. American Chemical Society, Washington, pp. 167-182.

Kiene,R.P. and Bates,T.S. (1990) Biological removal of dimethyl sulphide from seawater. *Nature*, 345, 702-745.

Kirk,J.T.O. (1981) A Monte Carlo study of the nature of the underwater light field and the relationship between optical properties in turbid waters. *Aust. J. Mar. Freshwater Res.*, 32, 51-532.

Kirk,J.T.O. (1983) Light and photosynthesis in aquatic ecosystems. Cambridge University Press, Cambridge, 401 pp.

Kirwood,D.S. (1989) Simultaneous determination of selected nutrients in sea water. *Cons. int. Explor. Mer* (CM Papers and reports), C29.

Klaveness,D. (1972) *Coccolithus huxleyi* (Lohm.) Kamptn II: The flagellate cell, aberrant cell types, vegetative propagation and life cycles. *Br. Phycol. J.*, 7, 309-318.

Klaveness,D. and Paasche,E. (1971) Two different *Coccolithus huxleyi* cell types uncapable of coccolith formation. *Arch. Mikrobiol.*, 75, 382-385.

Klaveness,D. and Paasche,E. (1979) Physiology of coccolithophorids. *In* Levandowsky,M. and Hutner,S.H. (eds.), Biochemistry and physiology of Protozoa, 2nd edition. Academic Press, New York, pp. 191-213.

Kuenzler,E.J.and Perras,J.P. (1965) Photophatases of marine algae. *Biol. Bull. mar. biol. Lan.*, 128, 271-284.

Lewis,M., Warnock,R.E. and Platt,T. (1986) Photosynthetic response of marine picoplankton at low photon flux. *Can. Bull. Fish Aquatic Sci.*, 214, 235-250.

Linschooten,C., Van Bleijswijk,J.D.L., Van Emburg,P.R., De Vrind,J.P.M., Kempers,E.S., Westbroek,P., De Vrind-De Jong,E.W. (1991) Role of the light-dark cycle and medium composition on the production of coccoliths by *Emiliania huxleyi* (Haptophyceae). *J. Phycol.*, 27,82-86.

Malin,G., Turner,S.M. and Liss,P. (1992) Sulphur: The plankton/climate connection. *J. Phycol.*, 28, 590-597.

Manton, I. (1986) Functional parallels between calcified and uncalcified periplasts. *In* Leadbeater,B.S.C. and Riiding,R. (eds.), Biomineralization in lower plants and animals. Oxford University Press, Oxford, pp.157-172.

Margalef,R. (1978) Life forms of phytoplankton as survival alternatives in a unstable environment. *Oceanol. Acta*, 1 ,493-509.

Matrai,P.A. and Keller,M.D. (1993) Dimethylsulphide production in a large scale coccolithophore bloom in the Gulf of Maine. *Cont. Shelf. Res.*, 13, 831-843.

McClain,E.P, Pichel,W.G. and Watson,C.C. (1985) Comparative performance of AVHRR-based multichannel sea surface temperatures. *J. Geophys. Res.*, 90, 11,587-11,601.

McIntyre,A., Ruddiman,W.F. and Jantzen,R. (1972) Southward penetrations of the North Atlantic Polar Front: Faunal and floral evidence of large-scale surface water mass movements over the last 225,000 years. *Deep-Sea. Res.*, 19, 61-77.

Mitchelson,E.G. (1984) Phytoplankton and suspended sediment distributions in relation to physical structure and water-leaving colour signals. PhD Thesis, University of Wales, Bangor, 126 pp.

Mitchelson,E.G., Jacob,N.J. and Simpson,J.H. (1986) Ocean colour algorithms from the Case 2 waters of the Irish Sea in comparison to algorithms from Case 1 waters. *Cont. Shelf Res.*, 5, 403-415.

Morel,A. and Ahn,Y-H. (1991) Optics of heterotrophic nanoflagellates and ciliates: A tentative assesment of their scattering role in oceanic waters compared to those of bacterial and algal cells. *J. Mar. Res.*, 49, 117-202.

Morel,A. and Prieur,L. (1977) Analysis of variations in ocean color. *Limnol. Oceanogr.*, 22, 709-722.

Müller-Karger.F.E., McClain,C.R., Sambrotto,R.N. and Ray,G.C. (1990) A comparison of ship and CZCS mapped distributions of phytoplankton in the Southeastern Bering Sea. *J. Geophys. Res.*, 95, 11,483-11,499.

Murphy,J. and Riley,J.P. (1962) A modified single solution method for the determination of phosphate in natural waters. *Anal. chim. Acta*, 27, 31-36.

Nimer,N.A and Merrett,N.J. (1992) Calcification and utilization of inorganic carbon by the coccolithophorid *Emiliania huxleyi* Lohman. *New Phytol.*, 121, 173-177.

Okada,H. and McIntyre,A. (1977) Modern coccolithophores at the Pacific and North Atlantic oceans. *Micropaleontology*, 23, 1-55.

Okada,H. and McIntyre,A. (1979) Seasonal distribution of modern coccolitophores in the NW Atlantic Ocean. *Mar. Biol.*, 54, 319-328.

Paasche,E. (1964) A Tracer study of the inorganic carbon uptake during coccolith formation and photosynthesis in the coccolithophorid *Coccolithus huxleyi*. *Physiol. Plant.*, 1-82.

Parslow,J.S. and Harris,G.P. (1990) Remote sensing of marine photosynthesis. *In* Hobbs,R.J. and Mooney,H.A. (eds.), Remote sensing of Biosphere functioning. Springer-Verlag, New York, pp. 269-289.

Parsons,T.R., Maita,Y. and Lalli,C.M. (1984) A manual of chemical and biological methods for seawater analysis. Pergamon Press, Oxford, 173 pp.

Pingree,R.D. (1980) Physical oceanography of the Celtic Sea and English Channel. In Banner,F.T., Collins,M.B. and Massie,K.S. (eds.), The NW European shelf seas: The sea bed and the sea in motion, vol.2. Elsevier, London, pp. 415-465.

Pingree,R.D. (1984) Some applications of remote sensing to studies of shelf-sea hydrodynamics. In Nhoul,J.C.J. (ed.), Remote sensing of shelf sea hydrodynamics. Elsevier, London, pp. 287- 315.

Pingree,R.D. and Griffiths,D.K. (1978) Tidal fronts on the shelf-seas around the British Isles. *J. Geophys. Res.*, 83, 4,615- 4,622.

Pingree,R.D. and Griffiths,D.K. (1980) Currents driven by a steady uniform wind stress on the shelf seas around the British Isles. *Oceanol. Acta*, 3, 227-236.

Pingree,R.D. and Maddock,L. (1985) Stokes, Euler and Lagrange aspects of residual tidal transports in the English Channel and the Southern Bight of the North Sea. *J mar. biol. Ass. U.K.*, 65, 969-982.

Pingree,R.D. and Mardell,G.T. (1976) Bucket STD measurements. *Deep-Sea Res.*, 23, 551-555.

Pingree,R.D. and Mardell,G.T. (1981) Slope turbulence, internal waves and phytoplankton growth at the Celtic Sea shelf-break. *Phil. Trans. R. Soc. Lon. (A)*, 302, 663-682.

Pingree,R.D. and Mardell,G.T. (1986) Coastal tidal jets and tidal fringe development around the Isles of Scilly. *Estuar. coast. Shelf Sci.*, 23, 581-594.

Pingree,R.D., Mardell,G.T., Reid,P.C. and John,A.W.G. (1986) The influence of tidal mixing on the timing of the spring phytoplankton development in the Southern Bight of the North Sea, the English Channel and on the Armorican shelf. *In* Bowman,J., Yentsch,M. and Peterson,W.T. (eds.), Tidal mixing and plankton dynamics. Springer-Verlag, Berlin, pp. 164-192.

Pingree,R.D. and Harris,R.P. (1988) An *in vivo* fluorescence response in the Bay of Biscay in June. *J. mar. biol. Ass. U.K.*, 68, 519-529.

Pingree,R.D. and Le Cann,B. (1989) Celtic and Armorican slope and shelf residual currents. *Prog. Oceanogr.*, 23,303-338.

Pingree,R.D. and Le Cann,B. (1990) Structure, strength and seasonality of the slope currents in the Bay of Biscay region. *J. mar. biol. Ass. U.K.* ,70, 857-885.

Platt,T. (1986) Primary production of the ocean water column as a function of surface light intensity: Algorithms for remote sensing. *Deep-Sea Res.* ,33,149-63.

Platt,T, Caverhill,C. and Sathyendranath,S. (1991) Basin-scale estimates of oceanic primary production by remote sensing in the North Atlantic. *J. Geophys Res.*, 96, 15,147-15,159.

Platt,T. and Sathyendranath,S. (1988) Oceanic primary production: Estimation by remote sensing at regional and larger scales. *Science*, 241, 1613-20.

Platt,T. and Sathyendranath,S. (1993) Comment on "The remote sensing of ocean primary productivity: Use of a new data compilation to test satellite algorithms" by, William Balch *et al.*. *J. Geophys. Res.*, 98, 16,583-16,584.

Platt,T., Sathyendranath,S. Caverhill,C.M. and Lewis,M.R. (1988) Ocean primary production and available light: Further algorithms for remote sensing. *Deep-Sea Res.*, 35, 855-35,879.

Platt,T, Sathyendranath,S. and Ravindran,P. (1990) Primary production by phytoplankton: Analytic solutions for daily rates per unit area of water surfaces. *Proc. R. Soc. London (B)*, 241, 101-111.

Poole,H.H. and Atkins,W.R.G. (1929) Photo-electric measurements of submarine illumination through the year. *J. mar. biol. Ass. U.K.*, 16, 297-324.

Price,J.C., (1988) An update on visible and near IR calibrations of satellite instruments. *Remote Sens. Environ.*, 24, 419-422.

Robertson,J.E., Robinson,C., Turner,D.R., Holligan,P.M., Watson,A.J., Boyd,P., Fernández,E. and Finch,M. (1994) The impact of a coccolithophore bloom on oceanic carbon uptake in the NE Atlantic during summer 1991. *Deep-Sea. Res.* (in press).

Robinson,I.S. (1983) Satellite observations of ocean colour. *Phil. Trans. Roy. Soc. London (A)*, 309, 415-432.

Robinson,I.S. (1985) Satellite oceanography: An introduction for oceanographers and remote-sensing scientists. Ellis Horwood, Chichester, 455 pp.

Robinson,I.S. (1989) Remote sensing information from the colour of the seas. *In* Herring,P.J., Campbell,A.K., Whitfied,M. and Maddock,L. (eds.), Light and life in the Sea. Cambridge University Press, Cambridge, pp. 19-38.

Ruddiman,W.F. and McIntyre,A. (1981) The North Atlantic during the last deglaciation. *Palaeogeog. palaeoclimat. palaeoecol.*, 35, 145- 214.

Ruddiman,W.E., Molino,B., Esmav,A. and Pokras,E. (1980) Evidence bearing on the mechanism of rapid deglaciation. *Clim. Change*, 3, 65-82.

Sathyendranath,S. and Platt,T. (1993) Remote sensing of water column primary production. *ICES mar. Sci. Symp.*, 197, 236-243.

Sathyendranath,S., Platt,T., Caverhill,C.M., Warnock,R.E. and Lewis,M.R. (1989) Remote sensing of oceanic primary production: Computations using an spectral model. *Deep-Sea Res.*, 36, 431-453.

Sikes,C.S. and Wilbur,K.M. (1982) Functions of coccolith formation. *Limnol. Oceanogr.*, 27, 18-26.

Simpson,J.H., Tett,P.B., Argote-Spinoza,M.L., Edwards,A., Jones,K.J. and Savidge,G. (1982) Mixing and phytoplankton growth around an island in a stratified sea. *Cont. Shelf Res.*, 1, 15-31.

Singh,S.M. (1988) Atmospheric correction algorithm for ATM data. *In* Proceedings of the NERC 1987 Airborne Campaign Workshop. NERC, Swindon, pp.19-28.

Sinha,B. and Pingree,R.D. (1993) ATM images of a coccolithophore bloom off Lands End in June 1992. *In* Proceedings of the NERC 1992 Airborne Campaign Workshop. NERC, Swindon, pp. 97-116.

Snyder,J.P. (1982) Map projections used by the Geological Survey. *U.S. Geol. Survey Bull.*, 1,532, 313pp.

Smayda,T.T. (1970) The suspension and sinking of phytoplankton in the sea. *Oceanogr. Mar. Biol. Annu. Rev.*, 8, 353-414.

Smith,R.C. and Baker,K.S. (1978) The bio-optical state of ocean waters and remote sensing. *Limnol. Oceanogr.*, 23, 247-259.

Smith,R.C and Baker,K.S. (1981) Optical properties of the clearest natural waters (200-800nm). *Appl. Opt.*, 20, 177-184.

Smith,R.C. and Baker,K.S. (1989) Stratospheric ozone, middle ultra-violet radiation and phytoplankton productivity. *Oceanography*, 2, 4-10.

Smith,R.C., Eppley,R,W. and Baker,K.S. (1982) Correlation of primary production as measured onboard ships in Southern California coastal waters and as estimated from satellite chlorophyll images. *Mar. Biol.*, 66, 281-288.

Sturm,B. (1981) Ocean colour remote sensing and quantitative retrieval of surface chlorophyll in coastal water using Nimbus CZCS data. *In* Gower,J.F.R. (ed.), Oceanography from space. Plenum Press, New York, 267-279.

Tangen,T. (1979) Dinoflagellate blooms in Norwegian waters. *In* Taylor,D.L. and H.H.Sliger (eds.), Toxic dinoflagellate blooms. Elsevier, North Holland , pp. 179-182.

Talling,J.F. (1957) The phytoplankton population as a compound photosynthetic system. *New Phytol.*, 56, 133-149.

Tassan,S. (1987) Evaluation of the potential of the Thematic Mapper for marine applications. *Int. J. Rem. Sens.*, 8, 1,455- 1,478.

Taylor,A.H., Watson,A.J., Ainsworth,M., Robertson,J.E. and Turner D.R. (1991) A modelling investigation of the role of phytoplankton in the balance of the carbon at the surface of the North Atlantic. *Global Biogeochem. Cycles*, 5, 1-4.

Thierstein,H.R., Geitsenauer,K.R. and Molfino, B. (1977) Global synchroneity of late Quaternary coccolith datum levels: Validation by oxygen isotopes. *Geology*, 5, 400-404.

Trees,C., Aiken,J., Hirche,H.J. and Groom,S.B.(1992) Bio-optical variability across the Artic Front. *Polar Biol.*, 12, 455-461.

Turner,S.M., Malin,G., Liss,P.S., Holligan,P.M. and Harbour,D.S. (1988) The seasonal variation of dimethylsulphide and dimethylsulphoniopropionate concentrations in nearshore waters. *Limnol. Oceanogr.*, 33, 364-375.

Uthermöl,H. (1958). Zur vervollkommung der quantitavien phytoplankton-methodik. *Mitt. Int. Ver. Theor. Angew. Limnol.*, 9, 1-38.

Van Bleijswijk,P., Van der Wal,P., Kempers,R., Veldhuis,M., Young,J.R., Muyzer,G., De Vrind-De Jong,E. and Westbroek,P. (1991) Distribution of two varieties of *Emiliania huxleyi* (Haptophyceae) in the NE Atlantic region as determined by immunofluorescence and coccolith morphology. *J. Phycol.*, 27, 566- 570.

Vairavamurthly,A.M., Andreae,O. and Ivrson,R.L. (1985) Biosynthesis of dimethylsulphide and dimelthylsulphoniopropionate by *Hymenomas carterae* in relation to sulphur source and salinity varations. *Limnol. Oceanogr.*, 30,59-70.

Viollier,M. and Sturm,B. (1984) CZCS data analysis in turbid coastal water. *J. Geophys. Res.*, 89, 4,977-4,985.

Viollier,M., Tanre,D. and Deschamps,P.Y. (1980) An algorithm for remote sensing of ocean colour from space. *Boundary-layer Meteorol.*, 18, 247-267.

Wahl,D.D and Simpson,J.J. (1990) Physical processes affecting the objective determination of near-surface velocity from satellite data. *J. Geophys. Res*, 95, 13,511-13,528.

Walsh,J.J. (1989) How much shelf production reaches the deep sea? *In* Berger,W.H., Smetacek,V.S. and Wefer,G. (eds.), Productivity of the ocean: Present and past. John Wiley, Berlin, pp. 175-191.

Westbroek,P., Brown,C.W., Van Bleijswik,J., Brownlee,C., Brummer,G.J., Conte,M., Egge,J., Fernández,E., Jordan,R., Knappersbutch,M., Stefels,J., Veldhuis,M., Van der Wal,P. and Young,J. (1993) A model system approach to biological climate forcing: The example of *Emiliania huxleyi*. *Global Planet. change*, 8, 27-46.

Westbroek,P., De Jong,E.W., Van der Wal,P., Borman,T., De Vrind, J.P.M., Van Emburg,P.E. and Bosch,L. (1983) Calcification in coccolithophoridae: Wasteful or functional? *Biogeochem. Ecol. Bull.*, 35, 291-299.

Westbroek,P.E., De Vrind-De Jong,E.W., Van der Wal,P., Borman,A.H. and De Vrind,J.P.M. (1985) Biopolymer-mediated calcium and manganese accumulation and biomineralization. *Geol. Minjbouw*, 64, 5-15.

Wilson,A.K. (1986) Calibration of ATM data. *In* Proceedings of the NERC 1985 Campaign Workshop. NERC, Swindon, E29-E42.

Yentsch,C.S. and Menzel,D.W. (1963) A method for the determination of phytoplankton by fluorescence. *Deep-Sea Res.*, 10, 221-231.

Young,J.R. and Westbroek,P. (1991) Genotypic variation in the coccolithophorid species *Emiliania huxleyi*. *Mar. Micropal.*, 18, 5- 23.